Effect of Traverse Rate in Ultrasonic Water Jet Peening on Surface Properties of Wrought Ti-6Al-4V

by

Danielle Griffin

Submitted in partial fulfilment of the requirements

for the degree of Master of Applied Science

at

Dalhousie University

Halifax, Nova Scotia

December 2022

Table of Contents

List of Tables

List of Figures

Abstract

Ti-6Al-4V is a popular alloy employed in numerous industrial applications. However, it exhibits poor wear resistance that leads to galling, seizure, and generation of wear debris. Surface modification techniques are commonly used to enhance the surface properties of materials. Ultrasonically pulsed water jet (UPWJ) peening is a relatively new technology that may possibly improve the surface properties of materials without excessive plastic deformation, detrimental thermal effects, or surface contamination. However, the influence of UPWJ peening parameters on the surface properties and wear resistance of titanium alloys is largely unknown. In this study, wrought Ti-6Al-4V was subjected to UPWJ peening at varying traverse speeds. The surfaces of the unpeened and peened wrought material were characterized by measurement and analysis of their surface roughness and scratch hardness through use of SEM and CLSM. Reciprocating wear tests were conducted on unpeened and peened wrought Ti-6Al-4V, and the wear tracks were analysed with SEM, CLSM, and EDS. It was found that UPWJ peening resulted in higher surface roughness than the unpeened material, although this was especially evident at low traverse speeds. Low traverse speeds also resulted in lower scratch hardness, although the scratch hardness was improved at higher traverse speeds. It was observed that UPWJ was detrimental to the wear resistance of the Ti-6Al-4V. At low traverse speeds, the material was highly susceptible to adhesive wear. At high traverse speeds, the material was found to experience an increased amount of abrasive wear.

Acknowledgements

I wish to express my sincere gratitude to numerous people that were vital to this study for their contributions and support. Foremost, my sincerest gratitude for my supervisor, Dr. Kevin Plucknett, for providing me with the opportunity to complete the MASc program at Dalhousie University. I am extremely appreciative of his patience, understanding, accommodations and guidance throughout the pandemic and MASc.

I would also like to thank the rest of my thesis committee: Dr. Zoheir Farhat and Dr. Fadi Oudah for their encouragement, insights, and recommendations. I also thank VLN Advanced Technologies, Inc and NSERC for their contributions and support to this research.

This study could not have been completed without the guidance and lab support of all my incredible coworkers. I am especially appreciative of Patricia Scallion, Zhila Russell, Mark Amegadzie, and Paria Siah Pour for their training, patience, knowledge, and skills. Moreover, thank you to Dr. Farhat and the Advanced Tribology Laboratory group for their expertise in wear testing and use of their equipment.

I am indebted to my brilliant friends: Jeremy Cadence, Rielle Jensen, Thomas Brennan, Solomon Somers, and Margaret Wilson. They have supported me immensely throughout my time at Dalhousie University, and never fail to help me laugh and relax. Finally, I am so thankful for my parents, Tim and Paula Griffin, and my brother and sister-in-law, Alex and Hannah Griffin. I could not have wished for a more loving or encouraging family.

Chapter 1: Introduction

Titanium alloys have found widespread use in a variety of industries such as aerospace and biomedical applications due to their advantageous mechanical and chemical properties [1-14]. In the aerospace industry, titanium alloys have become a vital engineering material due to their high strength-weight ratios and excellent corrosion resistance. Aircraft components previously made from high-strength steels are being replaced with those made from titanium alloys, to reduce aircraft weight and fuel consumption [15-20]. In biomedical applications, implants are commonly made from titanium alloys also due to their excellent corrosion resistance and strength, as well as high biocompatibility. Artificial joints such as the hip and knee are routinely made from titanium alloys, as well as dental implants [5-7].

In particular, Ti-6Al-4V has become one of the most popular titanium alloys for use in many industries [2, 5, 6, 10]. Ti-6Al-4V has high strength, excellent corrosion resistance, and reasonable ductility, due largely to its crystal structure which contains two distinct crystalline phases. The hexagonal close-packed (HCP) α-Ti phase is characterised by excellent corrosion resistance, as well as impressive thermal and chemical stability [4, 16, 21]. The body-centred cubic (BCC) β-Ti phase has improved ductility and strength in comparison to the α phase [4, 21].

However, titanium alloys are notorious for their poor tribological properties, which may be a result of its crystal structure [1, 3]. Compression of the titanium α phase leads to an increased number of slip planes, such that it behaves similarly to a cubic structure, which intrinsically contains numerous slip planes [3]. Hence the alloy has good ductility and strength while exhibiting poor wear resistance. Titanium and its alloys have been observed to have a strong propensity for adhesive wear, leading to galling and seizing [3, 5-7, 12, 13]. Wear tracks on titanium alloys have been found to feature ridges, deep grooves, and significant wear debris caused by cyclic adhesion and shearing [3]. In aerospace, damaged components due to wear must be replaced. This is a significant cost, as the aircraft cannot function while the part is produced, installed, or inspected. Furthermore, there are consequently potential safety concerns. In biomedical applications,

wear debris from titanium-based implants has been found to accumulate in surrounding tissue and is able to enter the bloodstream [5, 6, 10, 21, 22]. This is often detrimental to the patient's health and requires revision surgery to replace the damaged implant.

Wear behaviour is largely impacted by the surface properties of the material rather than its bulk properties [23]. Surface modification may be employed to improve the overall performance and thus the material's wear properties. A commonly applied surface modification technique is peening, where the material surface is impinged by a peening medium [24-27]. The impingement causes plastic deformation at the surface, leading to a surrounding elastic restraint and induced subsurface compressive residual stress. Conventional peening techniques include shot peening, laser shock peening, cavitation peening, and continuous water jet peening. Ultrasonically pulsed water jet (UPWJ) peening, which utilises an ultrasonically pulsed water stream, has been developed as a possible improvement of continuous water jet peening. This method relies on the water hammer effect to achieve a greater effective impact pressure at the material surface [28-30]. However, the influence of UPWJ peening parameters, such as the traverse speed, on surface properties are relatively unknown.

The influence of UPWJ peening traverse speed on the surface properties of Ti-6Al-4V must consequently be evaluated, which is the focus of the present thesis. This includes a comparison of the surface properties of unpeened wrought Ti-6Al-4V with Ti-6Al-4V that has been treated by UPWJ peening using varying traverse speeds. This study involves analysis and measurement of both the unpeened and UPWJ peened surface roughness, as well as evaluation of scratch hardness with and without UPWJ peening. This assessment is further supported by studying the dry reciprocating wear behaviour of both unpeened and peened materials. The purpose of this study is thus to measure and observe the influence of UPWJ peening traverse speed upon the surface properties of wrought Ti-6Al-4V. The primary objective for this research is to study and comprehend the effects of UPWJ peening upon the tribological response of wrought Ti-6Al-4V. Hence, the scope of work for this project involves:

1. Observation and comparison of the surface roughness of unpeened Ti-6Al-4V to the surface roughness of wrought Ti-6Al-4V peened at various traverse speeds.
2. Measurement and comparison of the resulting scratch hardness of each UPWJ peening traverse speed to that of the unpeened Ti-6Al-4V material.
3. Measurement and comparison of the specific wear rates of Ti-6Al-4V peened at various traverse speeds to the specific wear rate of unpeened Ti-6Al-4V.
4. Inspection of wear tracks of unpeened and peened Ti-6Al-4V materials and determine the primary wear mechanism.

External contributions to this study include Andrew Tieu from VLN Advanced Technologies, Inc., who performed the UPWJ peening for this study. Additionally, Mark MacDonald from Dalhousie University completed machining of the Ti-6Al-4V samples prior to peening. Testing of the samples was completed by the author, as well as data collection and analysis. To the author's knowledge, the influence of traverse speed upon the surface properties of wrought Ti-6Al-4V has not yet been studied by any research group.

The overall thesis structure is as follows. The second chapter of the thesis contains a comprehensive literature review of titanium alloys, their wear behaviour, and surface peening techniques, and outlines both the current research and research gaps. The experimental procedures used for this study are detailed in Chapter 3. Chapter 4 exhibits the data gathered and discusses the results found from this study. Finally, the overall conclusions and some future recommendations for extending this work are found in Chapter 5.

Chapter 2: Literature Review

2.1 Material Background

2.1.1 Titanium Alloys and Their Applications

Titanium alloys have found application in a wide range of industries due to their unique properties. They are typically characterised by high strength-weight ratios, high specific strength, stability at mid-temperatures, non-magnetism, biocompatibility, and impeccable corrosion resistance [1-12, 15-17, 31]. These properties have made them desirable in numerous fields such as the aerospace, marine, biomedicine, automotive, performance sports, and chemical industries [1-4, 7, 8, 13, 14]. Ti-6Al-4V is a popular titanium alloy in many applications; it accounts for approximately 60% of all titanium alloy products [2].

In aerospace engineering, there has been considerable interest in replacing steel components with titanium alloy for over 40 years [1, 3, 15]. In comparison with ferrous alloys, titanium alloys are favourable due to their high strength-weight ratios, their specific modulus, specific strength, and toughness [1, 15, 16, 31]. Aircraft weight may be significantly reduced by substituting high-strength steels for titanium alloys, decreasing fuel consumption, and increasing profit [15-20]. As a result, many aircraft contain titanium alloys in their fuselage, such as the Boeing 777 [31]. Primary components of aircraft landing gear as showing in Figure 2–1, traditionally made from high-strength steel, have also become increasingly manufactured from titanium alloys. The high strength steel components would have to be replaced at least once over the course of the aircraft's lifetime due to severe stress corrosion; replacement is not required for titanium components due their high stress corrosion resistance [31]. Steel hydraulic tubing has also been replaced with titanium-based tubing, with possible weight savings of 40 % [31]. In comparison to aluminium or ferrous alloys, the manufacturing costs of titanium are much higher. However, savings from reduced part replacement and diminished fuel cost outweigh the initial costs [31]. Military fighter aircraft have also integrated titanium alloys into their designs and structures. Due to their higher manoeuvrability and speed, the material used in military fighter aircraft must be able to withstand high thermal and

mechanical loads. A military fighter aircraft may contain more than 50 % titanium in its fuselage, and titanium accounts for 35 to 50 % of the weight of a modern fighter aircraft [31].

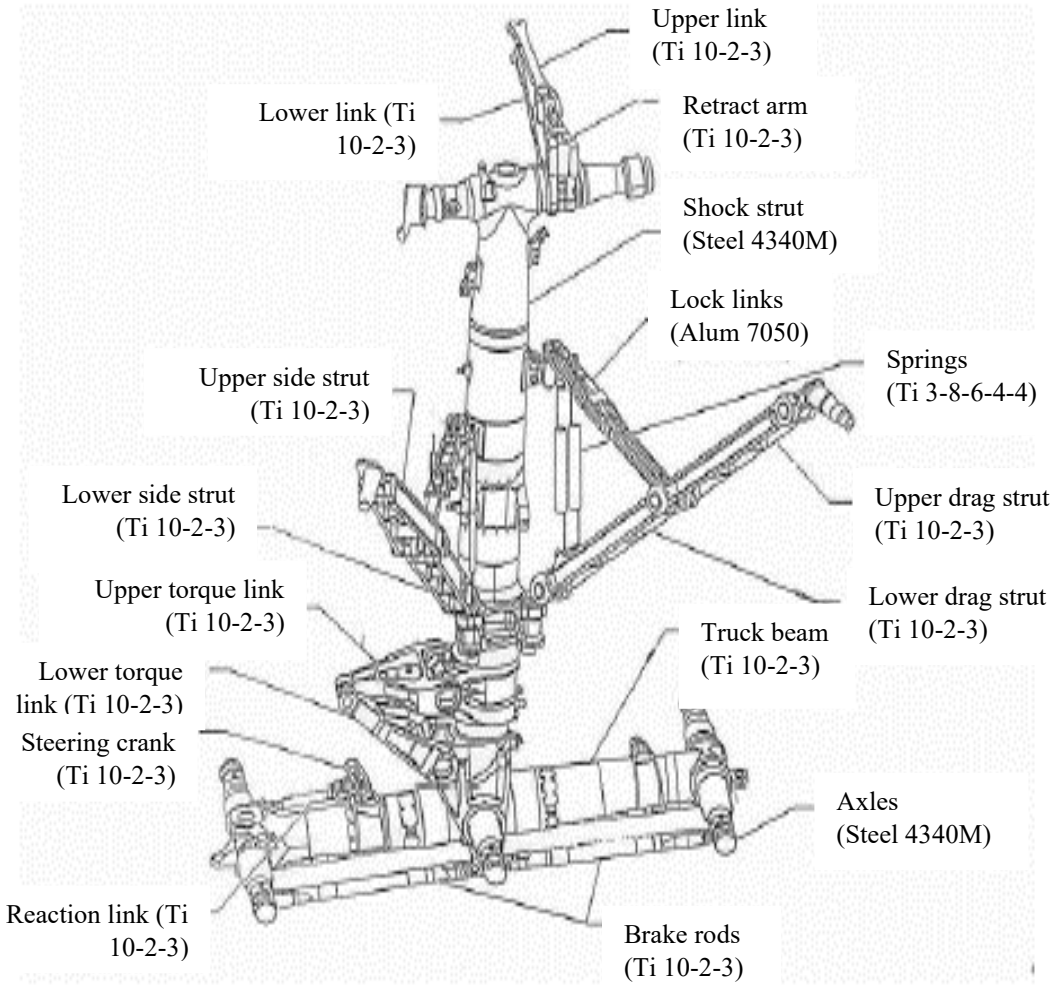

Figure 2—1: Materials of primary components of landing gear of Boeing 777 aircraft [18].

Titanium alloys are becoming increasingly common in the biomedical field for artificial bones, joints, and dental implants [5-7]. Their high biocompatibility, good mechanical properties, low density, and excellent corrosion resistance of titanium alloys means that they present favourable mechanical and chemical behaviour suitable for orthopaedic and dental use [6, 21, 22]. Commercially pure titanium (CP-Ti, referred to as grade 2) and Ti-6Al-4V (grade 5) alloy are the most common titanium-based materials found in medical applications [6, 7, 10]. In dental and orthopaedic implants, titanium alloys have been widely used due to their high strength and fracture toughness under loadbearing conditions [6]. In these applications, the surface properties of the implant

may have a significant impact upon the success and biocompatibility of the implant. Surface chemistry, surface topography and surface roughness may aid or hinder the process of osteointegration, the mechanism by which bone may chemically bond with the metal and begin to grow into the implant. Osteointegration has been observed in titanium alloy implants, further making titanium and its alloys highly promising engineering material for biomedical applications [6]. Ti-6Al-4V is the most widely used alloy for hip implants, knee implants, bone screws, and plates, where good mechanical properties are vital for success [6]. One of the most common applications of titanium alloys is total hip arthroplasty (THA), which involves replacing a degraded hip joint with an artificial one [6, 21]. The artificial joint consists of a stem and articulating bearing (composed of a femoral head and cup) and stem as shown in Figure 2–2, where the cup and stem are produced with titanium alloys [6]. Similarly, the femoral and tibial components of knee joint replacements are often made from titanium with a polyethylene articulating surface.

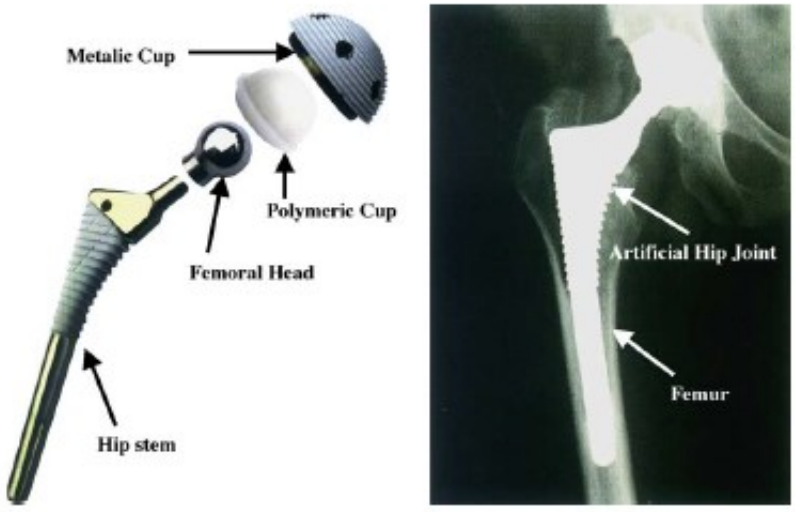

Figure 2—2: Schematic and x-ray of an artificial hip implant [21].

2.1.2 Titanium Crystallography

Titanium has two allotropic forms, α and β, which have significant impacts upon the properties of titanium alloys. Titanium has a close-packed hexagonal crystal structure up to a temperature of approximately 885˚C, above which it transforms into the β body-centred cubic structure [4, 7, 9, 16, 18, 19, 21, 30]. Titanium alloys may be separated into classes depending on the assemblage of these phases at room temperature: α, near-α, α-β,

and β alloys [4, 7, 9, 16, 21]. Alloying elements may be able to lower or raise the β-transus temperature to stabilise one of the phases [7, 21]. Hence, alloying elements for titanium may be separated into three categories: (i) α-stabilisers that raise the β-transus temperature, such as Al, O, N, C; (ii) β-stabilisers that lower the β-transus temperature, including Mo, V, Nb, Ta, Fe, W, Cr, Si, Co, Mn, H; (iii) neutrals that have a negligible effect on the β-transus temperature, such as Zr [7, 21]. Figure 2–3 displays several titanium alloys mapped onto a beta-isomorphous phase diagram.

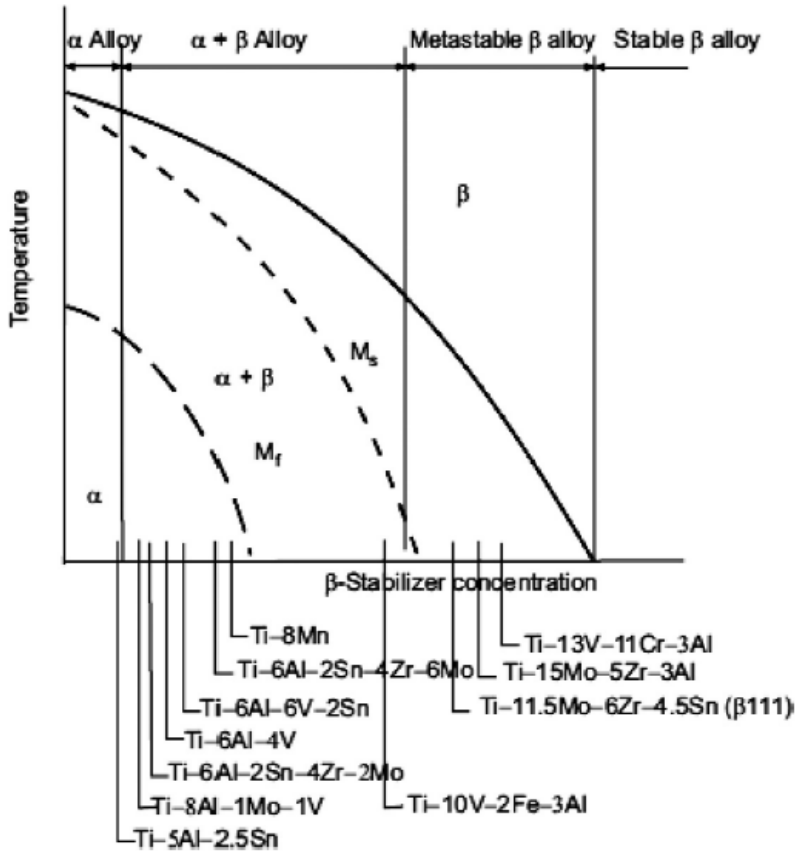

Figure 2—3: Compositions of titanium-based alloys mapped onto a pseudo binary β-isomorphous phase diagram [4].

The α alloys consist of a single solid solution of the α-phase, and possess low strength [4, 7]. However, they also show good ductility, fracture toughness, creep performance, and excellent corrosion resistance [4, 16, 21] These alloys are typically found in chemical and process engineering applications, where their high corrosion resistance and deformability are highly advantageous. Near-α alloys typically contain approximately 1 to 2 % of β-stabilizers, which results in a structure with less than 10% of

β-phase [7, 9]. The β-phase improves the strength and workability of the alloys [7, 19, 20].

The α-β class of titanium alloys, due to the presence of both phases, demonstrate higher strength but lower ductility than the α or near-α alloys [7, 19, 21]. These alloys typically possess 4 to 16 % of β-stabilizers to achieve 10 to 20 % of β-phase [7]. These are the most widely used titanium alloys for structural, aerospace, and biomedical applications [7, 9]. Ti-6Al-4V is the most popular α-β alloy, which represents more than 50% of all titanium alloys in use [4, 7, 9, 16].

The β alloys, also referred to as metastable β alloys, contain a small amount of α-stabilisers and 10-15% of β-stabilisers [7]. The β-stabilisers promote the retention of β-phase at room temperature, and the alloys can be heat treated by aging to achieve a very fine precipitation of α-phase dispersed in the β matrix [7, 9]. Beta alloys demonstrate high corrosion resistance, with equivalent or higher strength to that of the α-β alloys, with significantly higher ductility [4, 21]. The microstructure, elastic moduli and strengths of some titanium alloys are compared in Table 2–1.

Table 2—1: Comparison of titanium alloy microstructures and their elastic moduli, yield strength, and ultimate strength [21].

Alloy Designation	Microstructure	Elastic Modulus (GPa)	Yield Strength (MPa)	Ultimate Strength (MPa)
cpTi	α	105	692	785
Ti-6Al-4V	α/β	110	850-900	860-970
Ti-6Al-7Nb	α/β	105	921	1024
Ti-5Al-2.5Fe	α/β	110	914	1033
Ti-12Mo-6Zr-2Fe	Metastable β	74-85	1000-1060	1060-1100
Ti-15Mo-5Zr-3Al	Metastable β	82	771	812
Ti-35Nb-5Ta-7Zr	Metastable β	55	530	590

2.2 Wear Mechanisms

2.2.1 Adhesive Wear

Flat metal surfaces are never truly planar, asperities and a height distribution typically cover a metal surface [3]. When in contact with another surface, the asperities of each material are conjoined by plastic deformation. Thus, the real contact area is the summation of individual contact points at the asperities. The real contact area is influence by several factors including the surface topographies, the asperities' deformation properties, and the normal and tangential loads that cause junction growth. At regions of real contact, strong adhesion or cold-welding may occur to create a junction. Greater energy or friction force is required to shear the newly formed junction. Sliding motion under an applied load gives rise to junction formation between the surfaces, eventually giving way to junction shearing. As the sliding motion continues, new junctions are formed and subsequently sheared. When the adhesive strength is higher than either of the surfaces' cohesive strength, the junction ruptures within the weaker asperity. This results in material transfer from the weaker material to the counter surface and may detach to form loose wear particles [3]. An illustration of the adhesive wear mechanism is shown in Figure 2–4.

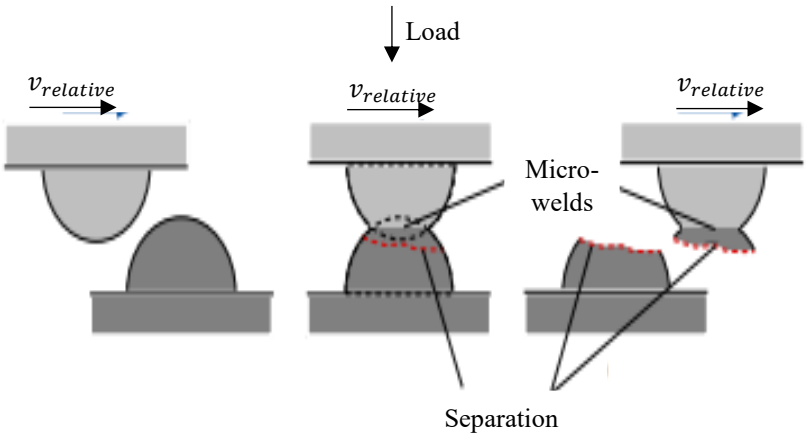

Figure 2—4: Adhesive wear mechanism before contact, during contact, and after contact [31].

Oxidational wear, or mild wear, is a type of adhesive wear to which most alloys are susceptible [3]. All metallic surfaces feature an oxide layer under atmospheric conditions, resulting in weak adhesion between oxide layers at the asperity tips and formed junctions have a low shear strength. A hard metal substrate may provide mechanical support for the oxide layer to protect against penetration. Otherwise, rubbing motion may easily remove the oxide layer to expose the metal underneath to contact. The exposed metal re-oxidises immediately unless in a vacuum or inert atmosphere. If the process of re-oxidisation dominates over the removal of the oxide film, the sliding surfaces become separated by the thin oxide film and minimal direct material contact occurs. This results in lowered friction and wear, but also creates fine oxidised debris [3]. However, should the oxide film be damaged faster than it can form, continuing direct material contact worsens and severe wear occurs. This results in surface roughening and coarse metallic debris. Scuffing, galling, and seizure may be observed in cases involving severe wear of varying surface damage. Scuffing is a localised form of surface damage caused by localised solid-state welding during direct material contact typically after the breakdown of a fluid or solid lubricant film, resulting in extreme friction and acute wear. Galling is similar to scuffing but results from unlubricated sliding and is characterised by much worse surface damage that consists of a severely roughened surface and transfer or displacement of large wear debris particles. Scuffing and galling are both destructive processes that may result in seizure of the surface with continued sliding, where excessive development of asperity junctions may cause failure of the sliding system [3].

2.2.2 Abrasive Wear

Abrasive wear occurs when material impinges on or moves along a softer material surface under load, resulting in the removal of material from the softer surface [3, 33, 34]. Plastic flow and brittle fracture may be present in abrasive wear, but plastic deformation is more prevalent in most cases of abrasive wear of metals and alloys [3]. During sliding, a particle may plough through a softer surface to produce a groove. Material is displaced or removed from the groove via a ploughing model or a micro-cutting model [1, 3]. The wear rate of abrasion is proportional to the applied load, and inversely proportional to the

hardness of the abraded material [3]. Abrasive wear also depends upon the hardness ratio between the abraded material and the abrasive. Abrasive wear may be defined as either two-body abrasion or three-body abrasion, although these may occur concurrently. In two-body abrasion, hard asperities on a counter surface remove material from the other surface. Three-body abrasion accounts for hard particles or wear debris that may become trapped in the wear path and abrade the softer material [33, 34]. Figure 2–5 illustrates the difference between two-body and three-body abrasive wear.

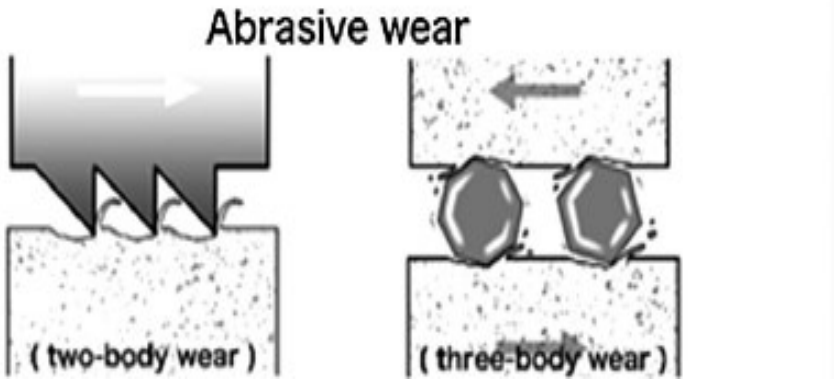

Figure 2—5: Abrasive wear mechanisms: left) two-body wear; right) three-body wear [33].

Often, abrasive wear may take place concurrently with adhesive wear. During adhesive wear, metal particles may transfer to the counterpart resulting in a rough counterpart surface. The transferred material may then abrade the soft metal surface, leading to severe abrasive wear [3]. The transferred material may also detach from the counter surface, becoming entrapped in the wear track. The transferred materials aids in abrading the softer surface [33].

2.3 Wear Resistance of Titanium Alloys

Despite their many advantageous mechanical and chemical properties, widespread use and increased industrial use of titanium alloys has been somewhat limited by their poor tribological behaviour, low hardness, poor abrasion resistance and low fatigue strength [1, 2, 6, 7]. They exhibit high and unstable friction, severe adhesive wear, low resistance to abrasion, vulnerability to fretting wear, and strong propensity to seize [3, 5-

7, 12, 13, 23]. Hence, the use of titanium alloys in industries has been hampered, especially in applications involving dynamic loading conditions [2, 3, 6]. The poor tribological behaviour of titanium alloys can be attributed to several characteristics including the electron configuration, crystal structure, ineffectiveness of lubrication, and low thermal conductivity [1, 3]. Titanium alloys experience abrasive, oxidative and adhesive wear. Titanium alloys are known to be relatively soft (200–350 HV), and thus have poor wear resistance as material is easily transferred to the counterpart and in turn abrades the titanium surface [3, 6, 21]. Titanium alloys are also vulnerable to oxidational wear, since titanium forms a relatively thin oxidation layer (5-10 nm) that may be easily penetrated by contacting asperities and be formed into oxidational debris [3, 10, 21]. However, the wear of titanium is dominated by adhesive wear. When a titanium-based surface slides against any engineering surface, whether it be metallic, ceramic, or polymeric, under a medium-to-high load, severe adhesion occurs and creates debris [3, 6]. Titanium's poor adhesive wear behaviour may be attributed to its crystallography that allows several slip systems to occur [1].

Adhesive wear involves direct metal contact, plastic deformation, cold welding, junction growth and material transfer. Titanium's susceptibility to adhesive wear is related to its plastic deformability and high ductility. The crystal structure of metals determines their plastic deformation mechanisms, and thus the metals wear behaviours. As discussed previously, titanium alloys have various orientations of α and β phases. The α phase features close-packed hexagonal crystal structure, whereas the β phase consists of a body-centred cubic crystal structure. Hexagonal structured metals typically have better friction and wear characteristics than cubic structured metals. At room temperature, hexagonal metals plastically deform by slip on the slip plane, which is the closed-packed basal plane (0001) [3]. Continuous junction growth requires slip to occur on different slip planes, thus the continuous junction growth is impossible for the hexagonal structure. The α titanium phase has an axial ratio c/a of 1.58787 due to compression of the lattice in the c-axis, whereas the ideal axial ratio for closest packing is 1.633 [3]. As a result, the interplanar spacing and atomic density of the plane are reduced, making it less favourable for slip. Instead, prismatic (1010) and first-order pyramidal (1011) slip are allowed [3]. Thus, the titanium α phase has multiple slip systems that cause it to behave similarly to a

cubic structure. It has good ductility, deforms easily, and exhibits poor tribological behaviour. Titanium β alloys, which are dominated by a cubic structure, have many slip systems that make these alloys highly ductile and stronger than the α or α-β alloys. However, these alloys suffer from a high degree of surface deformation, material transfer, higher average friction, and a much lower adhesive wear resistance [3]. Titanium and its alloys, in general, have low tensile and shear strengths, such that when adhesion occurs with other materials, fracture will occur in the titanium rather than at the junction. This results in large amounts of metal transfer and debris, increasing wear rates [1].

Titanium and its alloys are highly susceptible to adhesive wear leading to seizure and galling. Adhesion of titanium alloys is often evident by a high and unstable coefficient of friction when sliding occurs against itself or other engineering materials. In particular, titanium alloys have been found to exhibit cyclic 'stick-clip' adhesive behaviour. The 'stick' is the result of increased real contact area with increased tangential forces and junction growth, such that the two surfaces are in adhesive contact. As the applied force exceeds the adhesive strength, a sudden 'slip' between the two surfaces occurs as the junctions are ruptured. This repeating process results in fluctuations in friction traces. Wear tracks of Ti-6Al-4V have been observed to feature deep grooves that are generated by ploughing, and recurrent transverse ridges and adhesive spots caused by the 'stick-slip' process [3]. Figure 2–6 shows the stick-slip wear pattern found in Ti-6Al-4V, and Figure 2–7 shows severe adhesive wear.

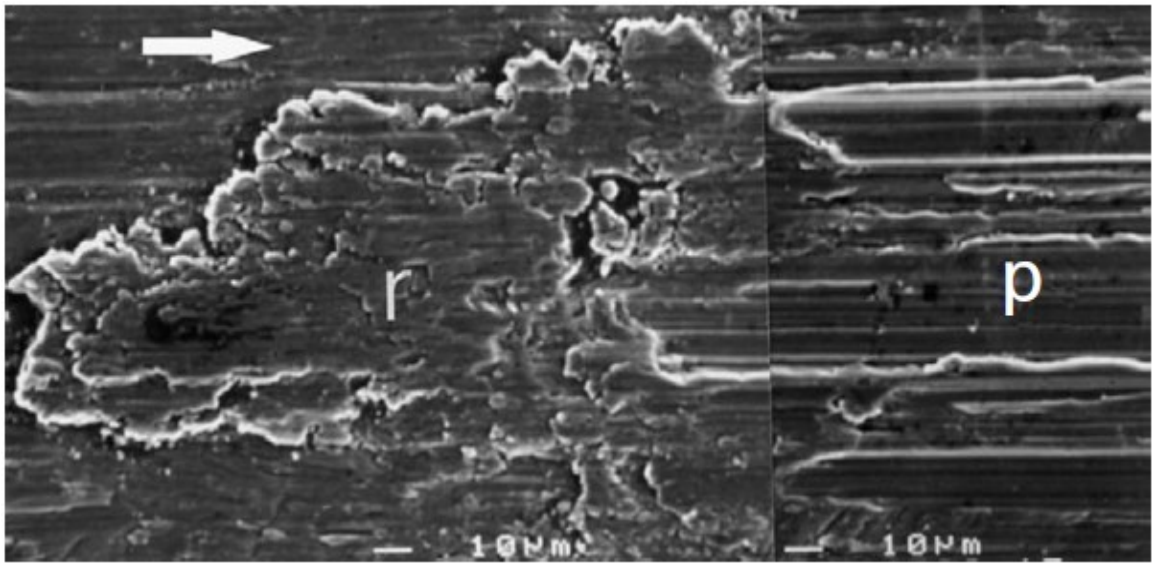

Figure 2—6: Worn tracks on a Ti-6Al-4V disc that show adhesive areas (indicated by 'r') and deep ploughing (indicated by 'p') [3].

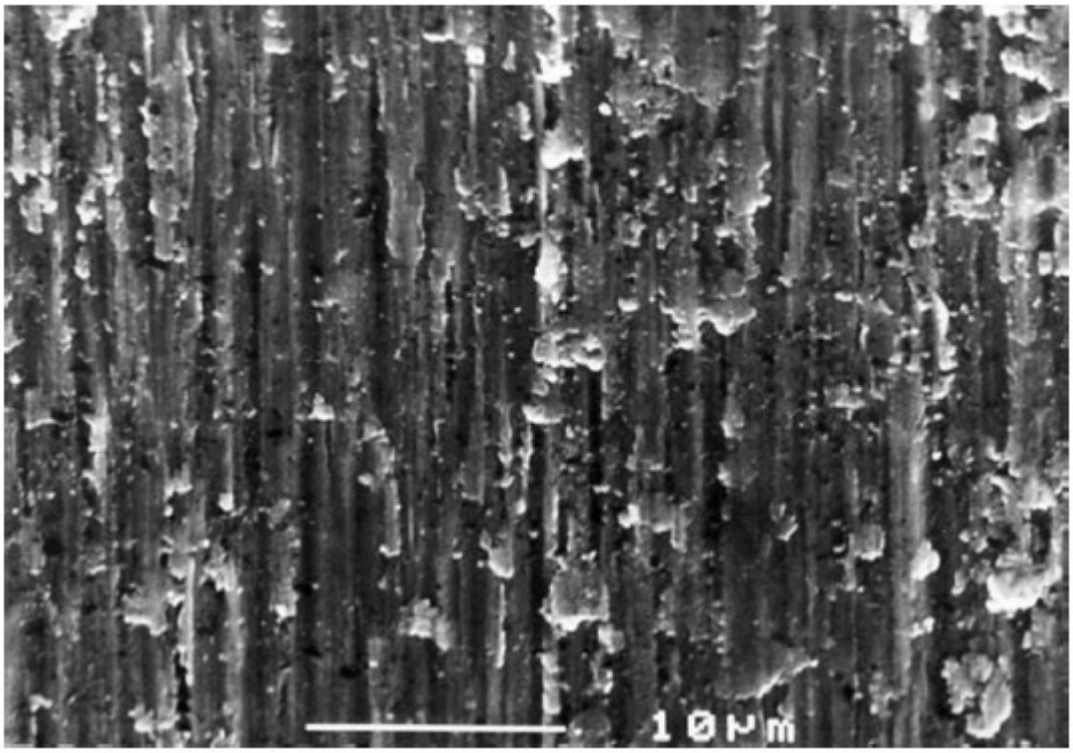

Figure 2—7: Adhesive wear features on Ti-6Al-4V with craters and deep ploughing grooves [3].

The poor wear behaviour of titanium has prompted issues across several industries. For instance, in the biomedical field, the wear resistance of titanium poses a serious issue with harmful consequences. Sliding parts made from titanium have a tendency to gall and eventually seize, resulting in the creation of adhesion couplings and mechanical instability of oxide passive layers [6]. For implants, oxide passive layers are vital to maintaining biocompatibility and avoiding corrosion within the body. Moreover, the alloys' high coefficient of friction and poor wear resistance results in the formation of wear debris around the implant [5, 6, 10, 21, 22]. This debris may become imbedded in surrounding tissue, causing toxicity, inflammation, and significant pain [5]. Aseptic loosening may also occur due to poor wear resistance, as wear debris is released into the bloodstream and inflames surrounding tissue. This instigates bone resorption (osteolysis) that leads to loosening of the implant, which may only be revised with surgery and implant replacement [6]. Consequently, 10 % to 20 % of total joint replacements with a titanium head and polymer cup must be replaced within 15 to 20 years [6, 10, 21]. Aseptic loosening caused by the release of wear debris into the bloodstream accounts for approximately 80 % of cases [10, 21]. To combat this issue, a significant amount of research has developed focusing on surface treatments of titanium alloys for implant use [5, 7, 8, 21, 23]. Additionally, surface treatments of titanium alloys may aid in promoting osteointegration [6, 21].

2.4 Surface Peening Techniques

The wear behaviour of a material is known to be impacted largely by the material's surface performance rather than its bulk properties [23]. Hence, much research has been aimed at the usage of surface modification technologies to impart favourable surface attributes to materials in the hopes of improving their wear behaviour. An appropriate surface treatment is able to improve surface performance, such as attaining a higher hardness and wear resistance, while maintaining the bulk attributes of the material and lengthening a material's service life [23, 35]. Ti-6Al-4V has been subjected to numerous surface modification technologies to improve its tribological performance [23].

In biomedical applications, surface texturing by surface modification technologies has been extensively studied to improve the biocompatibility and tribological properties of titanium implants. Surface texturing and roughening to obtain artificial surface patterns such as dimples and grooves has proven favourable for cell and antibacterial adhesion and production on implant surfaces due to higher surface area [23, 36].

A common surface modification technique is peening, where the surface of a material is bombarded with high mechanical forces to impart compressive stresses at the surface and induce work hardening [25]. In this process, an impact is generated on a metal grain leading to plastic deformation of that grain and surrounding elastic restraint. This results in dislocation movement and proliferation, and subsequent hardening of the grain. As the dislocations multiply and intersect with one another, jogs are produced that act to pin the dislocations such that they can no longer propagate and move. Hence the grain hardness in the area of plastic deformation is greater than that in the original surface [24, 26]. These compressive stresses are greatest at the surface and lessen with depth, as shown in Figure 2–8, such that the bulk material at a great enough depth retains its original properties [30]. Additionally, the service life of parts is often affected by surface residual tensile stresses induced by previous machining operations [27]. The peening processes are designed to enhance surface residual compressive stresses, thereby extending the part's service life, and improving its performance. Tensile residual stresses may be converted into compressive residual stresses by plastic deformation [24, 37]. In comparison to other surface modification methods, peening is relatively simple, cost effective, and industrially reliable [36]. Peening techniques may be classified as shot peening, laser shock peening, cavitation peening, and water jet peening [27, 38].

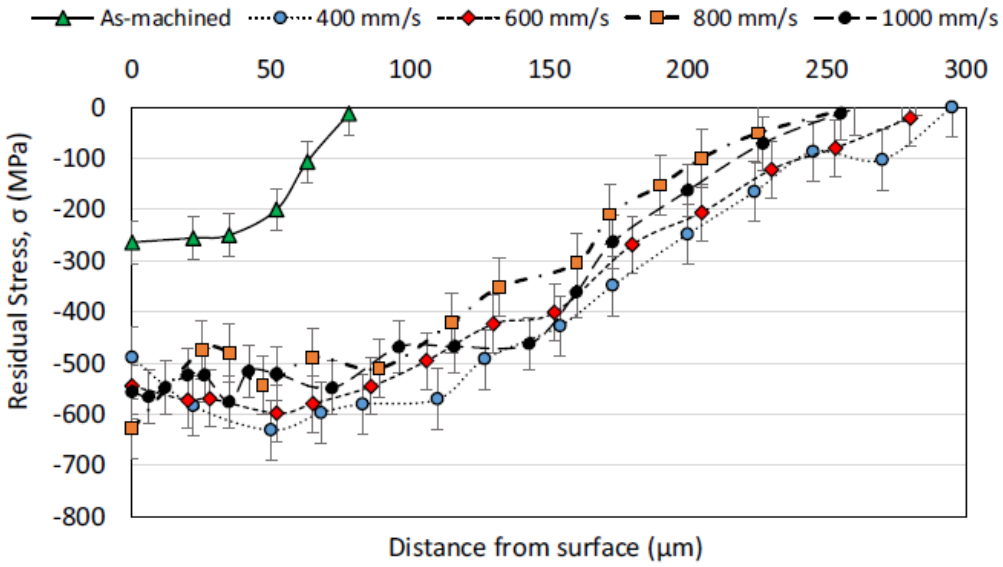

Figure 2—6: Residual stress in peened materials as a function of depth from the peened surface [30].

2.4.1 Shot Peening

Shot peening has been widely used in industrial applications to remove residual tensile stresses and improve surface hardness of metallic components [24]. It is a cold working method designed to improve surface mechanical properties of engineering materials [38]. It was first introduced in the 1950s for aerospace applications but has since been applied to many engineering materials across a variety of industries [35, 38]. This method typically uses compressed air to fire multiple hard spherical projectiles at controlled velocity towards the material surface [35, 37-40]. The projectile shots may be made of glass, metals, or ceramics, that are directed through a gun working on compressed air, as seen in Figure 2–9 [38, 40]. As the shots impact the material surface, the material is elasto-plastically deformed and dimples are formed on the material surface [35, 38]. Residual compressive stresses are formed on the substrate surface during the recovery process upon rebounding the shots [38]. The shots may be made of metals, glass and ceramics of varying diameter chosen by the operator. Shot peening can be completed wet or dry. Wet shot peening involves the use of ceramic beads placed in liquids that contain corrosion inhibitors [2]. During the process, a liquid film is formed on the surface

that reduces friction and cools the surface. Ceramic beads may be considered to be advantageous for energy conservation and for environmental protection due to their high intensity, toughness, hardness, good surface finish, and high productivity [2].

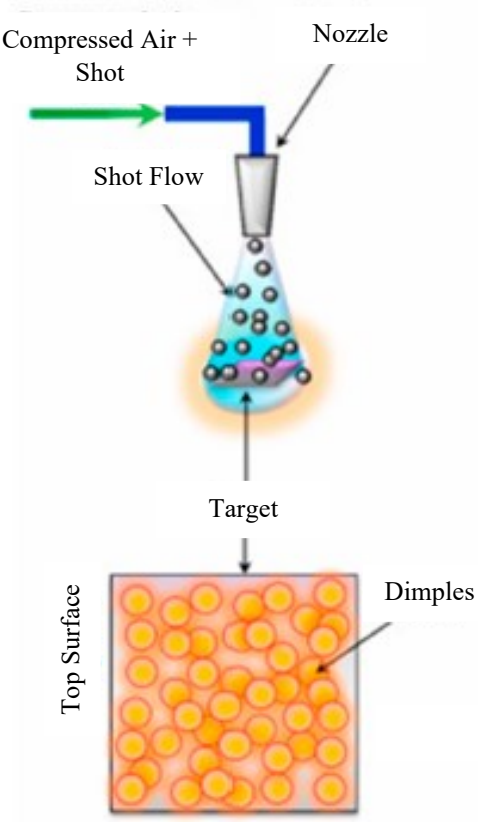

Figure 2—7: Diagram of the shot peening process [38].

Shot peening is an inexpensive, simple, flexible, and efficient method of improving surface properties and fatigue strength [24, 38]. Shot peening has been used to improve the fatigue and tribological properties of titanium alloys by work hardening the surface layer [11]. However, this method of peening results in extreme surface roughness and surface deterioration [24, 30]. Uniform peening intensity across the material surface is not guaranteed, and it is also difficult to obtain a compressive residual stress layer depth greater than 1 mm, since increasing parameters such as the intensity or coverage has adverse effects on the surface roughness and micro-cracks [14, 38, 40]. Due to the surface roughening, secondary surface treatments may be required for wear applications [38]. Additionally, the use of a shot peening medium may result in contamination of the

material surface [35]. Therefore, shot peening is not recommended for components that require deep compressive residual stress distribution and low surface roughness [14].

2.4.2 Laser Shock Peening

Laser shock peening technology was initially developed in the late 1960s and involves utilising laser-induced shockwaves to strengthen the surface of a material [14, 25, 39]. A pulsating laser light is aimed at the material surface, with a typical pulse length of 0.15 – 0.30 ns [37]. A transparent layer is required to reduce plasma produced on the material surface and increase the shock wave's intensity, a water stream is commonly used for this layer as a simple and cost-effective method [37]. After the laser light has passed through the transparent layer it hits an optional opaque sacrificial layer. The opaque layer is typically made from aluminium, zinc, or copper; and is used to protect the material from direct thermal contact with laser-induced plasma [35]. The opaque layer also provides a consistent surface condition for interaction with the laser beam. A diagram of the laser shot peening method is shown in Figure 2–10. Direct contact between the metal surface and laser-induced plasma often forms a thin melt layer on the material surface. Depending on the laser conditions and metal properties, surface discolouration will appear or a melt layer 15 – 25 μm in thickness [37]. As the laser light reaches the absorption layer, ionisation occurs in the heated zone and a shock wave is produced [35]. The shock wave with high amplitude propagates from the surface into the material, causing plastic deformation. Material resistance to plastic deformation results in compressive residual stress [14, 37, 39, 40].

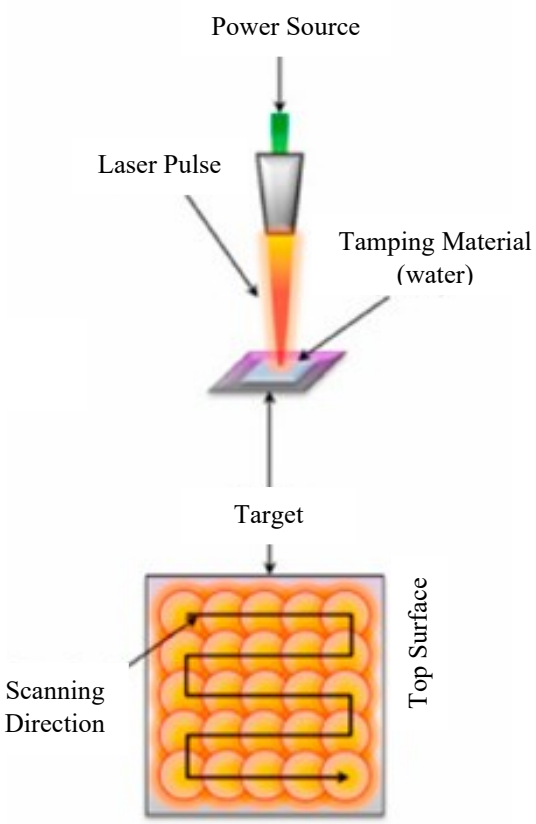

Figure 2—8: Diagram of the laser shock peening process [38].

Laser shock peening is able to generate a compressive residual stress layer with a depth of approximately 0.5 to 2 mm, deeper than that generated by conventional shot peening [14, 35]. Due to the deeper compressive residual stress layer, surfaces treated with laser shot peening exhibit better fatigue strength than surfaces treated with shot peening. Additionally, laser shot peening results in less surface roughness than shot peening [14]. However, laser shock peening has a risk of melting the surface of a material, as the temperature at the heating point may reach upwards of 10, 000˚C, making this treatment unsuitable for alloys with low melting temperature [30, 35, 39, 40]. Furthermore, laser shot peening results in lower values of compressive residual stress and inhomogeneous work hardening in comparison to shot peening [14].

2.4.3 Cavitation Peening

Cavitation is another shotless peening method, where plastic deformation is induced by pressure waves and microflows from collapsing bubbles and cavitation clouds [35]. In this process, the workpiece is immersed in water in a container. Since fluid temperature has an effect on the dynamics of cavitation bubbles, a temperature control must be used. A high-pressure water jet containing fine microscopic cavitation bubbles is injected into the water, aimed at the workpiece surface [26]. Turbulent flow in the surrounding water is generated, producing a continuous stream of cavitation bubbles. The cavitation method is illustrated in Figure 2–11. Due to the surrounding pressure, the cavitation bubbles rapidly shrink and eventually collapse, resulting in micro jets and shock waves [24, 26]. This creates impact loads on the material surface that plastically deform the material, inducing compressive residual stresses and increasing the surface hardness [24, 25].

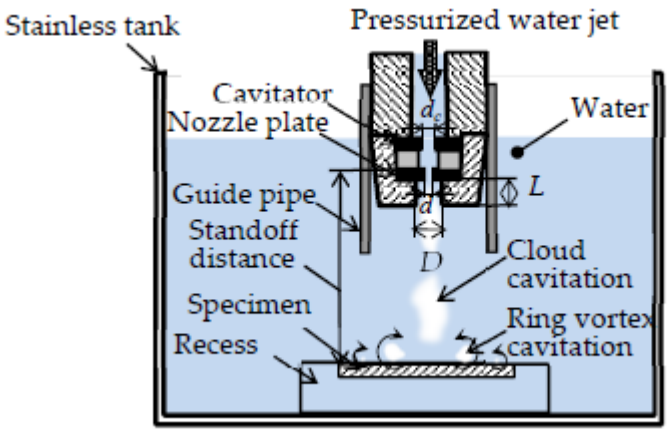

Figure 2—9: Diagram of the cavitation peening process [41].

As this method lacks a shot peening medium, there is no risk of contamination of the material surface by material transfer [35, 41]. Unlike laser shot peening, cavitation peening poses no risk of harmful thermal effects such as the presence of a heat affected zone due to the lack of a heat source [37]. It is capable of treating workpiece with complex geometries and is considered to be environmentally friendly, as it does not pollute the water and involves reduced dust and hazardous gases [24, 45]. In addition to

this, the method is relatively inexpensive and may be completed in one step for a variety of materials [24, 29].

2.4.4 Water Jet Peening

Continuous water jets have been extensively used in industrial applications such as cutting, cleaning, and the removal of surface layers [28, 42, 44]. Only recently have they been applied as a surface modification method to improve surface properties, originally as a method of improving the fatigue life of steels in 1984 [42-44].

Similar to cavitation peening, water jet peening utilises water jets to induce plastic deformation and compressive residual stress. However, the two methods depend upon different mechanisms to achieve this effect. Cavitation peening relies upon the production and collapse of cavitation bubbles to generate shockwaves and microjets at the material surface, whereas water jet peening strictly relies upon the impact caused by water droplets continuously impinging upon the target material as seen in Figure 2–12 [35, 39, 44-46]. The high-pressure water jet produces a small amount of plastic deformation, resulting in a layer of compressed stress and work hardening of the material surface [25-27, 40, 45, 47]. Water jet peening has similar advantages to cavitation peening such as its suitability for treating workpieces with complex geometries. It also is considered environmentally friendly as it does not produce polluted water, has reduced dust, and does not involve hazardous gases [45]. Water jet peening is capable of achieving total coverage of the workpiece, without risk of contamination by material transfer or thermal effects [29, 30, 39, 40, 44-46]. This method can also be completed in one step for various materials and is inexpensive [29]. This process does not require the workpiece to be submerged underwater, removing some complexity of the apparatus. However, continuous water jet peening requires high pressures to attain suitable hardening of the material surface.

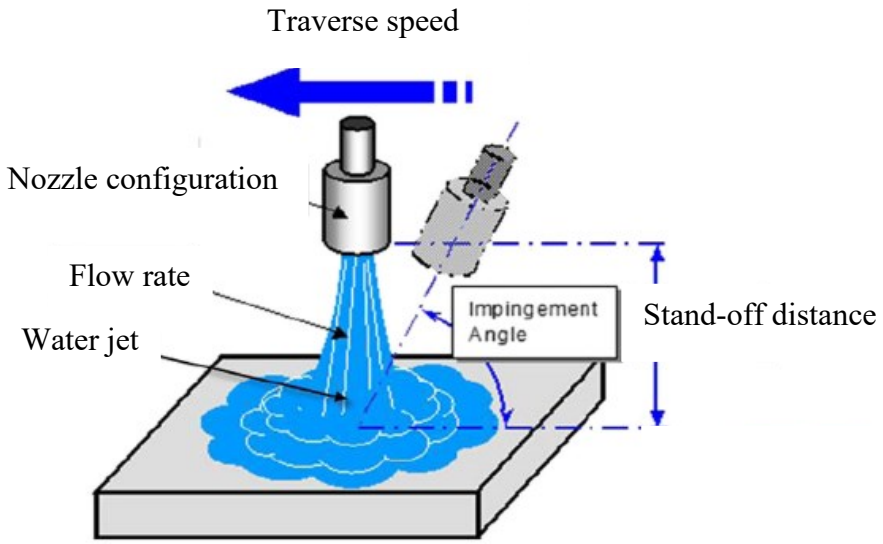

Figure 2—10: Diagram of continuous water jet peening [37].

Using pulsed water jets in place of continuous water jets has recently garnered attention as a possible improvement of water jet peening. The impact of a single droplet of water has a much greater effective impact pressure than the stagnation pressure produced by a continuous water jet [28, 29]. The continuous waterjet produces a maximum pressure at the material surface, called the stagnation pressure, which may calculated as [30]:

$$P_S = \frac{1}{2}\,\rho\, v_0^2 \qquad \text{(Equation 2–1)}$$

where ρ is the water density and v_0 represents the jet velocity.

Pulsed water jets have recently become a topic of interest as a possible improvement of the conventional water jet peening method. One approach for achieving a pulsed water jet is by ultrasonically modulating the continuous stream through the use of a sonotrode [28, 48]. The sonotrode oscillates in the acoustic chamber to create pressure fluctuations, which are amplified by a transmitting cone. A nozzle is attached to the transmitting cone, from which the water exits, and the pressure fluctuations are converted to velocity fluctuations [42, 48]. Portions of water with different velocities flow together

in the free stream, causing the water jet to separate into discrete water clusters [28, 48]. A schematic of this method and the separation of water clusters is displayed in Figure 2–13. The impact of various water clusters results in a greater impact pressure than the stagnation pressure of a continuous water jet [30, 42]. This is known as the water hammer effect, described by the following equation developed in 1933 [28, 30, 42, 48]:

$$P_i = \frac{v\rho_1 c_1 \rho_2 c_2}{\rho_1 c_1 + \rho_2 c_2} \qquad \text{(Equation 2–2)}$$

where v is the impact velocity of the liquid, and the densities and speed of sound in the liquid and solid are accounted for by ρ_1, ρ_2, c_1, and c_2, respectively. The material surface is periodically impacted by the water clusters, resulting in plastic deformation and subsequently inducing residual compressive stresses [29, 48].

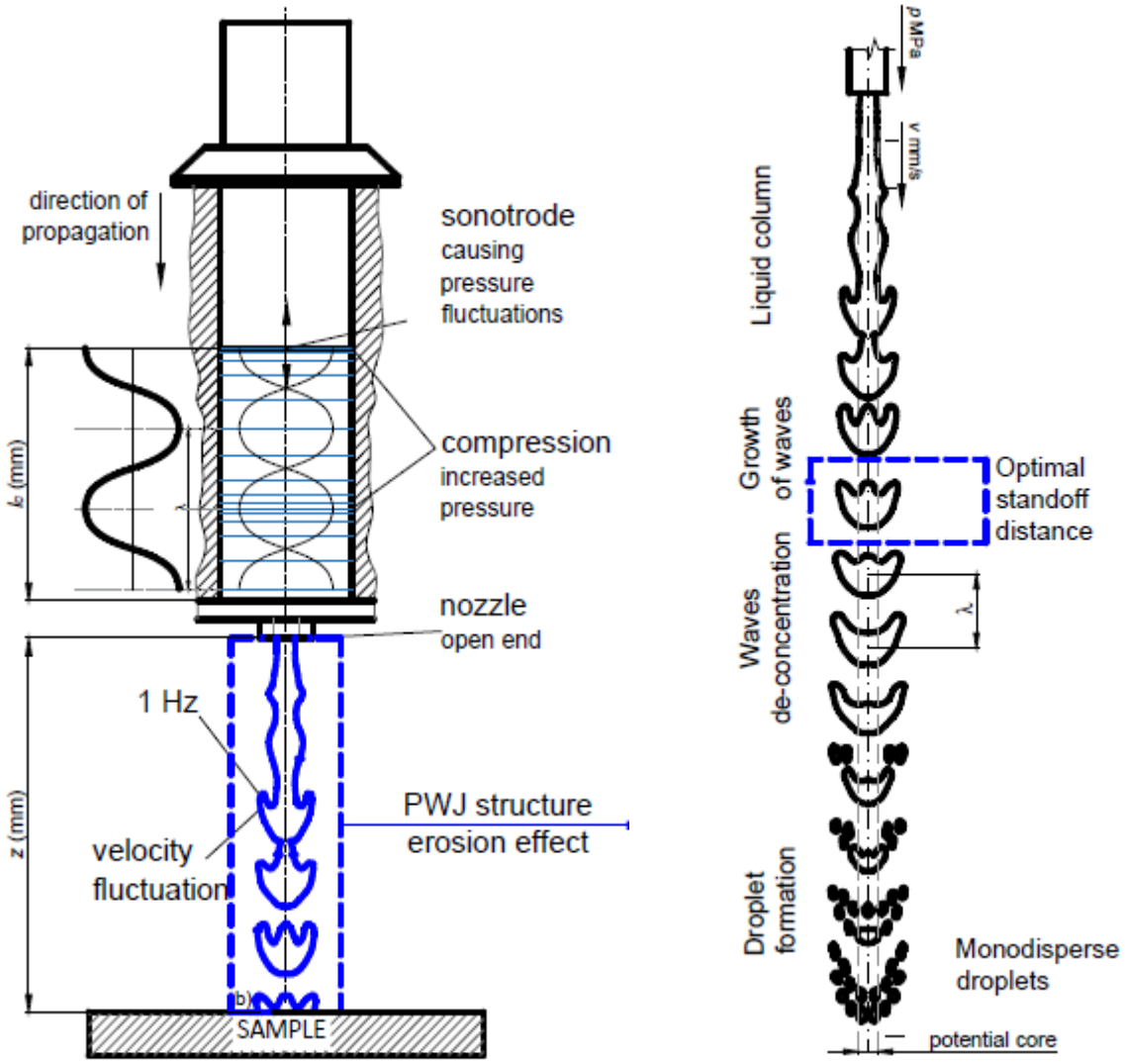

Figure 2—11: Diagram of ultrasonic water jet peening: left) the apparatus; right) separation of a continuous water flow into water clusters [42].

Ultrasonically forced modulation is the most simple and practical method of obtaining a pulsed water jet offers the ability to realise a wide range of water droplet velocities and volumes [28, 42]. Ultrasonic water jets are much more efficient than continuous water jets with identical hydraulic conditions [42]. Ultrasonic water jet peening requires lower operating pressures than continuous water jet peening, reducing the input cost of the process [27]. This method, like conventional water jet peening and cavitation peening, avoids possible contamination of the material surface due to the absence of a peening medium and produces a clean surface [27, 42]

2.5 Current Research

There has already been extensive research completed on the effects of water jet peening, as well as surface modification techniques of Ti-6Al-4V. Arola and McCain demonstrated the effect of pressure upon the surface topography of Ti-6Al-4V with abrasive water jet peening. They subjected samples of wrought Ti-6Al-4V to abrasive water jet peening with garnet abrasives at varying pressure up to 280 MPa. They found the surface morphology of the metal to be highly dependent upon the operating parameters. It was found that the highest water jet pressure resulted in the roughest material tested [49].

Arola et al. compared the effects of water jet and abrasive water jet peening processes on the surface topographies of wrought titanium alloys. The water jet pressure was varied up to 280 MPa and used on samples of commercially pure titanium and Ti-6Al-4V. It was found that water jet peening resulted in far less surface roughness than abrasive water jet peening. Water jet peening resulted in a maximum surface roughness increase of 1.5 μm [50].

Azhari et al. investigated the effects of water jet peening parameters on aluminium alloy 5005. From this research it was found that increasing the number of passes, pressure, and standoff distance increased the resulting surface roughness and hardness. The traverse rate was also varied from 500 to 1,500 mm/min. Lower traverse speeds produced rougher surfaces than higher traverse speeds. A lower traverse speed allowed for additional overlap of traverse paths and more time for water molecules to impinge the material surface, thus increasing surface roughness [40].

Barriuso et al. studied the roughening of biomaterials by water jet peening. Two traverse speeds of 0.05 and 0.1 m/min were tested on Ti-6Al-4V. At the lower traverse speed, the alloy was observed to feature significantly more pits, undercuts and large intrusions than the samples treated at the higher traverse speed. The higher traverse speed resulted in a lower surface roughness. However, little to no deformation or hardness gradient was found in the Ti-6Al-4V subsurface when the cross sections were examined [51].

Ganesh et al. observed the dry sliding wear behaviour of Ti-6Al-4V exposed to shot peening with a steel shot medium. Wear testing using a pin and rotating disc method demonstrated the presence of titanium oxide in the wear tracks in the as-received wrought Ti-6Al-4V. The peened samples showed a decrease in surface roughness in comparison to the as-received sample. The microhardness of the Ti-6Al-4V was improved, with a significant decrease in wear rate. The coefficient of friction was also reduced in the shot peened samples [5].

Islam et al. surface treated multiple Al-Si alloys with high pressure water jet technologies with increasing pressure and studied the effects on the alloys' tribological properties. The group studied dry reciprocating wear tests of the treated Al-Si alloys and found the water jet produced a hard compressed subsurface that improved the material's wear resistance [47].

Srivastava et al. varied the processing parameters of ultrasonic water jet peening on stainless steel samples. The traverse speed was varied from 5 mm/s to 25 mm/s. At higher traverse speeds, there was a decrease in the amount of residual stress imparted to the material. This was found to be a result of increased exposure time at lower traverse rates, leading to more water droplet impingements and increased plastic deformation with deeper penetration. This was confirmed by a decrease in surface roughness with increasing traverse speed. [29]

2.5.2 Research Gaps

There has been considerable research surrounding the use of surface modification techniques to enhance the surface performance of various engineering alloys. However, the majority of this research has been focused on conventional methods, particularly shot peening. Although water jet peening has been extensively studied, the effects of ultrasonic water jet peening appear to be relatively unknown. As a recently developed technology, very little research has been completed on the influence of varying the processing parameters of ultrasonic water jet peening.

Furthermore, there is also a relatively limited amount of early work regarding the wear rates and surface improvements of titanium alloys [1]. In comparison to other

engineering alloys such as stainless steels or aluminium alloys, the use of titanium alloys in industrial applications is relatively new. Their poor tribological properties has limited their use, yet little research has been aimed at improving surface performance and wear behaviour.

The main driving industries for the improvement of titanium alloys comes from the aerospace and biomedical sectors. In aerospace applications, titanium alloys are valued for their high strength-weight ratio and good toughness [1]. In the biomedical fields, titanium alloys have become a choice material for hip and knee implants, where high corrosion resistance and biocompatibility are vital. Titanium and its alloys have been found to be highly biocompatible but demonstrate poor wear resistance in load-bearing implants [5, 6, 10, 21, 22]. Wear debris resulting from poor tribological properties are of concern as they may have severe health consequences for the patient, as well as result in required surgical revision [5, 6]. Hence, significant research is required to study possible enhancement of wear resistance in titanium alloys by surface treatments.

The following chapter details the process by which this study examined the influence of varying traverse speed of UPWJ peening upon the surface properties and wear behaviour of wrought Ti-6Al-4V.

Chapter 3: Experimental Procedure

3.1 Raw Materials

Alloy plates of commercial Grade 5 Ti-6Al-4V were obtained from McMaster-Carr for this study. The alloy plates, initially with dimensions 600 × 80 × 6.35 mm, were cut down to smaller samples with dimensions of 80 × 20 × 6.35 mm. The samples were afterwards lightly machined on the surfaces to guarantee flat and level surfaces for the peening process. The chemical composition of the wrought plates according to the Grade 5 specifications is show in Table 3–1.

Table 3—1: Chemical composition of Ti-6Al-4V according to Grade 5 ASTM standard specifications.

Alloy	Al	V	Fe	Ga	Cr	S	Si	Ti
Ti-6Al-4V	5.5-6.75	3.5-4.5	≤ 0.4	≤ 0.1	≤ 0.1	≤ 0.1	≤ 0.1	–

3.2 Water Jet Peening

The samples were not annealed prior to peening, such that any residual stresses from the machining processes would remain. Since annealing may not be used in a manufacturing scenario, the samples were peened in their ‘as-machined’ state to effectively mimic the use of water jet peening in an industrial setting.

The samples underwent UPWJ peening at VLN Advanced Technologies, Inc. (Ottawa, Ontario, Canada). The water jet system relies on a 125 HP NLB pump capable of applying a pressure of 107 MPa pressure at a flow rate of 6.31×10^{-4} m^3/s, and ultrasonic energy output to create forced water jet pulses. The jet pressure and stand-off distance were held at a consistent value for all tests. A back-and-forth peening pattern was employed in all tests to ensure full coverage of the sample surface, and to encourage uniformity while minimizing macroscopic surface changes. The scan strategy ran along the length of the target sample with an overlap of 0.1 mm. The nozzle also remained constant, with a circular shape and diameter of 1.4 mm for all tests, positioned

perpendicular (i.e., 90˚) to the target surface. Only the traverse rate speed was varied, from 200 to 1000 mm/s with increments of 100 mm/s. Table 3–2 displays the parametric peening conditions used for the entirety of the study, which were developed based on consultation with VLN Advanced Technologies, Inc. These are the optimal parameters found by VLN Advanced Technologies, Inc., to be feasible for peening of wrought Ti-6Al-4V. The traverse speeds tested are presented in Table 3–3 and the back-and-forth scan strategy is illustrated in Figure 3–1.

Table 3—2: Maintained UPWJ parameters.

UPWJ Parameter	Value
Water jet pressure (MPa)	69
Frequency (kHz)	20
Stand-off distance (mm)	25.4
Overlapping (mm)	0.1
Nozzle diameter (mm)	1.01
Nozzle orientation	Perpendicular (90°)
Scan strategy	Back-and-forth

Table 3—3: Traverse speeds tested in the present study.

Run	Traverse rate (mm/s)
1	1000
2	900
3	800
4	700
5	600
6	500
7	400
8	300
9	200

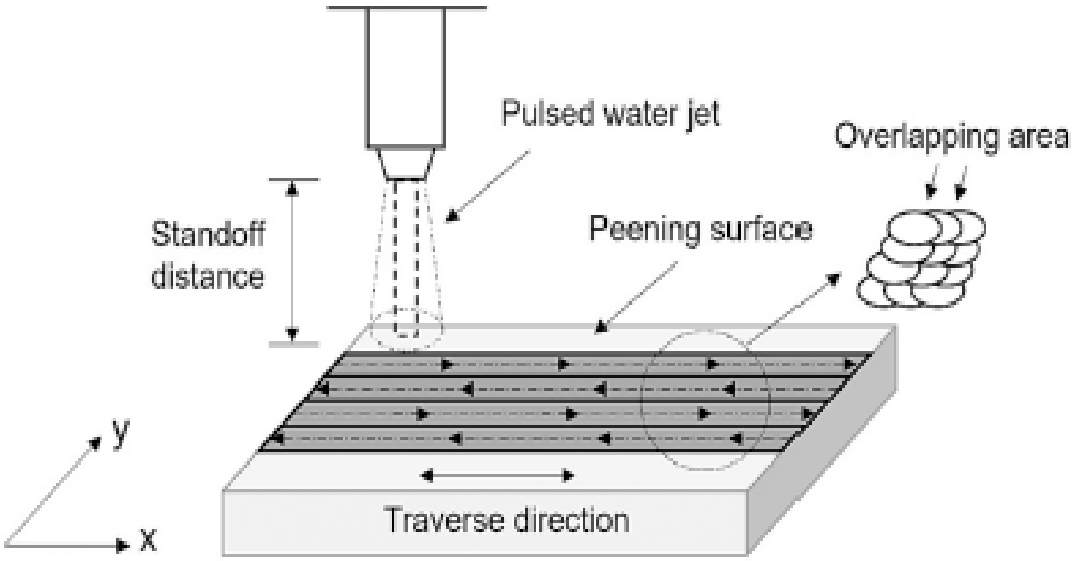

Figure 3—1: Schematic of the peening pattern used in the present study [30].

3.4 Material Characterisation

Crystalline phase analysis of the unpeened wrought Ti-6Al-4V was performed using X-ray diffraction (XRD; model AXS D8 Advance, Bruker Corp., Billerica, MA, USA) with a Cu-Kα radiation source and wavelength of 1.5406 Å. The test proceeded with a 2θ range of 5–120 degrees, with a scan step of 0.05 and counting time of 1 s for each step. The applied X-ray tube voltage was 40 kV with a current of 40 mA. The relative intensity, $R_{(x)}$, of each peak was calculated with the following:

$$R_{(x)} = \left(\frac{I_{(x)}}{I_{max}}\right) \times 100\% \qquad \text{(Equation 3–1)}$$

where $I_{(x)}$ is the intensity of reflection corresponding to the chosen peak, and I_{max} is the maximum peak intensity found in the data.

Surface characterisation of the peened and unpeened samples was completed with confocal laser scanning microscopy (CLSM; model VK-X1100, Keyence Corp., Osaka, Japan), which utilizes high-resolution optical imaging alongside laser-based 3D topographic imaging and metrology capabilities and can achieve nanometre-level height

resolution. To rid the surfaces of potential contamination, they were first cleaned with acetone and then dried with compressed air. Three areal measurements of 1000 μm^2 for each traverse rate were examined by CLSM using a 20-x magnification objective lens with a theoretical resolution of 535.7 nm. The arithmetic mean height (R_a) and the maximum height (R_z) of each peening test were recorded as per the requirements of the ISO 4288 standard. The mean and standard deviations were calculated for each measurement collected from each sample.

3.5 Single-Pass Scratch

Single-pass scratch tests were performed on each of the samples using a Universal Micro Tribometer (UMT-1; CETR, Campbell, CA, USA). These tests consist of sliding an indenter across the surface of a sample for a known scratch length and traverse velocity, under a known applied testing load. During the tests, the UMT-1 software records the dynamic numerical values for the indenter tip depth as well as the applied force over the course of the test run. It may also measure the dynamic coefficient of friction over the course of a single scratch test.

Although samples are usually polished for such tests to ensure a flat and even surface, these samples were left unpolished. The reason for this is that polishing of the samples may result in removal of any significant surface properties resulting from UPWJ. Moreover, testing these samples unpolished allows for better understanding of their possible behaviour in an industrial environment, where surfaces are highly unlikely to be polished prior to application. Hence, the samples were tested in either their wrought plus machined (i.e., unpeened) or peened states. Prior to each test, the sample surfaces were cleaned with acetone, and then dried with compressed air to ensure removal of possible surface contaminants, and the indenter was also cleaned with acetone to remove possible material transfer or debris. Five ‘single-pass’ scratches, 5 mm in length, were conducted on each of the samples with a Rockwell diamond indenter possessing a 200 μm tip radius. A constant nominal load of 4 kg force (39.2 N) was applied during the tests with a constant traversing velocity of 0.166 mm/s. A consistent test environment of room temperature (~23˚C) and relative humidity of 40-50% was maintained throughout testing.

The resulting scratches were subsequently analysed with the CLSM and the associated Keyence *Multifile Analyzer* software to assess the damage and make multiple measurements of the track width along the length of the scratch. The scratches were also assessed with scanning electron microscopy (SEM; model S-4700, Hitachi High Technologies, Inc., Tokyo, Japan) to obtain comparative results to those generated through use of the CLSM. This process utilised an electron accelerating voltage of 10kV, with an emission current of 15 nA. Multiple scratch widths for each track were manually measured from the SEM images and scaled to the appropriate size. For each data set of CLSM and SEM scratch widths, the scratch hardness was calculated according to the following relationship [52]:

$$HS_p = \frac{8P}{\pi W^2} \qquad \text{(Equation 3–2)}$$

where HS_p is the scratch hardness, P is the applied test load, and W is the scratch width. Once the scratch hardness had been obtained from each single-pass scratch of a sample, the sample's mean scratch hardness and standard deviation was calculated.

During the course of each single-pass test, the dynamic coefficient of friction was recorded by the UMT-1 software relative to the test time; the time and dynamic coefficient of friction data was collected in a text format, which was converted to graphs of dynamic coefficient of friction as a function of the test period for each single-pass scratch. Five graphs were obtained for each sample, although for ease of viewing three trendlines are presented in one graph.

Initial examination of scratches made on samples peened at traverse rates of 200, 300, and 400 mm/s indicated unreliable results. The scratches are not continuous and are inconsistent, making any measurement of the scratch widths (either manually or using the

CLSM) extremely difficult and unreliable. SEM images of these tracks can be seen in Figures 3–2, 3–3, and 3–4.

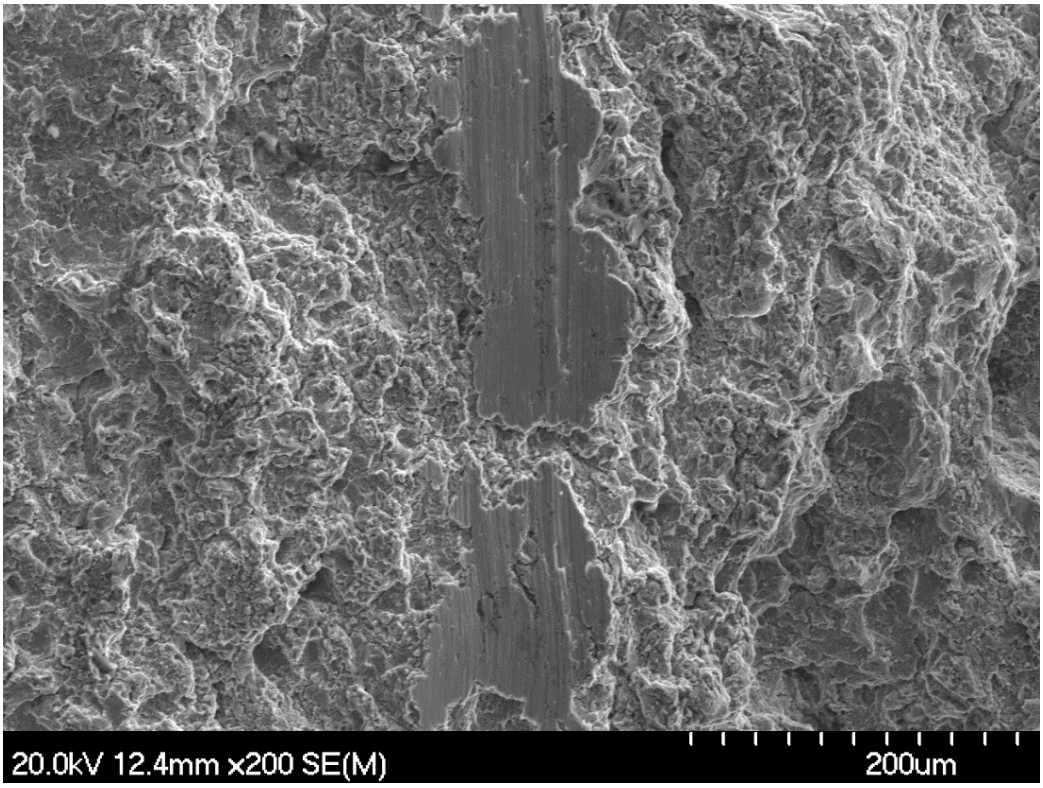

Figure 3—2: A single-pass scratch on Ti-6Al-4V peened at 200 mm/s.

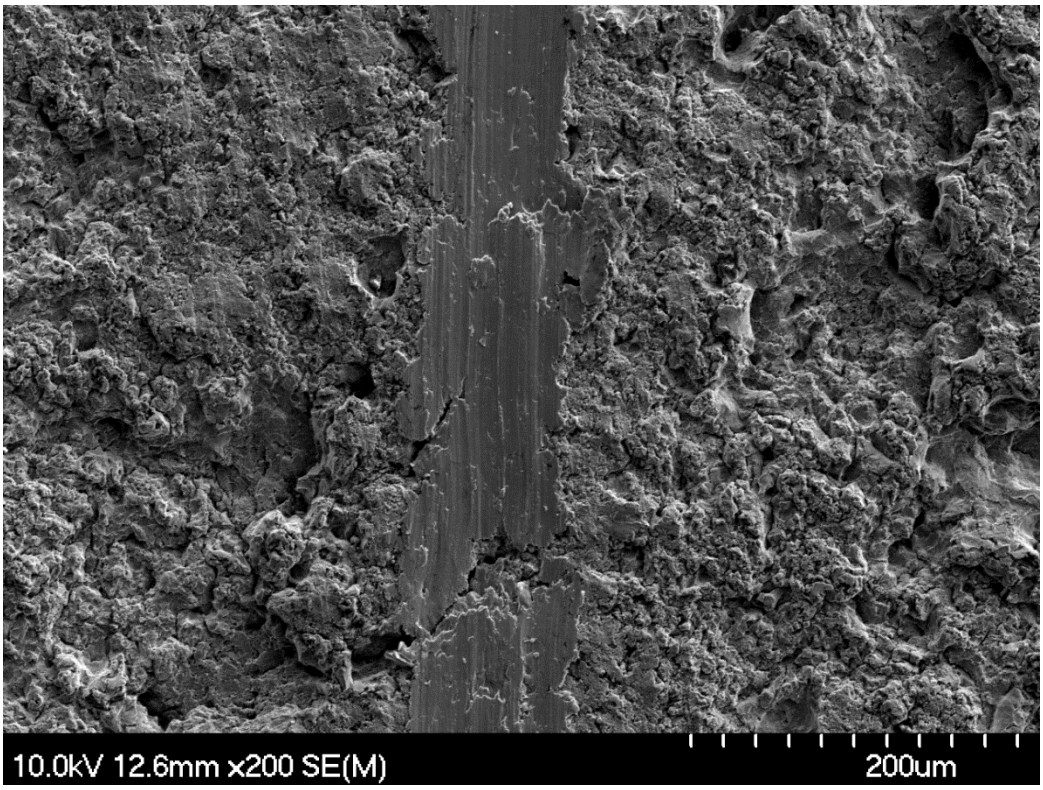

Figure 3—3: A single-pass scratch on Ti-6Al-4V peened at 300 mm/s.

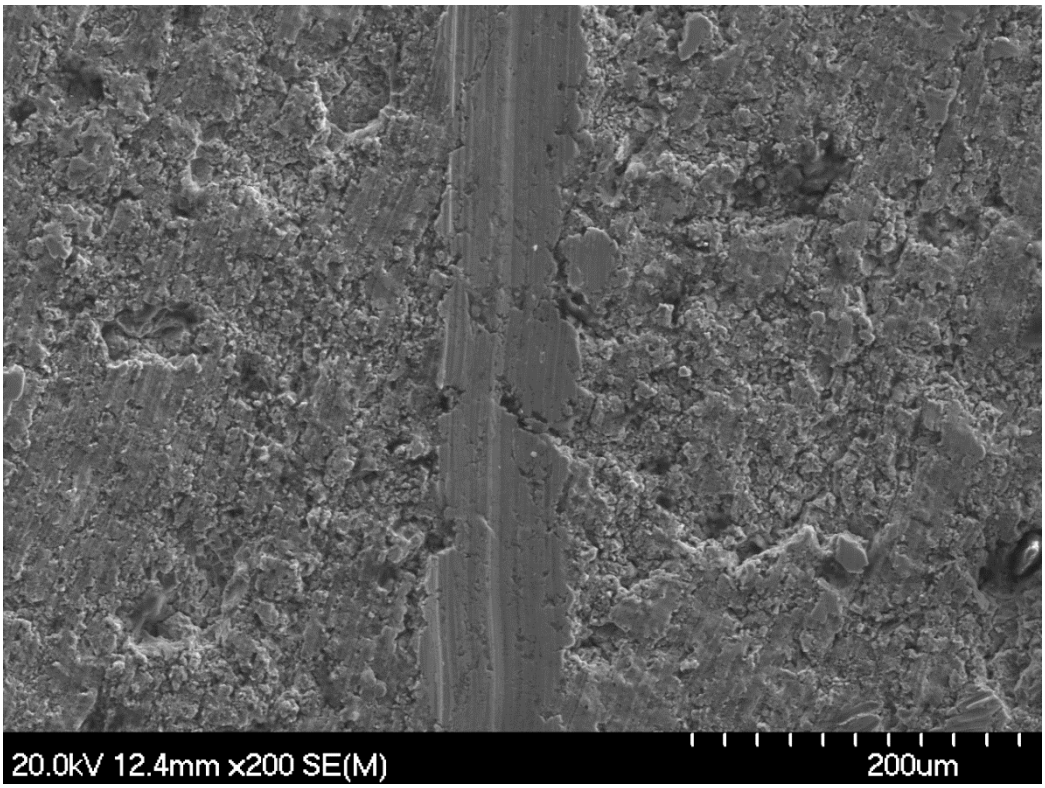

Figure 3—4: A single-pass scratch on Ti-6Al-4V peened at 400 mm/s.

From these examinations, it was deduced that traverse speeds of 200, 300, and 400 mm/s were unsuitable for further testing due to their acute surface roughness. The nature of the surfaces of these samples may cause machinery damage in testing, and any data gathered would be highly unreliable and likely inaccurate. For these reasons, the samples peened at 200, 300, and 400 mm/s were no longer included in the experimental procedure.

3.6 Dry Reciprocating Wear

Each of the samples were subjected to a series of reciprocating wear tests using the UMT-1 system. These tests involve sliding an indenter across the surface of a sample repeatedly for a known track length, with known frequency, period of time, and applied testing load. As with the scratch testing, these samples were tested unpolished to avoid removal of possible surface effects of UPWJ and to closer mimic their possible wear behaviour in a manufacturing scenario. Each sample was subjected to seven wear tests of varied applied nominal load. The load variations of each test performed on the peened samples can be seen below in Table 3–4, where each checkmark represents one test run.

Table 3—4: Reciprocating wear tests: Load variations and number of tests with each load.

Traverse Speed (mm/s)	Applied Load		
	1N	2N	5N
0	✓	✓ ✓ ✓	✓ ✓ ✓
500	✓	✓ ✓ ✓	✓ ✓ ✓
600	✓	✓ ✓ ✓	✓ ✓ ✓
700	✓	✓ ✓ ✓	✓ ✓ ✓
800	✓	✓ ✓ ✓	✓ ✓ ✓
900	✓	✓ ✓ ✓	✓ ✓ ✓
1000	✓	✓ ✓ ✓	✓ ✓ ✓

The wear tracks are 5 mm in length, using 3.175 mm diameter spherical nonporous alumina ceramic balls (McMaster-Carr) as the indenter material. The tests were each conducted at a frequency of 10 Hz for an hour. The testing environment was maintained consistently at room temperature (~23 ± 2˚C), with a relative humidity of 40-50%. The volume loss of each wear track was obtained with the CLSM Keyence *Multifile Analyzer* software, using a 5 x magnification objective lens. The volume measurements of the wear tracks were used to calculate the samples' mean specific wear rate, w_s (mm^3/Nm), according to the following relationship:

$$w_s = \frac{V}{P(vtd)} \qquad \text{(Equation 3–3)}$$

where V is the volume loss in mm^3, P is the applied load in N, v is the frequency in Hz, t is the test duration in seconds and d is the wear track length in meters. From the gathered data, the mean specific wear rate of each sample and the corresponding standard deviation was calculated.

The wear tracks were further assessed for tribological damage with SEM, using an electron accelerating voltage of 10kV and an emission current of 15 nA. Energy dispersive spectrometry (EDS) was employed alongside the SEM, as an X-ray characterization technique to identify elemental concentrations. Titanium, vanadium, aluminium and oxygen were mapped by concentration around and within each of the assessed wear tracks.

Chapter 4: Results and Discussion

4.1 Material Characterisation

The diffraction pattern of the unpeened Ti-6Al-4V sample, obtained by XRD, is shown in Figure 4–1.

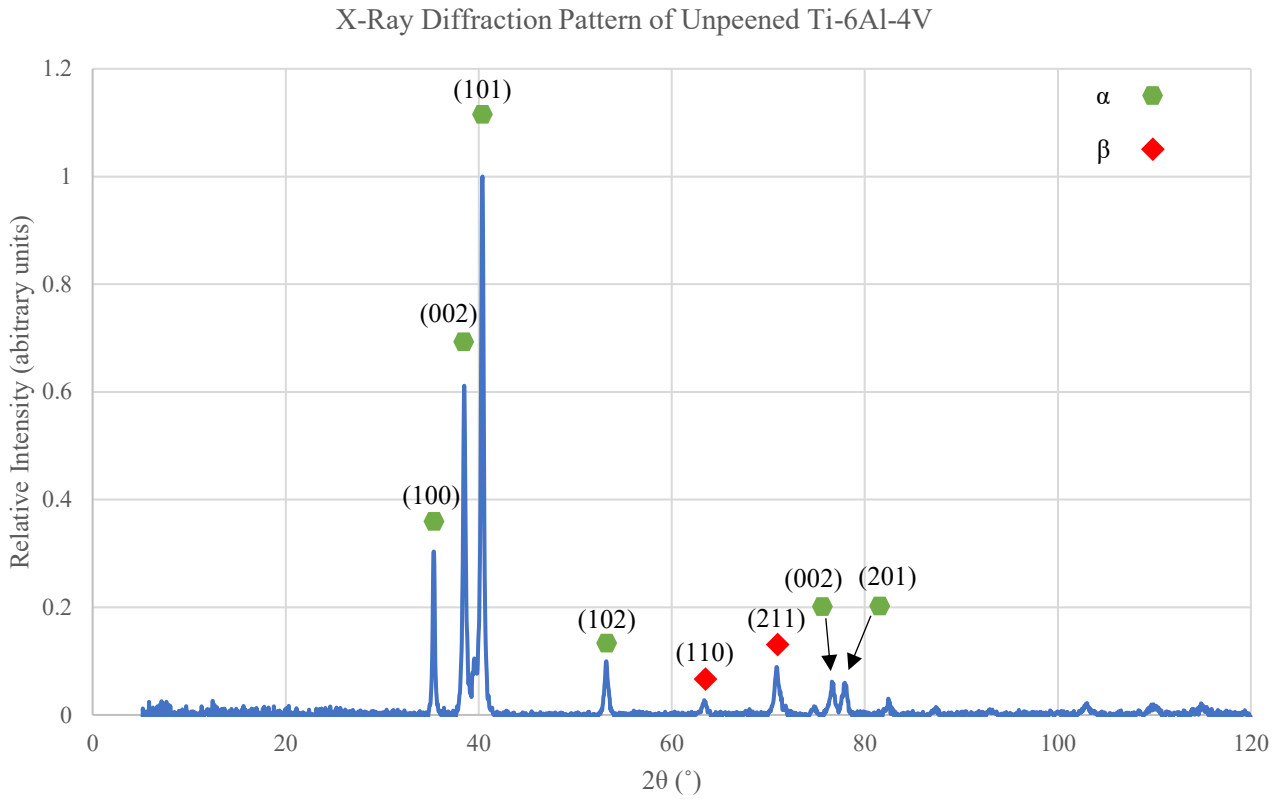

Figure 4—1: X-Ray diffraction pattern of unpeened wrought Ti-6Al-4V.

The XRD pattern obtained closely matched a Ti-6Al-4V PDF (PDF 04-002-8708) with a predominantly hexagonal crystal structure and small amount of body-centred cubic crystal structure. This is to be expected with Ti-6Al-4V alloys due to the vanadium content, which acts as a β-stabiliser by lowering the β-transus temperature. However, since the sample contains relatively limited amounts of β-stabilisers alloying elements, the peaks are predominantly of the hexagonal close-packed α phase. The highest peaks, in order of increasing intensity, occur at approximately 35˚, 38˚ and 40˚. These correspond to α patterns and planes of (100), (002), and (101), respectively. The XRD pattern overall

indicates a material with high strength due to the inclusion of the β body-centred cubic phase, but with poor tribological properties due to the high amount of hexagonal structure. This is similar to findings in other research and discussions of titanium crystal structures [1, 4, 7, 30]. However, prior work by Siah Pour et al., has shown that UPWJ peening has an effect upon the orientation of crystal planes and shifting of the diffraction pattern due to texture reorientation, as seen in Figure 4–2.

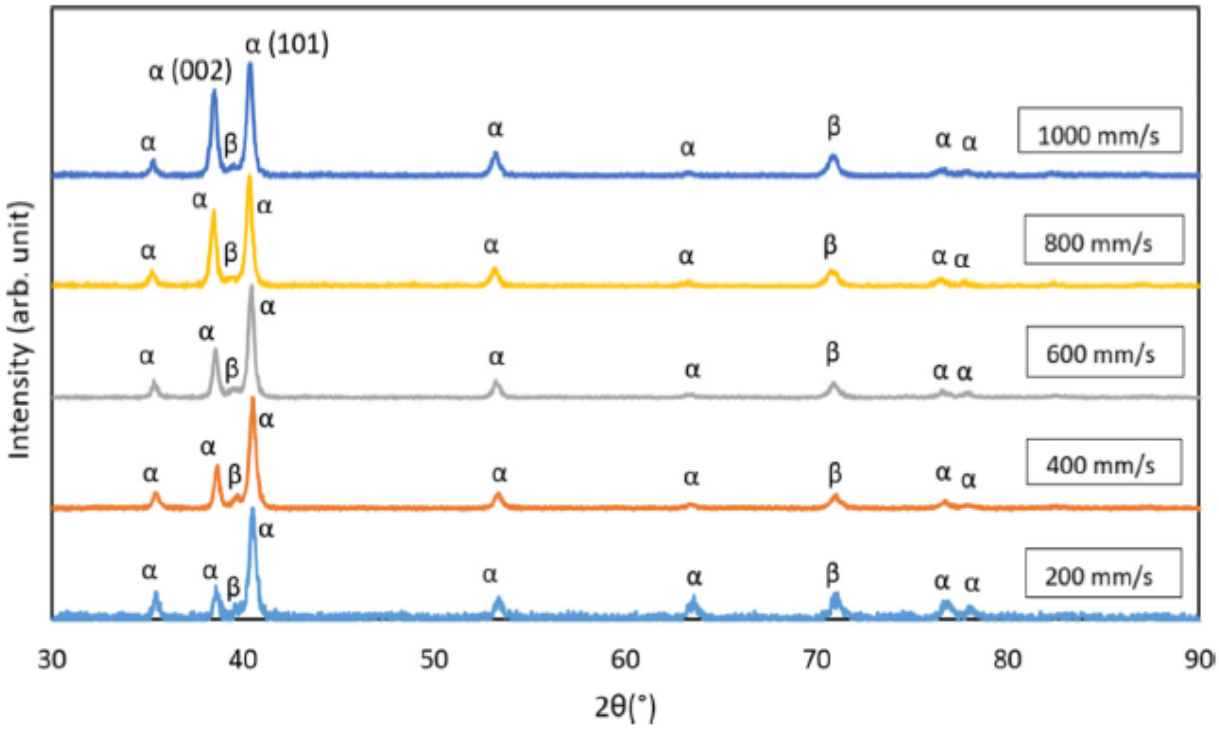

Figure 4—2: Shifting of Ti-6Al-4V diffraction pattern at various traverse speeds due to texture reorientation [30].

The unpeened and peened samples surfaces were analysed with CLSM to obtain the arithmetic mean height (R_a), and the maximum height (R_z) for each traverse speed. The mean of each measurement and its standard deviation were calculated for each sample and are presented in Table 4–1. These values were also plotted as a function of the sample's peening traverse speed, as shown in Figure 4–3 and Figure 4–4, where the unpeened sample is assigned a nominal traverse rate of 0 mm/s.

Table 4—1: Arithmetic mean height, R_a, and maximum height, R_z.

Material	Traverse Speed (mm/s)	R_a (µm)	R_z (µm)
Ti-6Al-4V	– (unpeened)	0.54 ± 0.06	7.2 ± 1.3
Ti-6Al-4V	200	22.8 ± 8.8	263.4 ± 167.1
Ti-6Al-4V	300	4.69 ± 0.07	58.3 ± 5.7
Ti-6Al-4V	400	1.87 ± 0.08	40.1 ± 7.5
Ti-6Al-4V	500	1.71 ± 0.14	34.1 ± 4.9
Ti-6Al-4V	600	1.28 ± 0.05	20.3 ± 2.0
Ti-6Al-4V	700	1.18 ± 0.09	15.7 ± 1.6
Ti-6Al-4V	800	1.16 ± 0.03	17.9 ± 1.9
Ti-6Al-4V	900	1.11 ± 0.07	16.2 ± 2.3
Ti-6Al-4V	1000	1.06 ± 0.03	14.1 ± 1.0

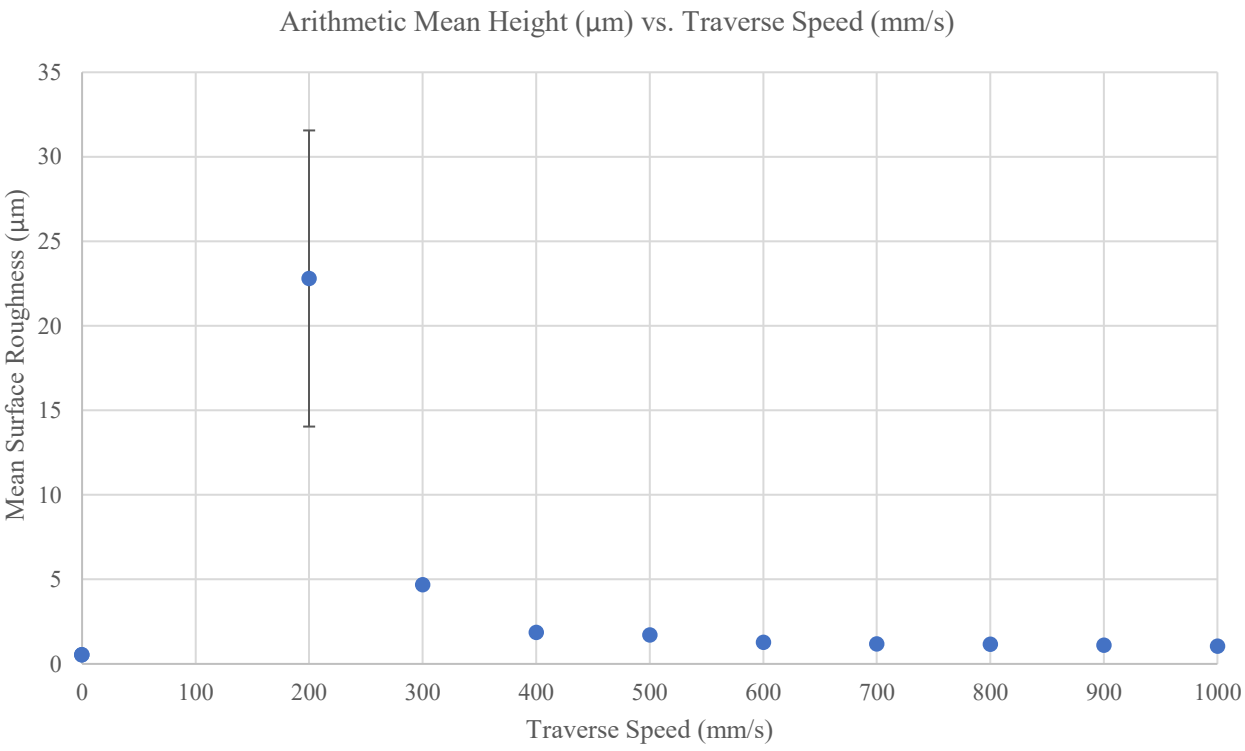

Figure 4—3: Arithmetic mean height relative to traverse speed.

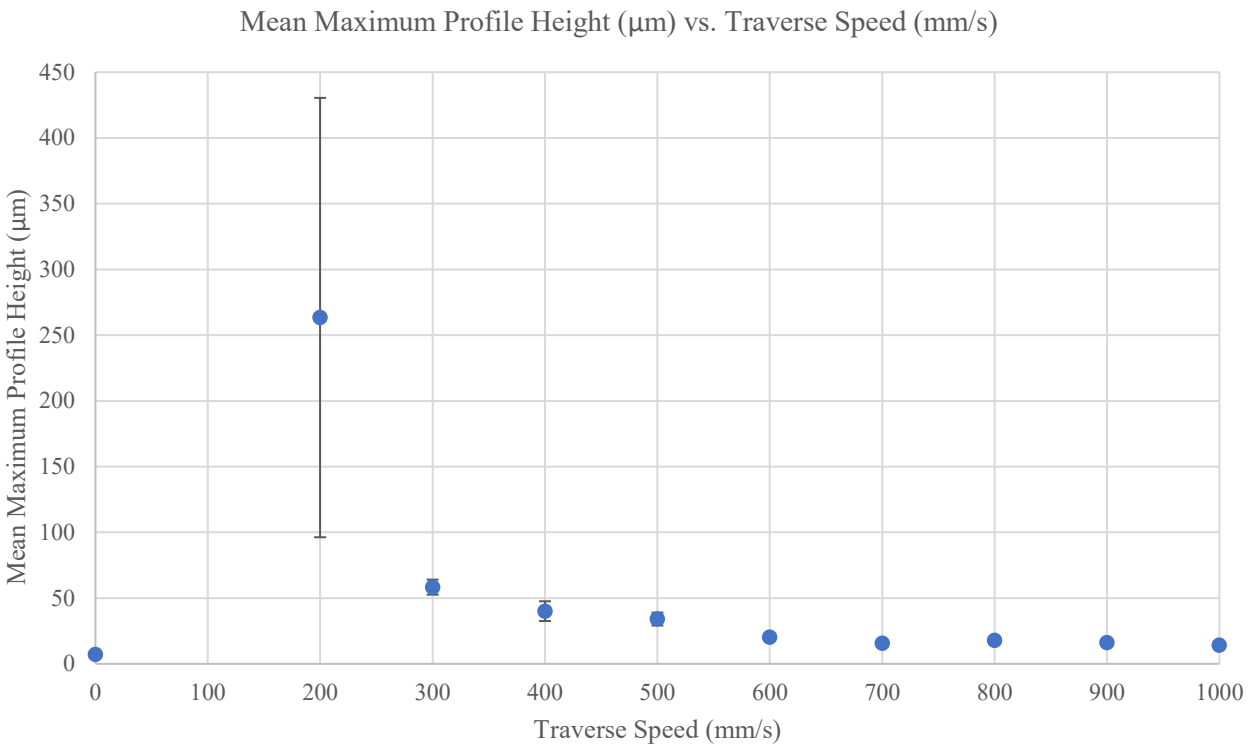

Figure 4—4: Mean maximum profile height relative to traverse speed.

From the data gathered it is evident that surface roughness of wrought material is increased by UPWJ and greatly affected by the process' traverse speed. At lower speeds, R_a is much greater than that of samples peened with high traverse rates. R_z is also shown to be much greater for lower traverse speeds. Relatively large standard deviations can also be seen at the lower traverse speeds, particularly for the sample peened at 200 mm/s, suggesting a highly varied surface morphology. Even at a traverse rate of 1000 mm/s, which produced the lowest surface roughness of the peened samples, the surface roughness was found to be almost double that of the unpeened material.

These findings are indicative of severe plastic deformation by UPWJ, especially at low traverse rates. At lower traverse rates, the pulsed water jet is allowed more time to release water clusters onto a surface region. The water clusters may repeatedly impinge a localised area, exposing the area to a severe, repetitive 'water hammer' effect. This results in severe localised plastic deformation of the material surface. Alternatively, at high traverse rates the peening process is allotted less time to impact a localised region. Water

clusters are more spread out over the material surface, such that there are fewer impingements. Hence the material experiences less of the water hammer effect and severe plastic deformation does not occur.

It appears that the surface roughness of the samples begins to plateau at a traverse rate of 700 mm/s. This suggests a limit to the effectiveness of varying the traverse rate in UPWJ. At a high enough traverse rate, the surface roughness of a peened sample will be close or equal to that of the unpeened sample as the water clusters are given minimal time to impact the surface. To achieve high surface deformation at these rates, other peening parameters such as the nozzle diameter or frequency may require adjustment to allow for increased water flow and thus impingements in a shorter period of time.

Similar results have been found by a handful of studies, where the traverse rate of conventional continuous water jet peening altered the surface morphology of materials [29, 40, 51]. In these studies, it was found that lowering the traverse rate increased the surface roughness, as the material is exposed to more water droplet impingements and resulting surface deformation to occur. However, it should be noted that the surface roughness of the samples may be affected by prior machining processes. Previous marks may contribute to a higher measured surface roughness after peening.

4.2 Scratch Hardness

Single-pass scratch tracks on the unpeened and peened samples were analysed by CLSM and SEM to obtain numerous scratch widths along the length of each track. As discussed previously, samples peened at 200, 300, and 400 mm/s were deemed unsuitable for further analysis due to their extreme surface roughness. CLSM images of the scratch tracks are shown in Figure 4–5 to Figure 4–11. SEM images of the scratch tracks are displayed in Figure 4–12 to Figure 4–18.

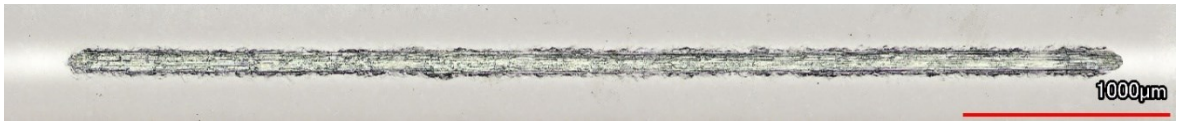

Figure 4—5: CLSM image of a single-pass scratch on unpeened Ti-6Al-4V.

Figure 4—6: CLSM image of a single-pass scratch on Ti-6Al-4V peened at 500 mm/s.

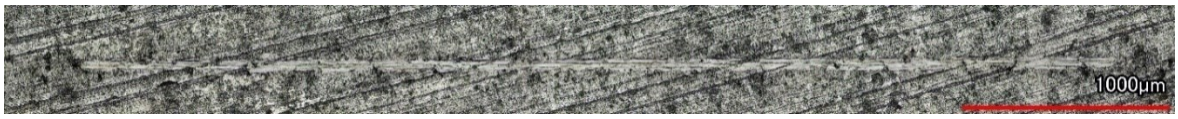

Figure 4—7: CLSM image of a single-pass scratch on Ti-6Al-4V peened at 600 mm/s.

Figure 4—8: CLSM image of a single-pass scratch on Ti-6Al-4V peened at 700 mm/s.

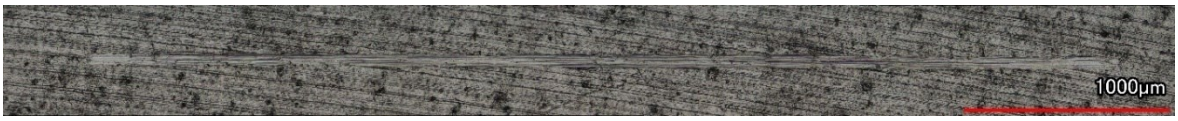

Figure 4—9: CLSM image of a single-pass scratch on Ti-6Al-4V peened at 800 mm/s.

Figure 4—10: CLSM image of a single-pass scratch on Ti-6Al-4V peened at 900 mm/s.

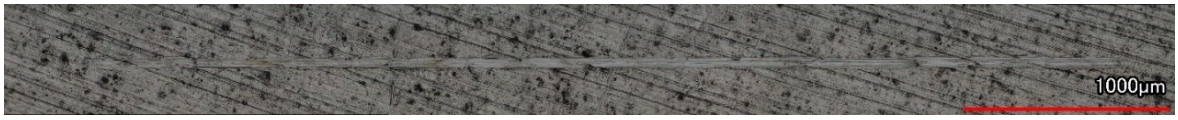

Figure 4—11: CLSM image of a single-pass scratch on Ti-6Al-4V peened at 1000 mm/s.

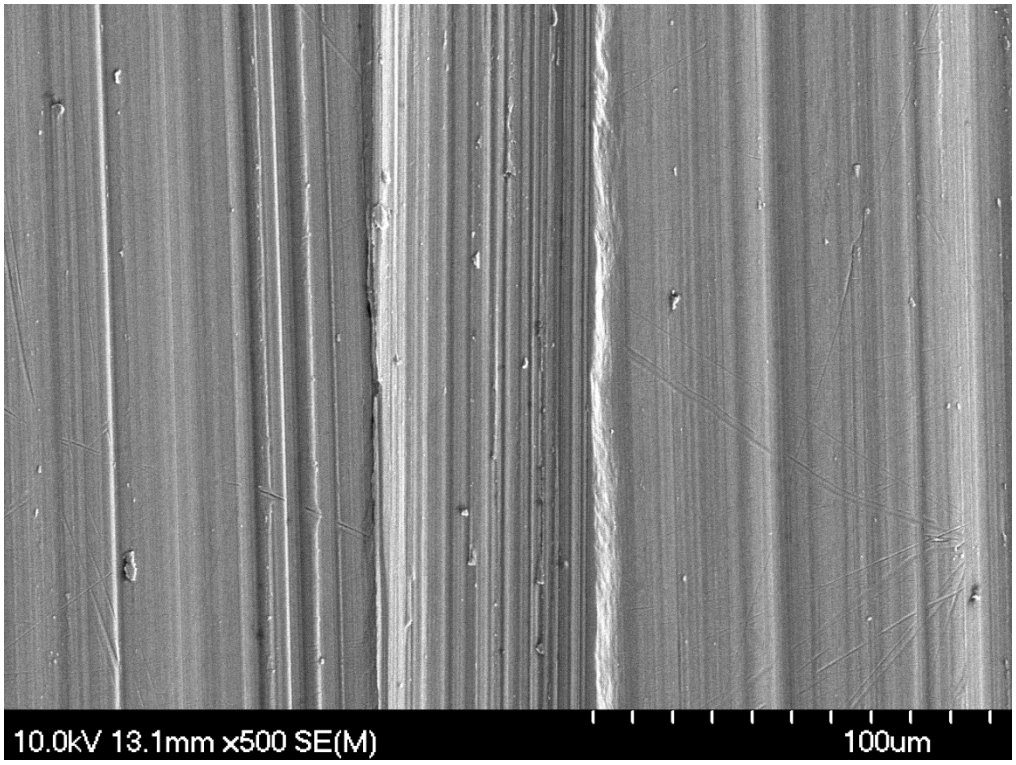

Figure 4—12: SEM image of a single-pass scratch on Ti-6Al-4V unpeened material.

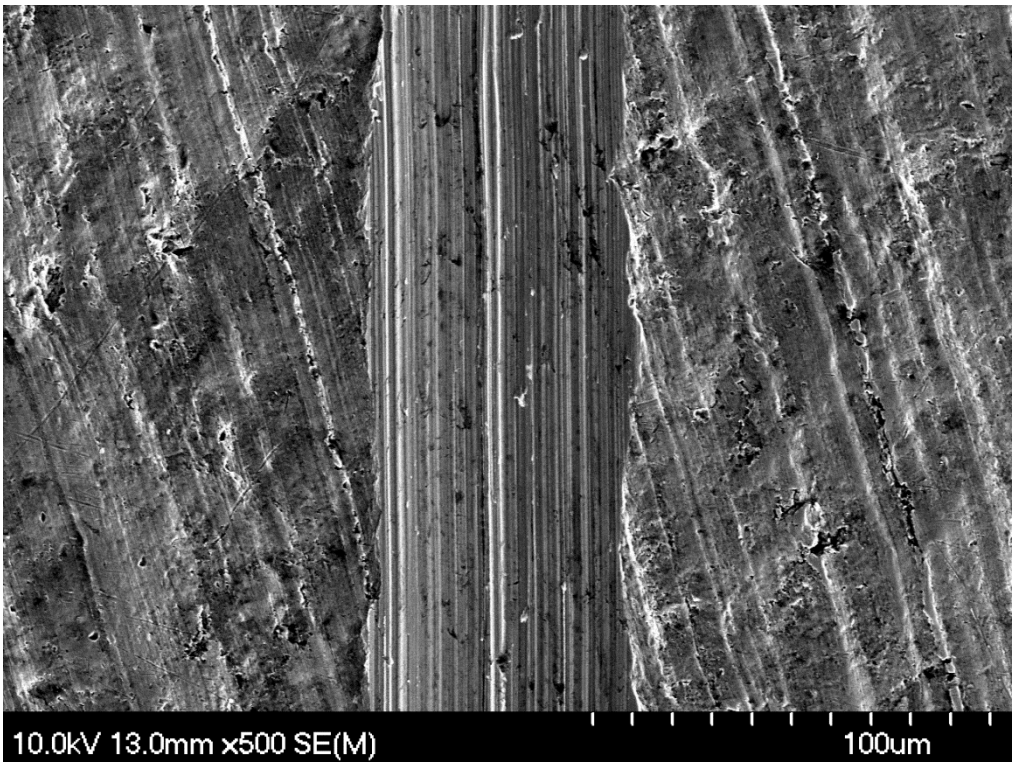

Figure 4—13: SEM image of a single-pass scratch on Ti-6Al-4V peened at 500 mm/s.

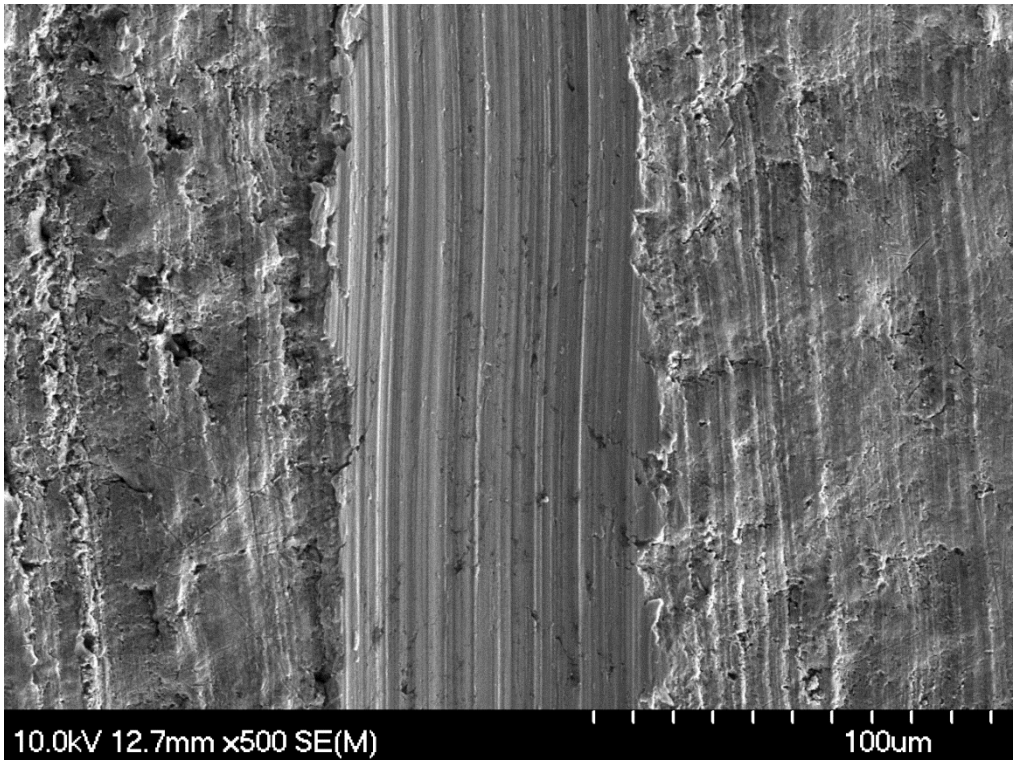

Figure 4—14: SEM image of a single-pass scratch on Ti-6Al-4V peened at 600 mm/s.

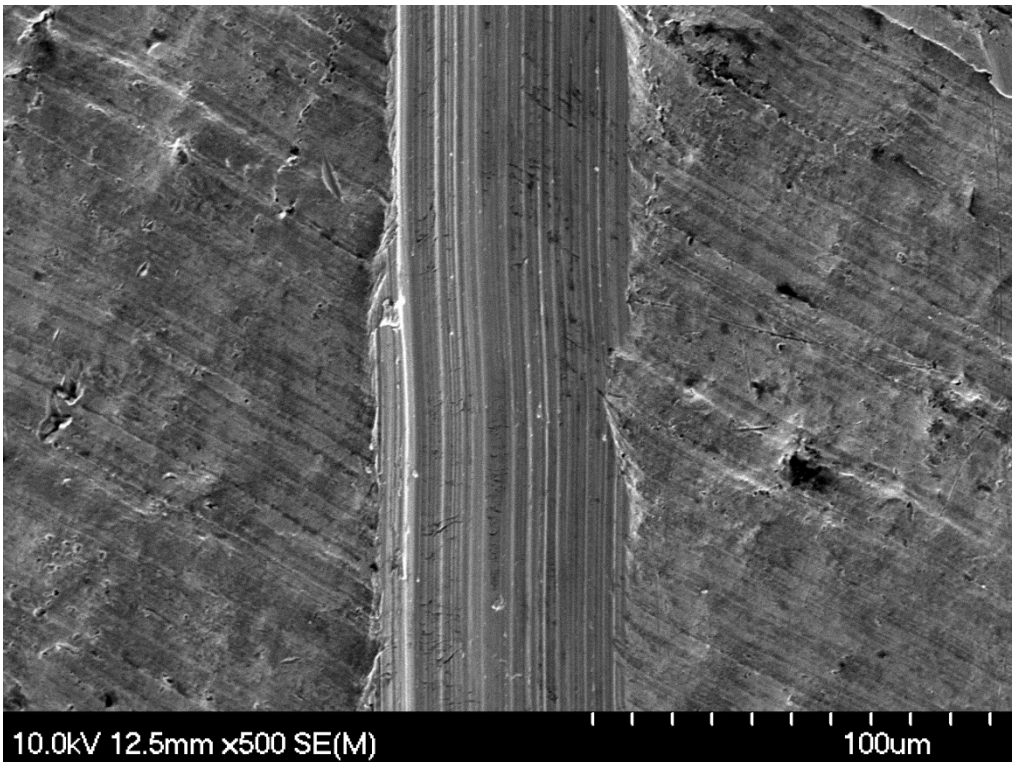

Figure 4—15: SEM image of a single-pass scratch on Ti-6Al-4V peened at 700 mm/s.

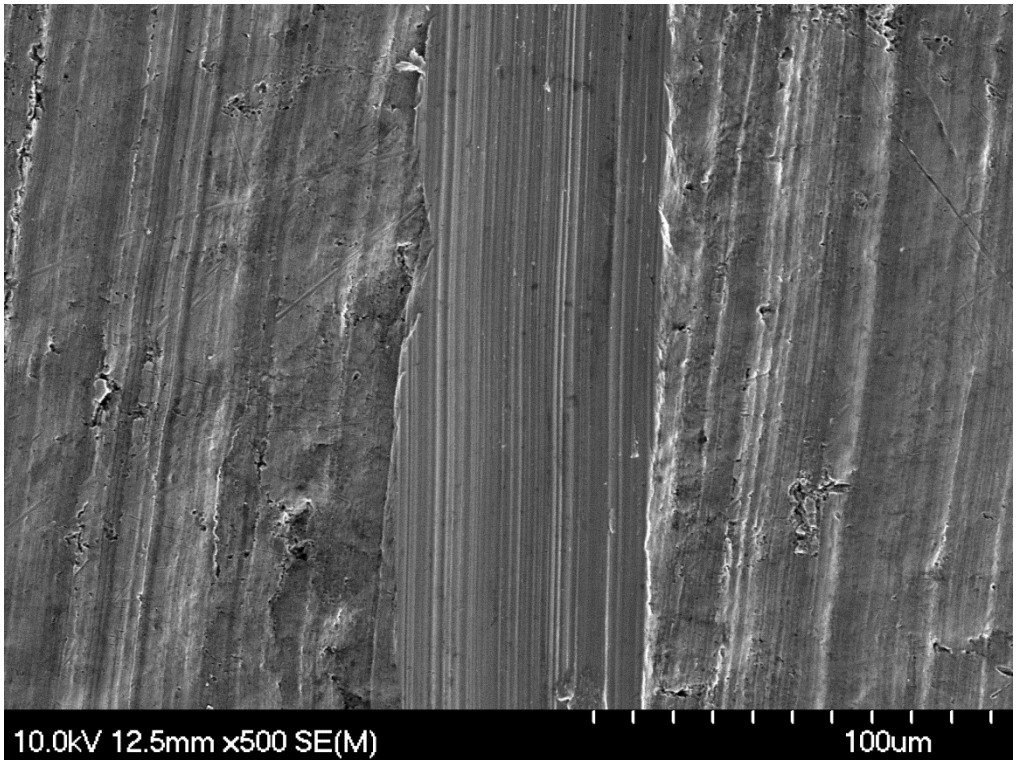

Figure 4—16: SEM image of a single-pass scratch on Ti-6Al-4V peened at 800 mm/s.

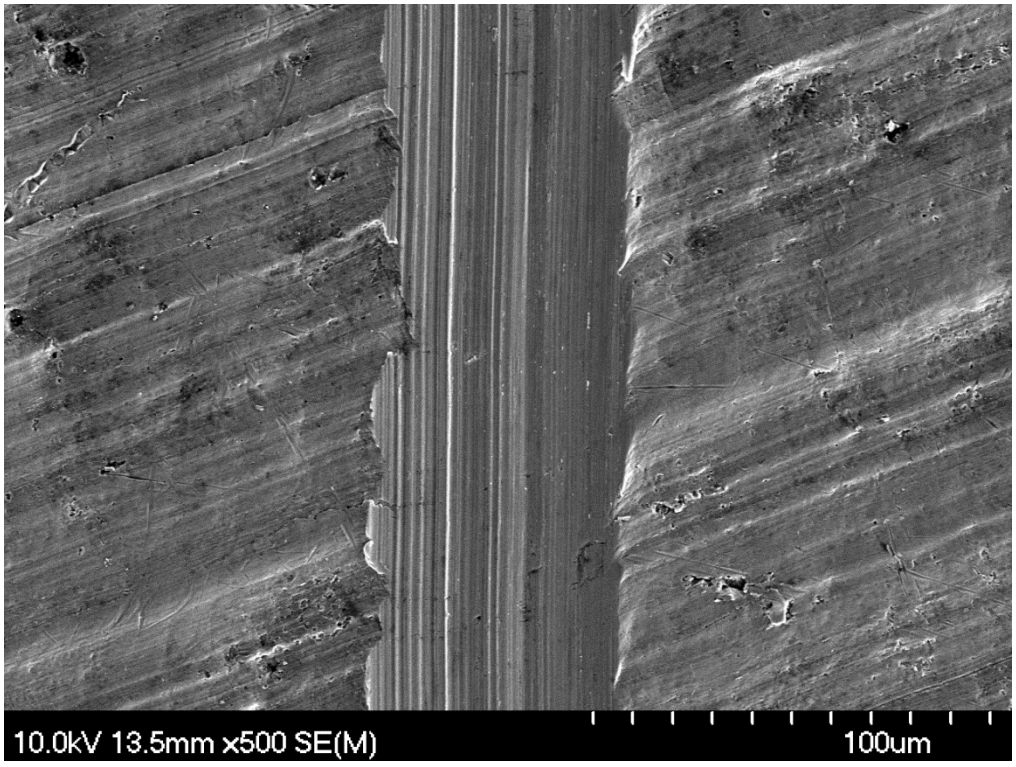

Figure 4—17: SEM image of a single-pass scratch on Ti-6Al-4V peened at 900 mm/s.

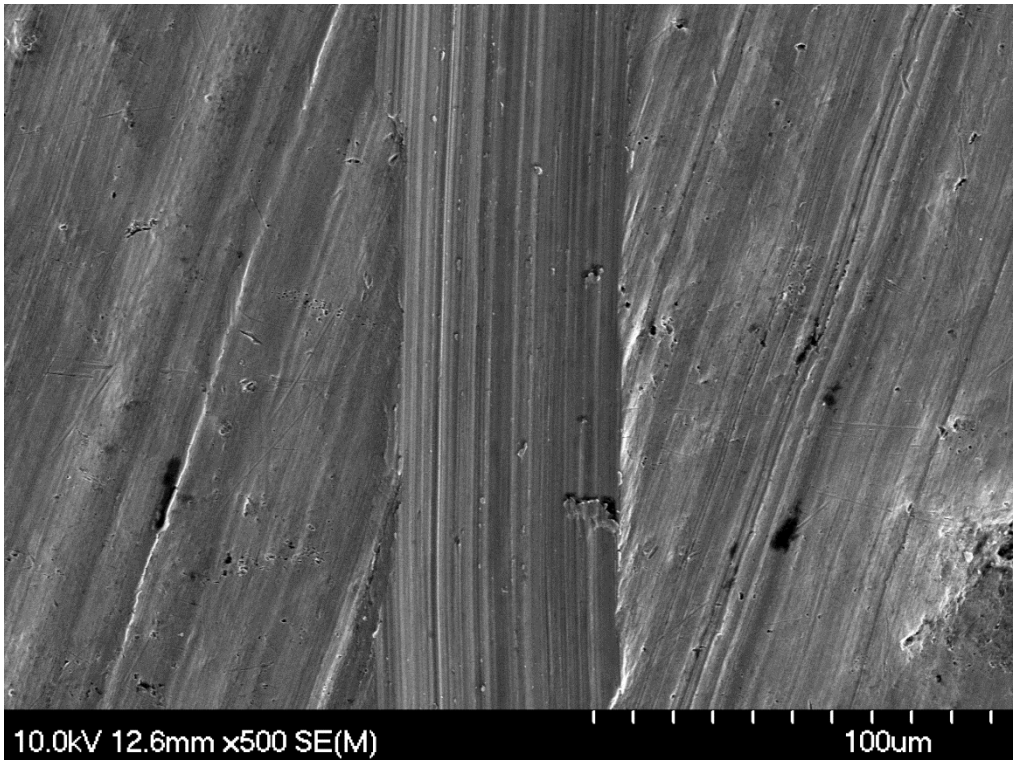

Figure 4—18: SEM image of a single-pass scratch on Ti-6Al-4V peened at 1000 mm/s.

From the gathered scratch widths measurements, either through software or manual measurement, the scratch widths were converted to scratch hardness values, HS_p, using Equation 3–2, as discussed previously; the results of these calculations are presented in Table 4–2. These results are also graphically presented in Figure 4–19 and Figure 4–20.

Table 4—2: Mean scratch hardness of peened samples, measured by CLSM or SEM.

Measurement Method	Material	Traverse Speed (mm/s)	Mean Scratch Hardness, HS_p (GPa)
CLSM	Ti-6Al-4V	Unpeened	3.61 ± 0.24
	Ti-6Al-4V	500	1.60 ± 0.06
	Ti-6Al-4V	600	3.34 ± 0.34
	Ti-6Al-4V	700	3.25 ± 0.28
	Ti-6Al-4V	800	4.06 ± 0.38
	Ti-6Al-4V	900	4.76 ± 0.29
	Ti-6Al-4V	1000	5.61 ± 0.30
SEM	Ti-6Al-4V	Unpeened	3.65 ± 0.20
	Ti-6Al-4V	500	1.91 ± 0.07
	Ti-6Al-4V	600	3.37 ± 0.63
	Ti-6Al-4V	700	3.56 ± 0.24
	Ti-6Al-4V	800	4.28 ± 0.24
	Ti-6Al-4V	900	5.34 ± 0.72
	Ti-6Al-4V	1000	6.29 ± 0.41

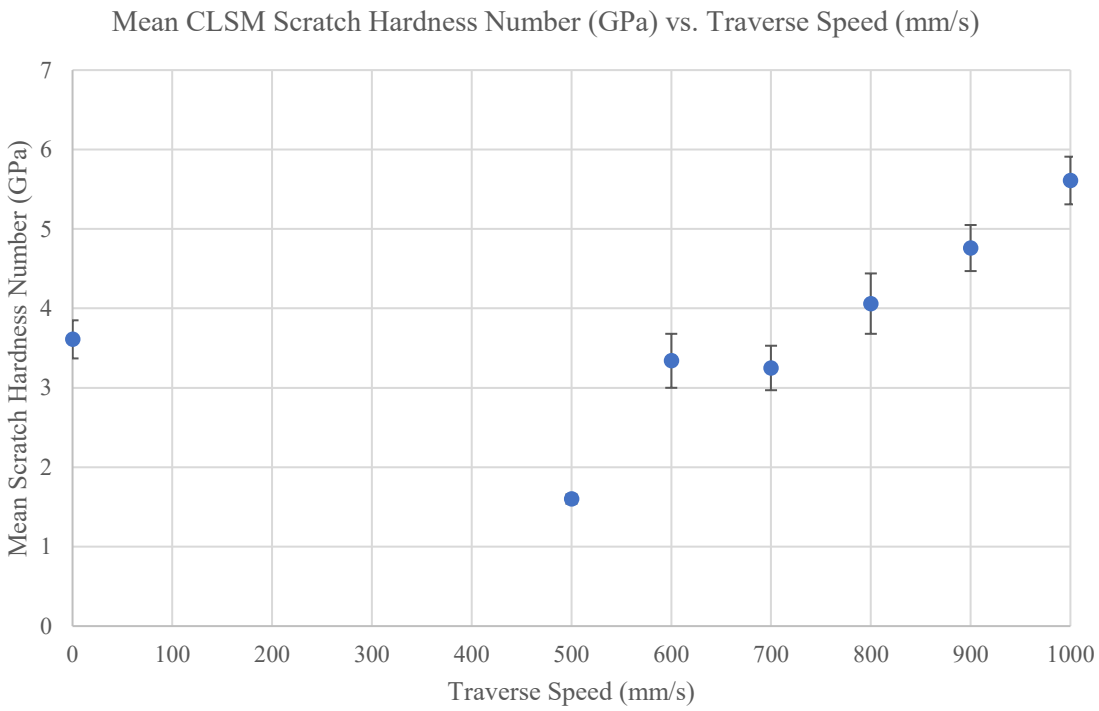

Figure 4—19: CLSM scratch hardness relative to traverse speed.

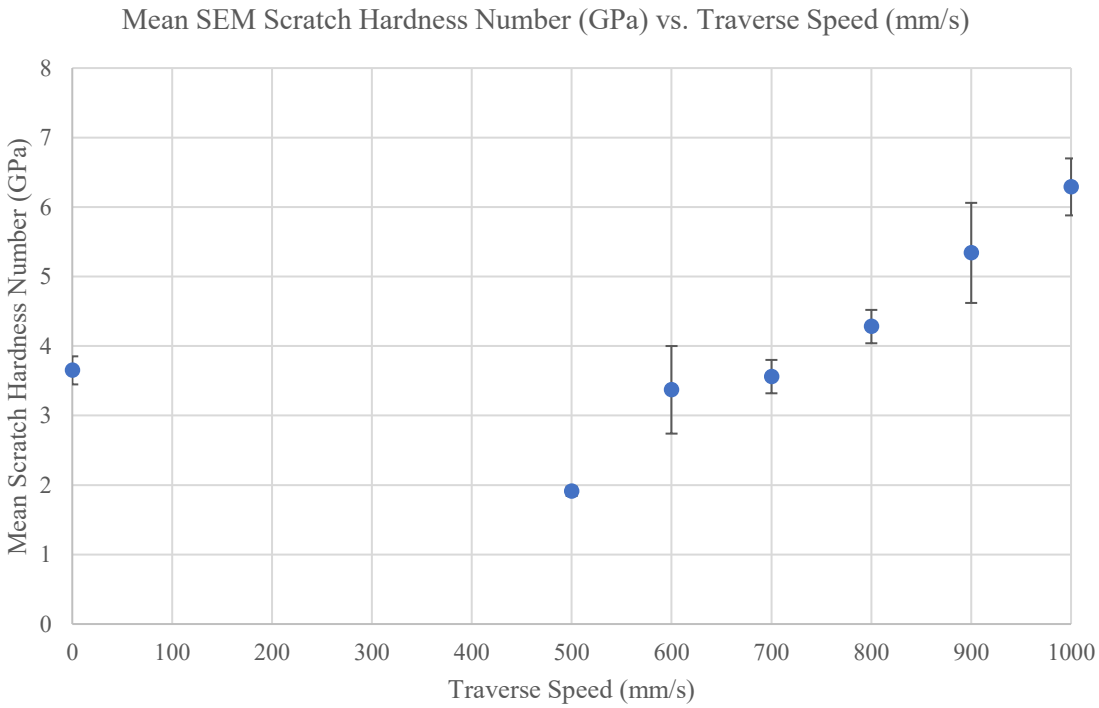

Figure 4—20: SEM scratch hardness relative to traverse speed.

The data gathered through SEM and CLSM are broadly similar to one another. Both sets of data indicate that the scratch hardness values of the Ti-6Al-4V material are heavily dependent upon the peening traverse speed employed. At traverse speeds lower than 800 mm/s, the resultant scratch hardness is lower than that of the unpeened wrought material. A traverse rate of 700 mm/s or 600mm/s results in a scratch hardness close to the scratch hardness of the unpeened material, while the sample peened at 500 mm/s demonstrated a considerable deterioration in scratch hardness. However, at traverse speeds equal to or above 800 mm/s the scratch hardness is seen to improve dramatically.

The trend in scratch hardness may be explained by comparison with the respective sample surface roughness. The scratch hardness is an indicator of the material's resistance to ploughing motion [52]. As other studies have found, titanium alloys are heavily susceptible to adhesive wear during dry sliding. During the sliding scratch test, as the indenter ploughs through the subject, asperities on both surfaces may cold weld together to form a junction. As the test continues, the junction shears in the softer material and may result in material transfer onto the surface of the harder counterpart. This creates a rough surface on the indenter, which aids in ploughing of the softer material [3].

As shown in the surface roughness data collected on each sample, traverse rates of 700 mm/s and below result in relatively high surface roughness. The traverse rate of 500 mm/s produced the highest surface roughness (disregarding the traverse rates below this that were found unsuitable for testing due to their extreme surface roughness), and the lowest scratch hardness. At traverse rates above 700 mm/s, the surface roughness begins to plateau. At the higher traverse rates, there is little variation in surface roughness. The benefits imparted by inducement of residual compressive stresses and resultant surface work hardening are greater than the detrimental effects posed by a greater surface roughness.

During the course of each scratch experiment, the dynamic coefficient of friction was recorded by the UMT-1 software. The collected data for three scratch tests with each traverse speed are presented in Figure 4–21 to Figure 4–27.

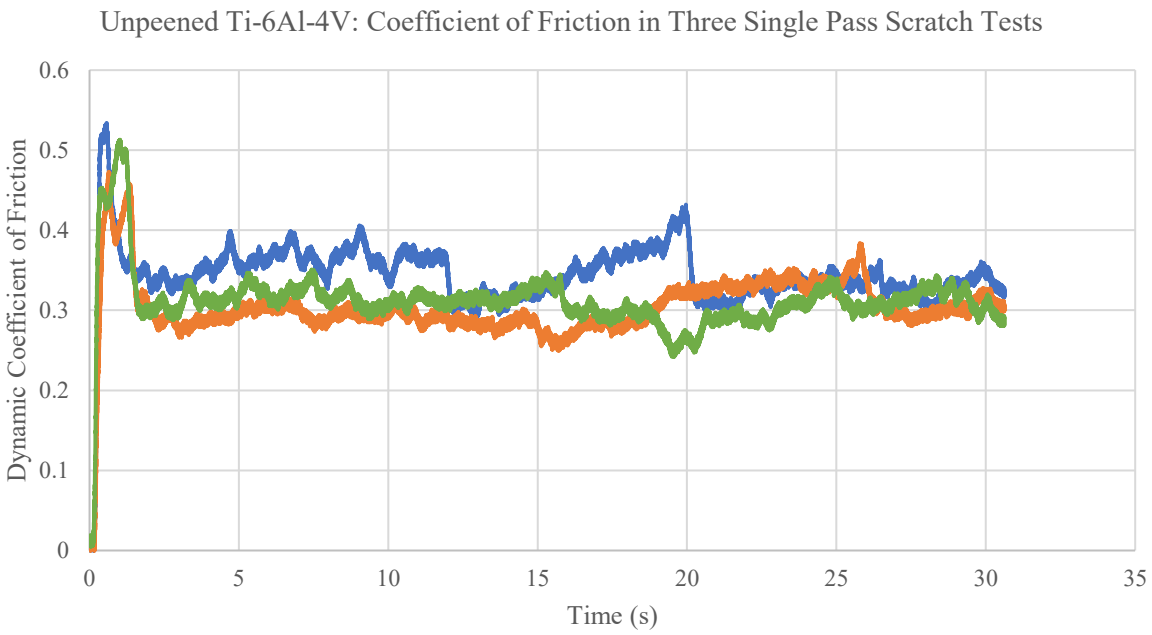

Figure 4—21: Dynamic coefficient of friction from three single-pass scratches on unpeened material.

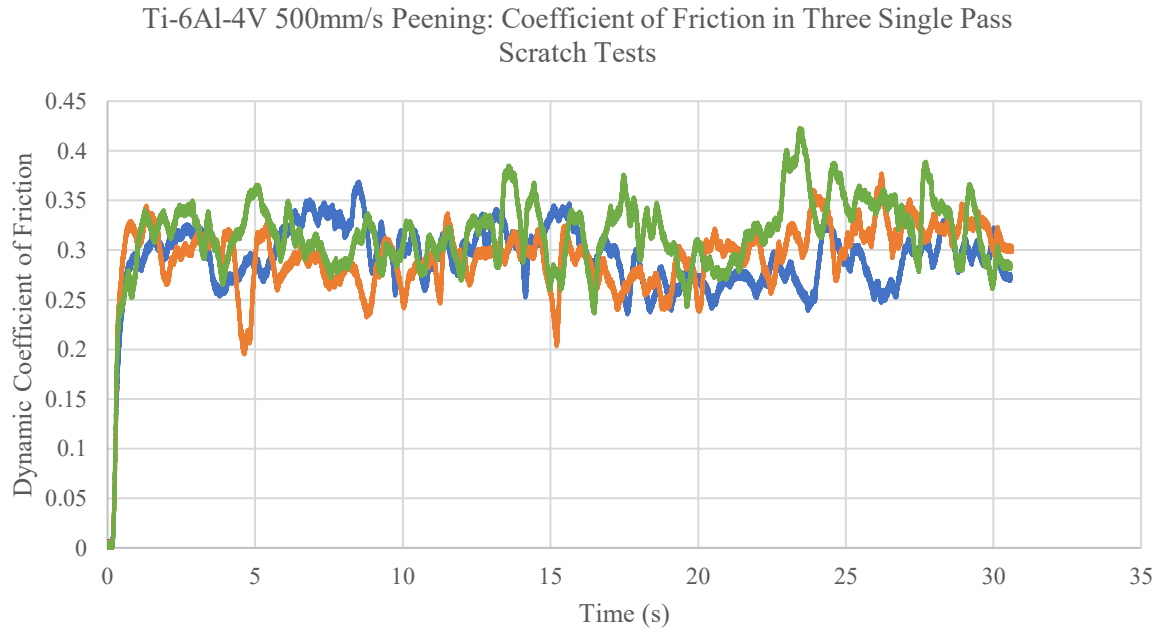

Figure 4—22: Dynamic coefficient of friction from three single-pass scratches on Ti-6Al-4V peened at 500 mm/s.

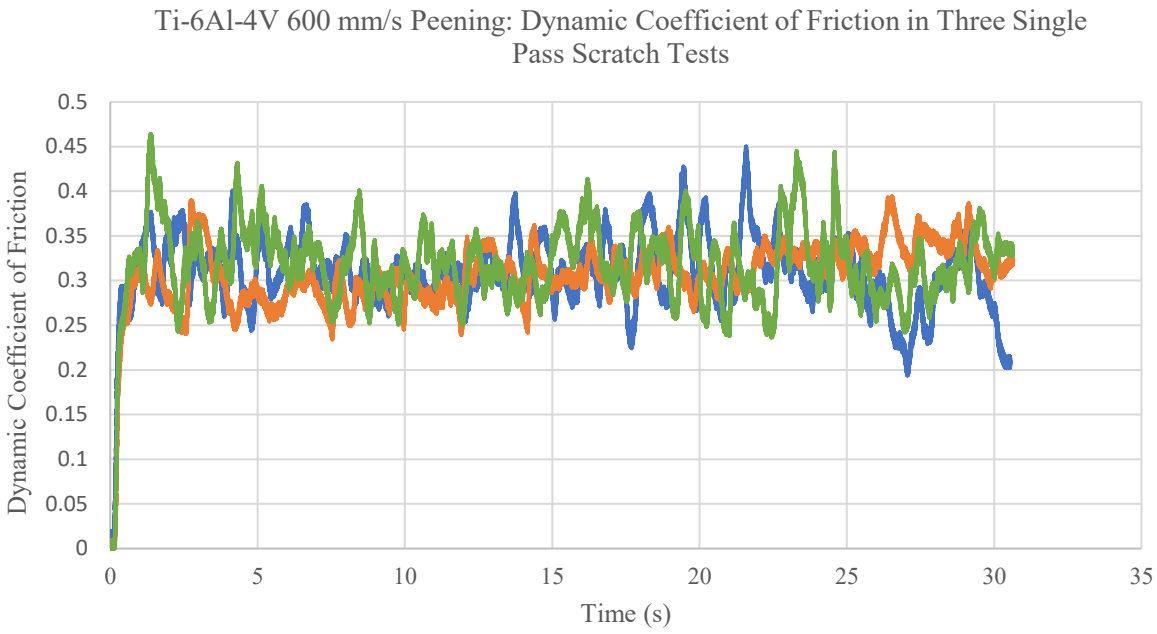

Figure 4—23: Dynamic coefficient of friction from three single-pass scratches on Ti-6Al-4V peened at 600 mm/s.

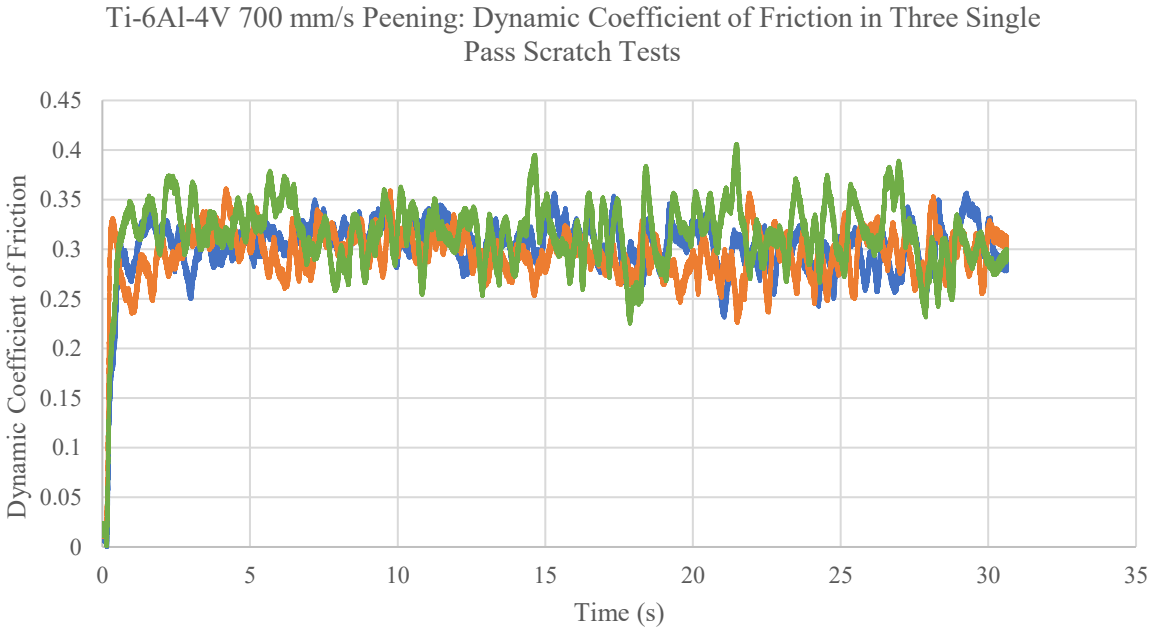

Figure 4—24: Dynamic coefficient of friction from three single-pass scratches on Ti-6Al-4V peened at 700 mm/s.

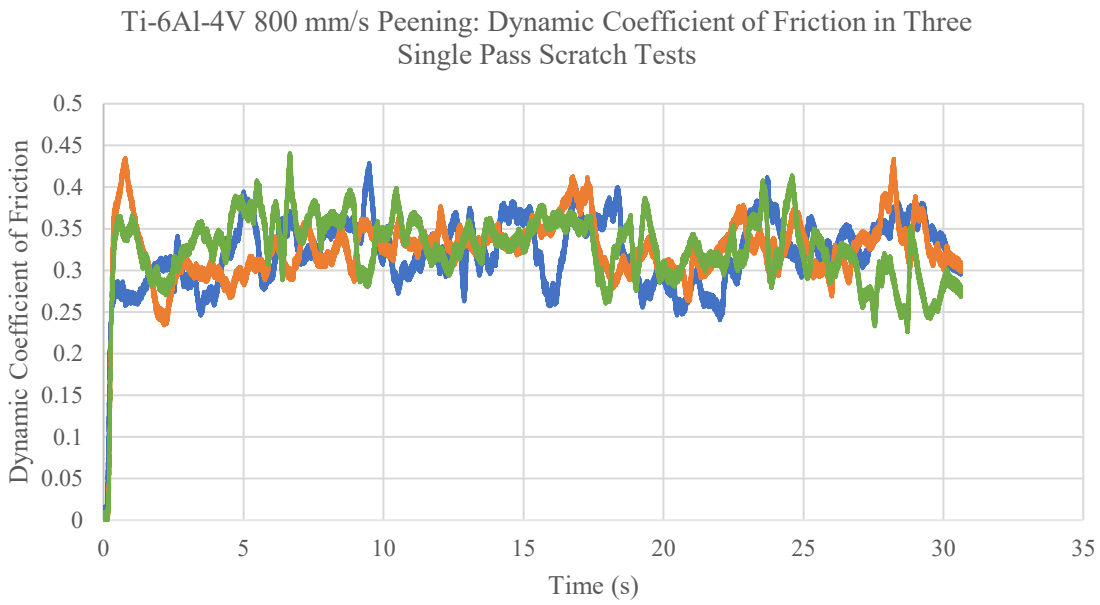

Figure 4—25: Dynamic coefficient of friction from three single-pass scratches on Ti-6Al-4V peened at 800 mm/s.

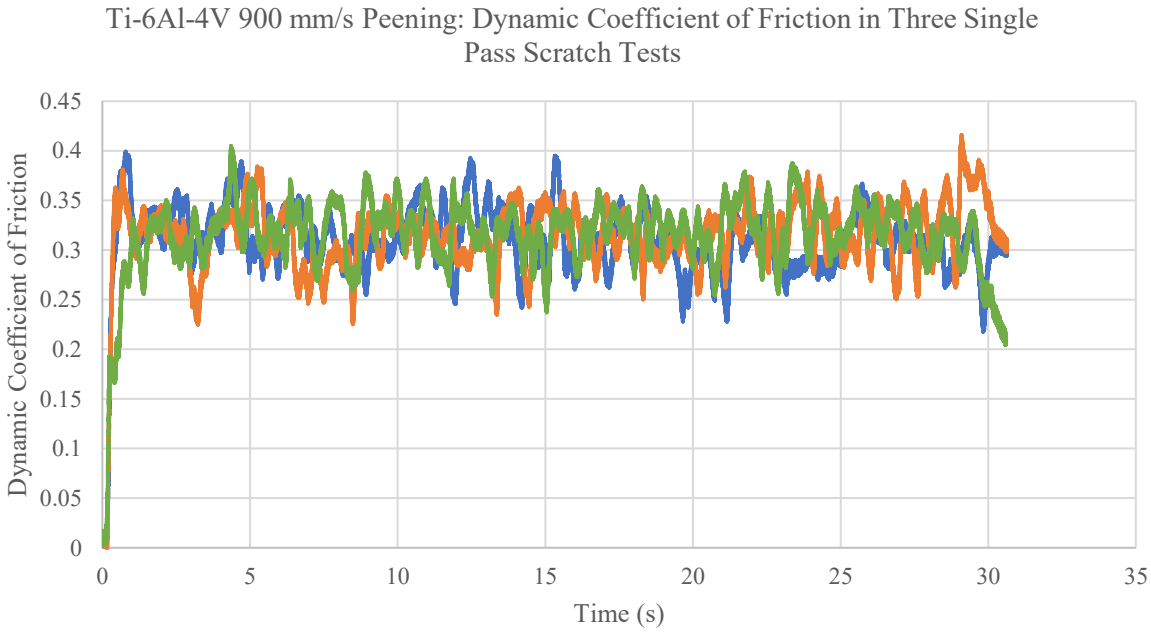

Figure 4—26: Dynamic coefficient of friction from three single-pass scratches on Ti-6Al-4V peened at 900 mm/s.

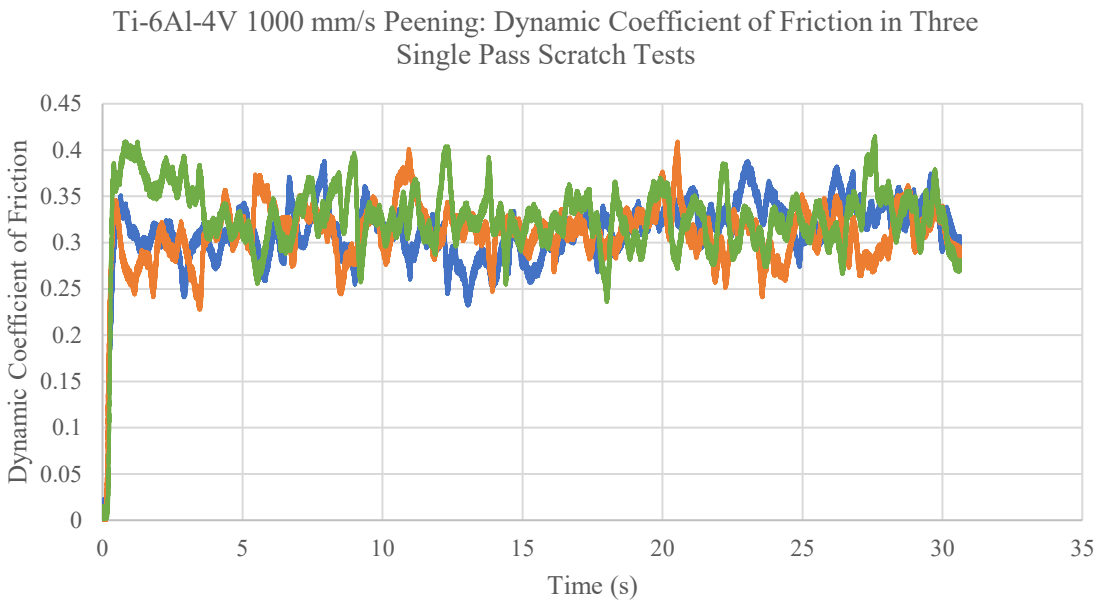

Figure 4—27: Dynamic coefficient of friction from three single-pass scratches on Ti-6Al-4V peened at 1000 mm/s.

The COF data of lower traverse speeds demonstrates greater variation in COF than the samples peened at high speeds. This indicated a greater presence of the 'stick-slip' tribological behaviour of titanium observed in other studies in addition to higher surface roughness [1, 3]. As adhesion occurs between the surfaces and junctions form, the software registers an increase in resistance to the sliding motion and thus an increase in the coefficient of friction. When the junction shears, the indenter is able to plough relatively easily (and registers a drop in resistance and coefficient of friction) until it encounters another junction. This behavior further supports the idea that the samples treated at lower peening speeds are more vulnerable to adhesive wear and subsequent junction shearing and ploughing, than the samples peened at higher traverse speeds with lower surface roughness.

Furthermore, the COF at higher traverse rates shows instability, implying that these samples still experience the cycle of adhesion and ploughing process. Although these samples may not experience the cycle to the same extent of the lower traverse rates, the process is still present. It suggests that the surface hardening benefits of UPWJ outweigh the disadvantages perpetuated by a higher surface roughness.

4.3 Reciprocating Wear

Each sample was subjected to multiple wear tests of varying nominal load. The resulting wear tracks were analysed by CLSM to obtain the volume loss and calculation of each sample's specific wear rate with Equation 3–3. Three-dimensional images obtained by CLSM of the wear tracks are presented in Figure 4–28 to Figure 4–34. The calculated specific mean wear rates are shown in Table 4–3 and are graphically presented in Figure 4–35.

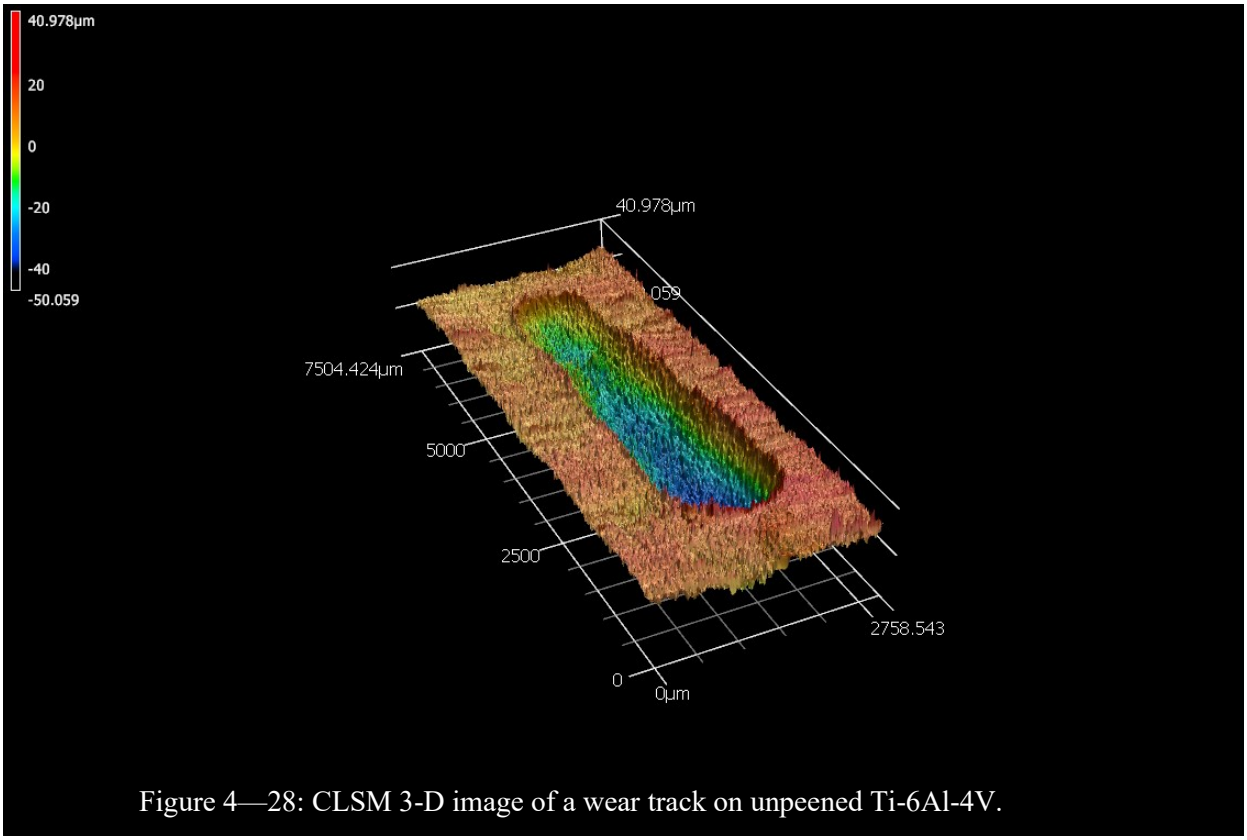

Figure 4—28: CLSM 3-D image of a wear track on unpeened Ti-6Al-4V.

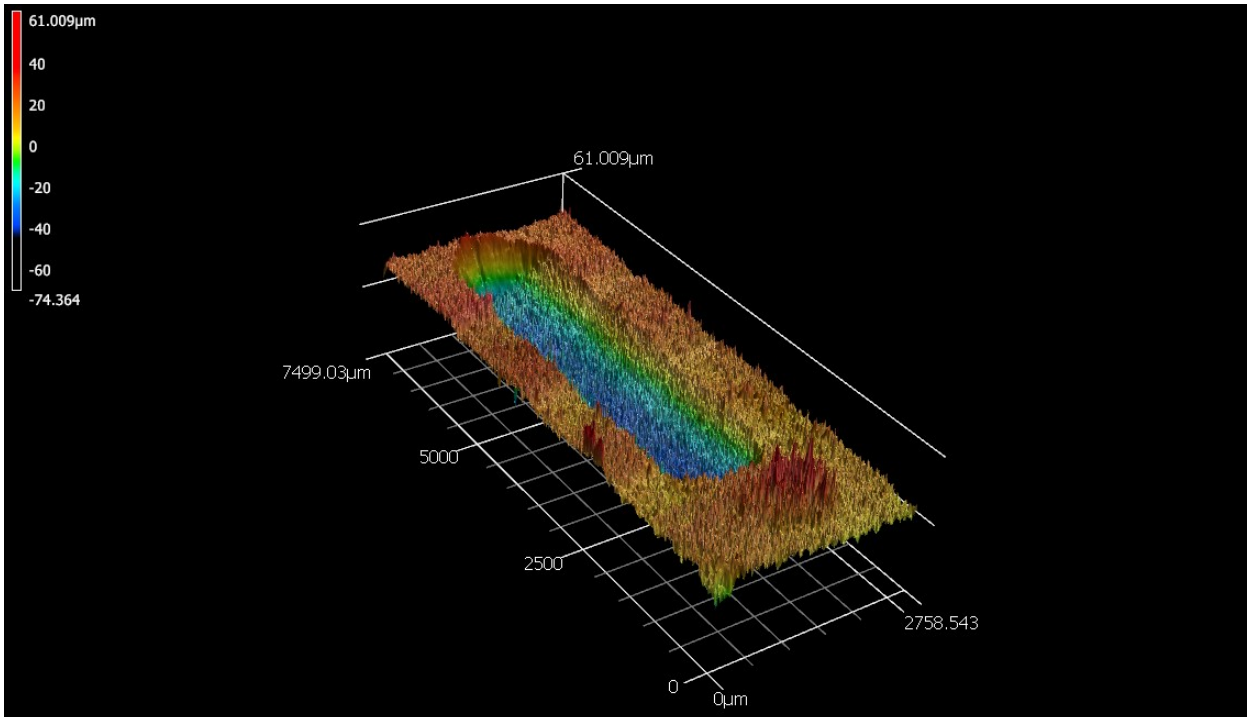

Figure 4—29: CLSM 3-D image of a wear track on Ti-6Al-4V peened at 500 mm/s.

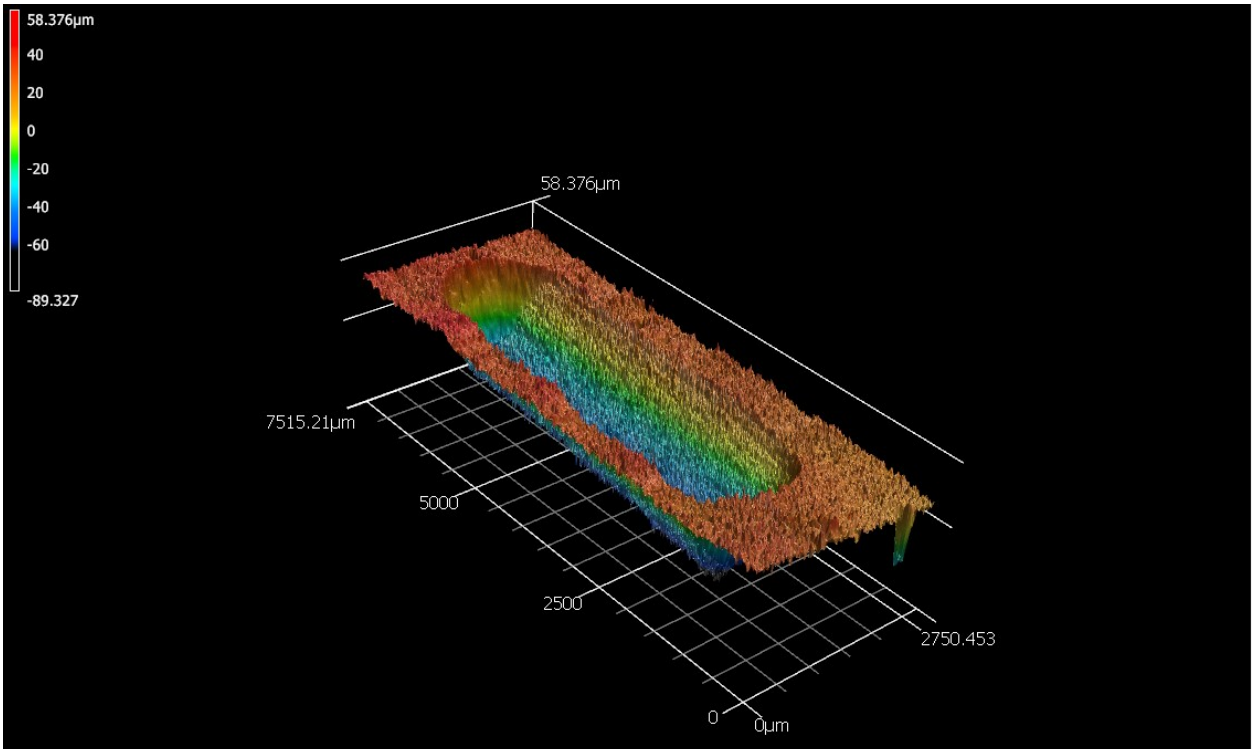

Figure 4—30: CLSM 3-D image of a wear track on Ti-6Al-4V peened at 600 mm/s.

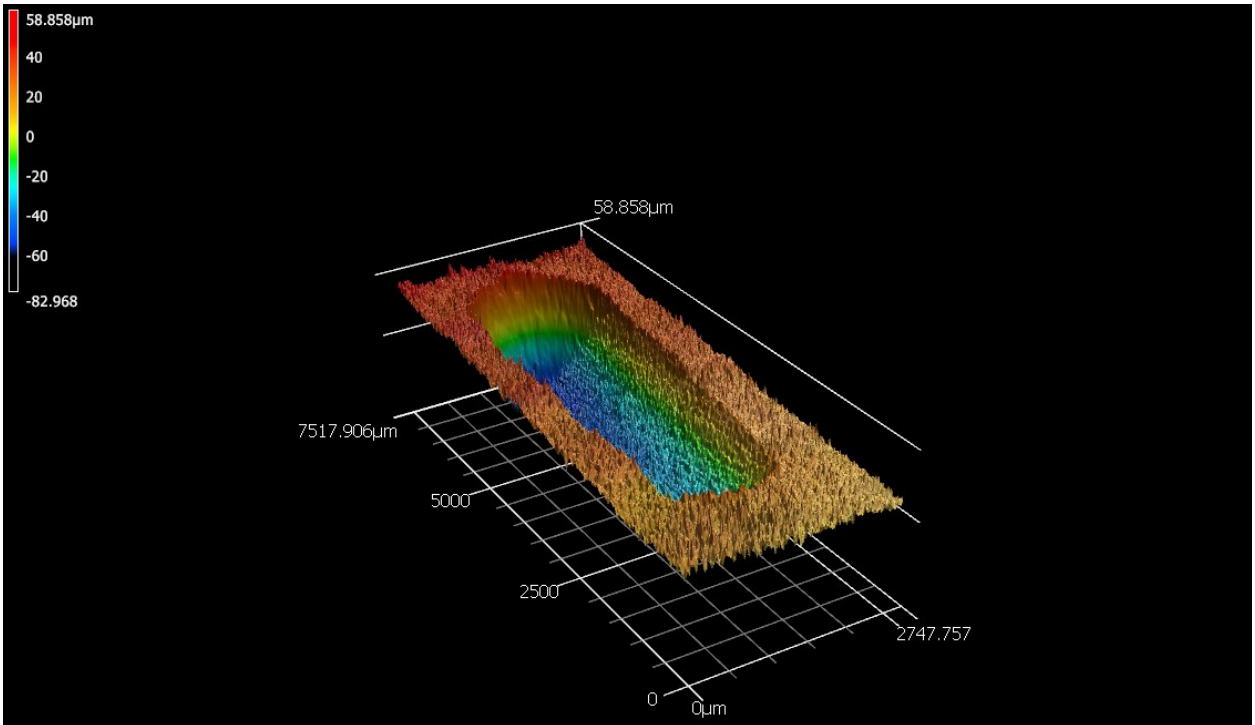

Figure 4—31: CLSM 3-D image of a wear track on Ti-6Al-4V peened at 700 mm/s.

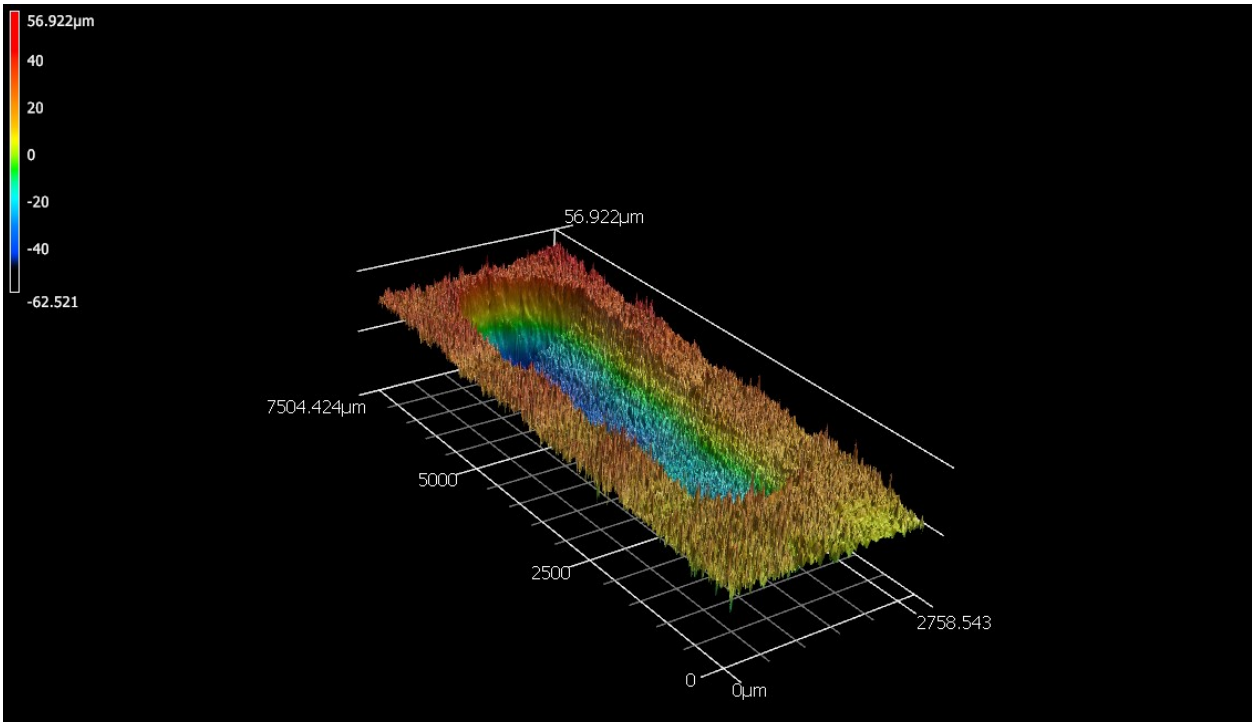

Figure 4—32: CLSM 3-D image of a wear track on Ti-6Al-4V peened at 800 mm/s.

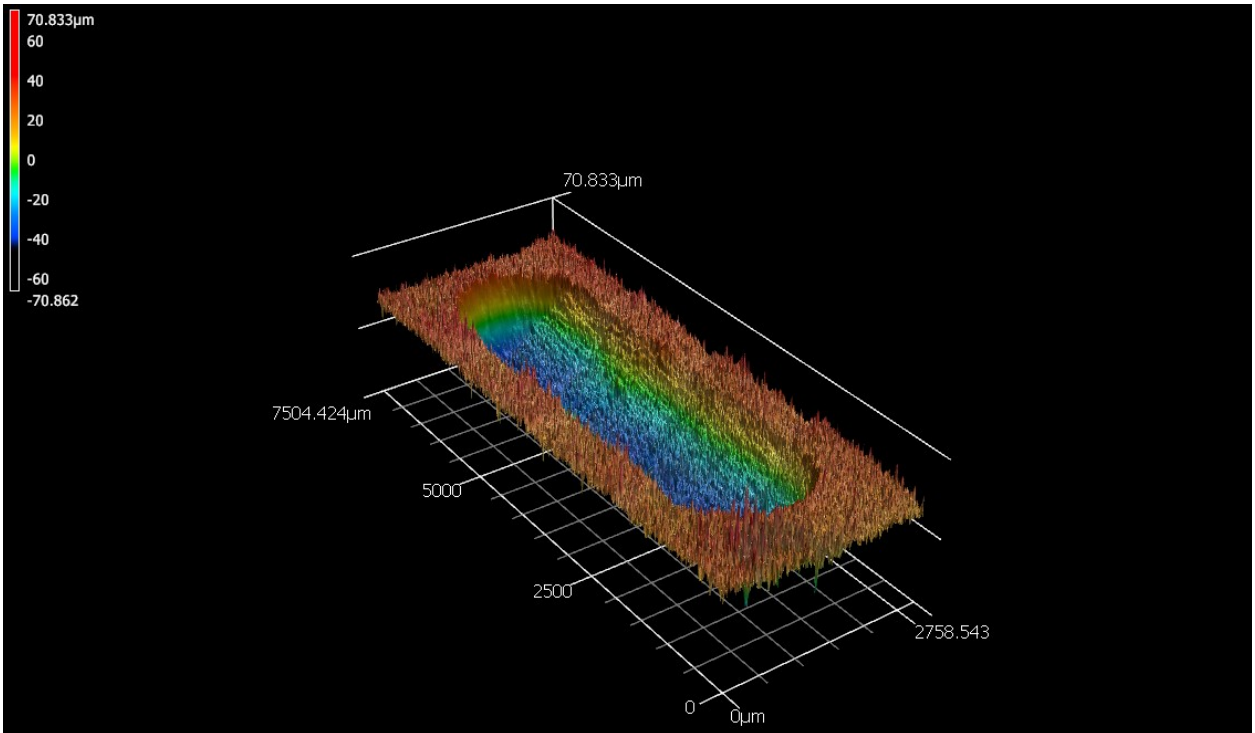

Figure 4—33: CLSM 3-D image of a wear track on Ti-6Al-4V peened at 900 mm/s.

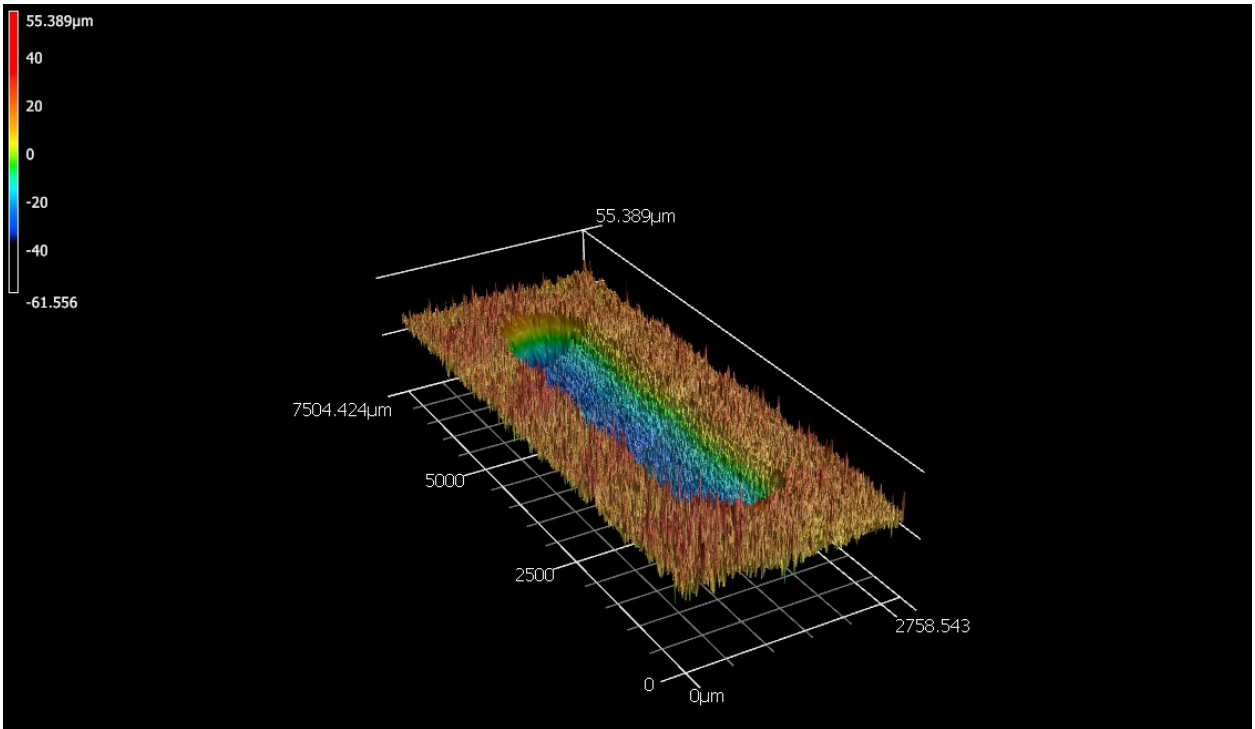

Figure 4—34: CLSM 3-D image of a wear track on Ti-6Al-4V peened at 1000 mm/s.

Table 4—3: Mean specific wear rates and traverse speed.

Material	Traverse Speed (mm/s)	Mean Specific Wear Rate (10^{-4} mm^3/Nm)
Ti-6Al-4V	– (unpeened)	3.89 ± 0.9
Ti-6Al-4V	500	9.08 ± 4.0
Ti-6Al-4V	600	9.10 ± 3.7
Ti-6Al-4V	700	7.52 ± 2.5
Ti-6Al-4V	800	7.10 ± 2.7
Ti-6Al-4V	900	7.27 ± 3.9
Ti-6Al-4V	1000	9.33 ± 4.0

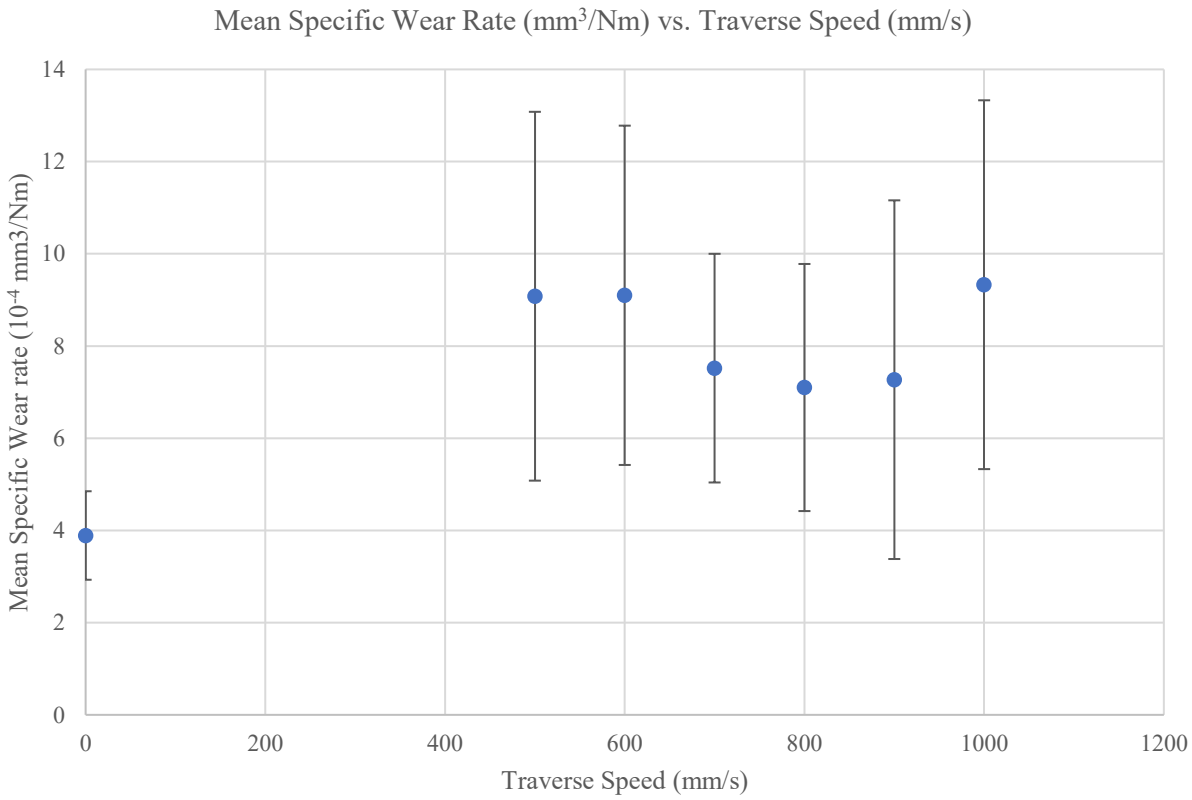

Figure 4—35: Mean specific wear rate relative to traverse speed.

The collected data indicates that the wear resistance of the wrought Ti-6Al-4V alloy was not improved by UPWJ peening. The unpeened sample possesses a much lower

mean specific wear rate than the peened samples, and with less variation. The lowest traverse rates show improving specific wear rate with increasing traverse rate up to 800 mm/s, which holds the lowest specific wear rate among the peened materials. However, samples peened at traverse speeds above 800 mm/s show an increasing wear rate.

The initial trend of a much higher increase in wear rate with lower traverse rates may be a result of increased surface roughness after UPWJ peening. A greater surface roughness implies a greater presence of asperities on the material surface. During a wear scenario, the asperities of two reciprocating surfaces conjoin together under an applied load and adhesion occurs. As reciprocating motion continues, the junctions rupture and initiate abrasive wear by two mechanisms. After the junction rupture, material from the softer surface may attach to the counter surface. This creates a rougher counter surface well suited for ploughing [1, 3]. Alternatively, the material transfer detaches from the counter surface and becomes loose wear debris. The wear debris may become trapped within the wear track, initiating three-body abrasive wear [33]. Thus, the samples that feature relatively high surface roughness from peening at lower traverse speeds may experience a higher level of adhesive and abrasive wear than the unpeened material.

The second trend of increasing wear rate for peening traverse speeds above 800 mm/s may be due to dominant abrasive wear. These samples also demonstrated a much higher scratch hardness than the unpeened material and featured lower surface roughness than samples peened below 800 mm/s, although still higher surface roughness than the unpeened material. As junction rupture takes place, shearing occurs in the relatively softer (as the counter surface was alumina) titanium material. However, the wear debris created from the ruptures, although less in volume due to less asperities in comparison to materials peened at lower traverse rates, is much harder. These hard particles may become trapped in the wear track, eventually abrading the softer titanium substrate underneath the work hardened surface. Thus, these samples demonstrate an increased wear rate when compared with the unpeened material.

The wear tracks were closely examined by SEM and EDS to analyse oxygen concentrations and debris in the wear tracks, which may be indicative of the operating

wear mechanism(s). Figures 4–36 to 4–42 display SEM images captured of wear tracks on peened surfaces.

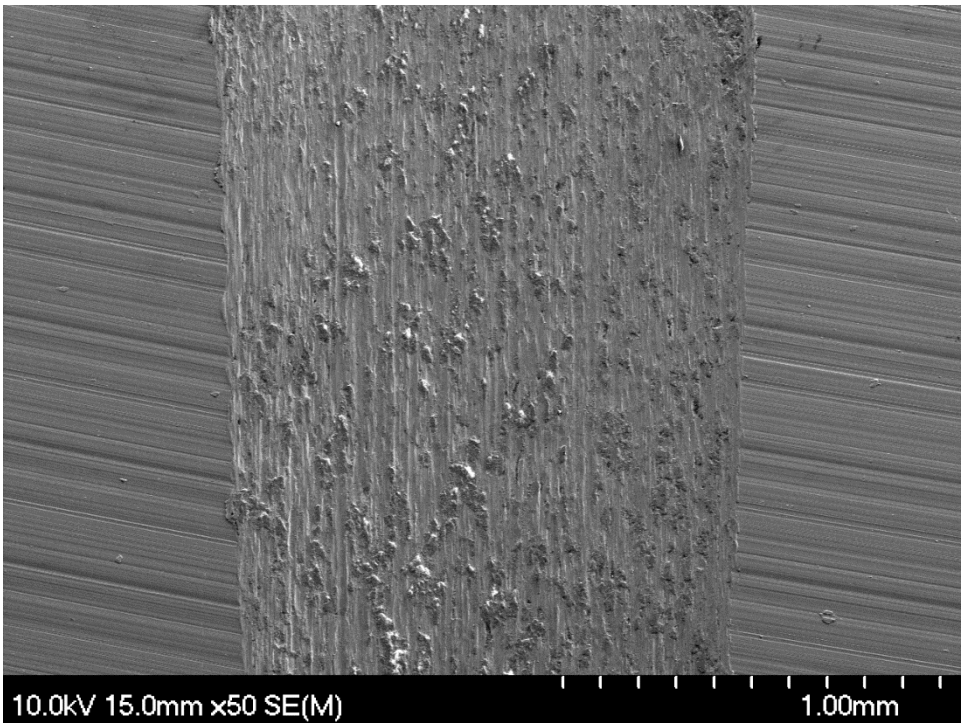

Figure 4—36: SEM image of a wear track on unpeened Ti-6Al-4V.

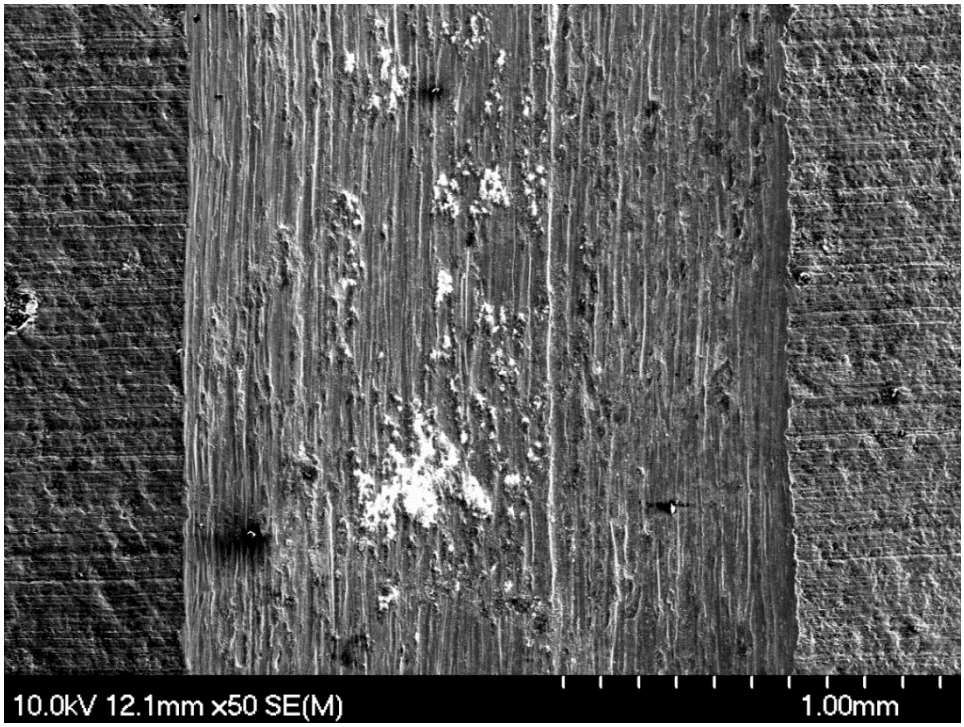

Figure 4—37: SEM image of a wear track on Ti-6Al-4V peened at 500 mm/s.

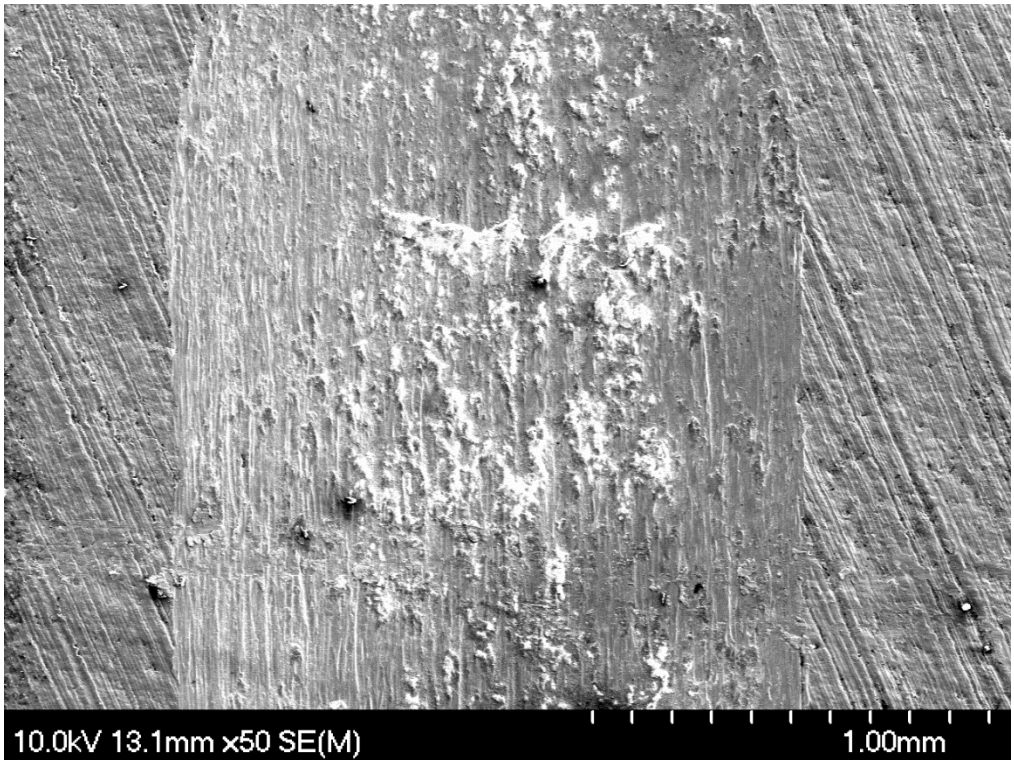

Figure 4—38: SEM image of a wear track on Ti-6Al-4V peened at 600 mm/s.

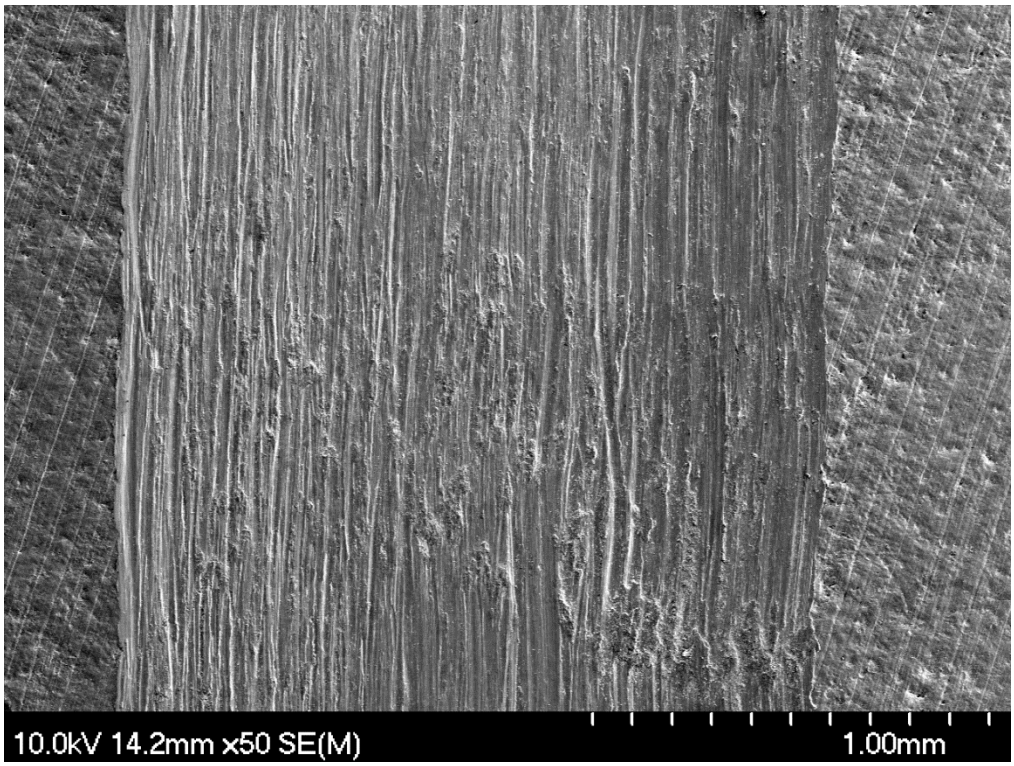

Figure 4—39: SEM image of a wear track on Ti-6Al-4V peened at 700 mm/s.

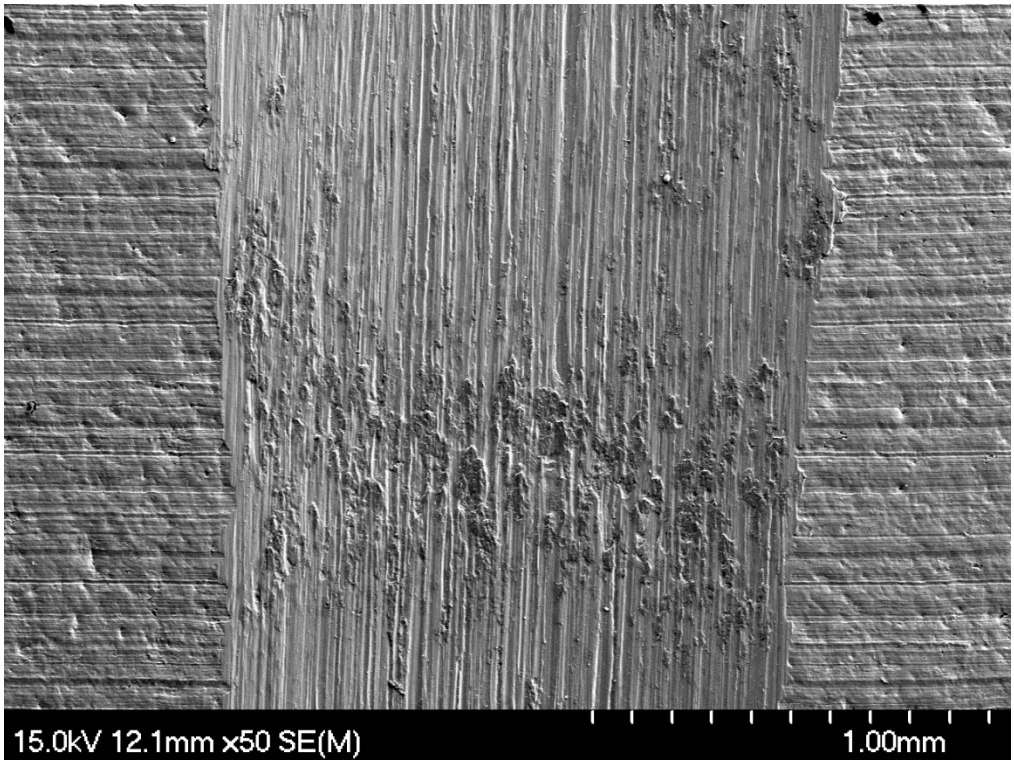

Figure 4—40: SEM image of a wear track on Ti-6Al-4V peened at 800 mm/s.

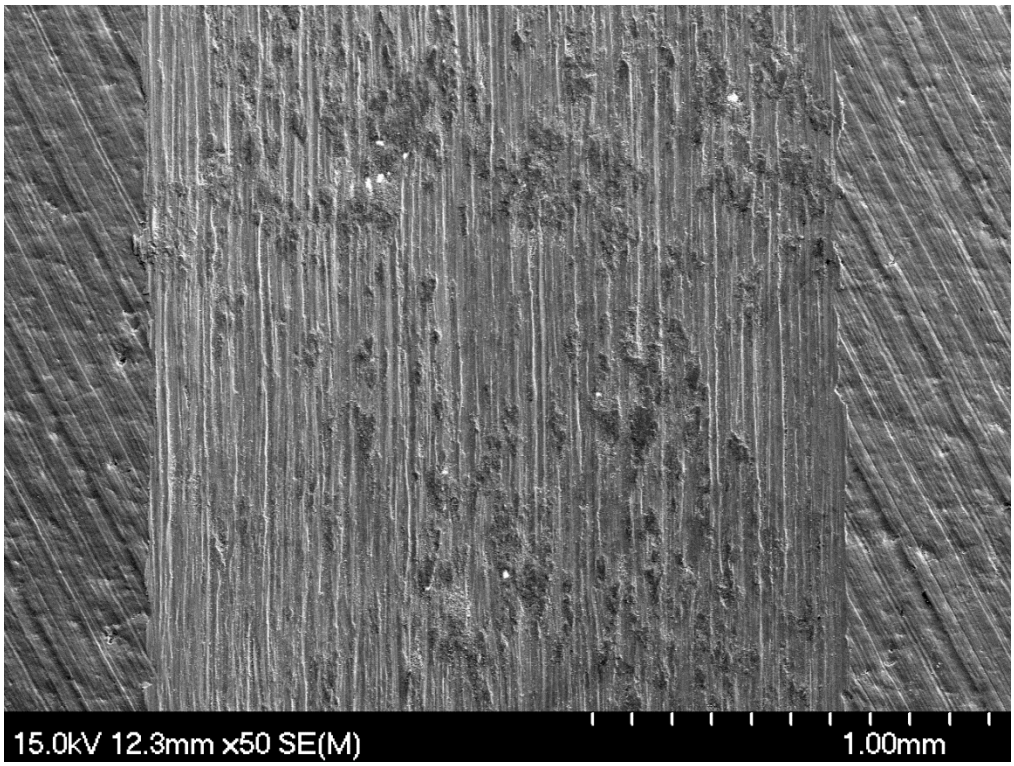

Figure 4—41: SEM image of a wear track on Ti-6Al-4V peened at 900 mm/s.

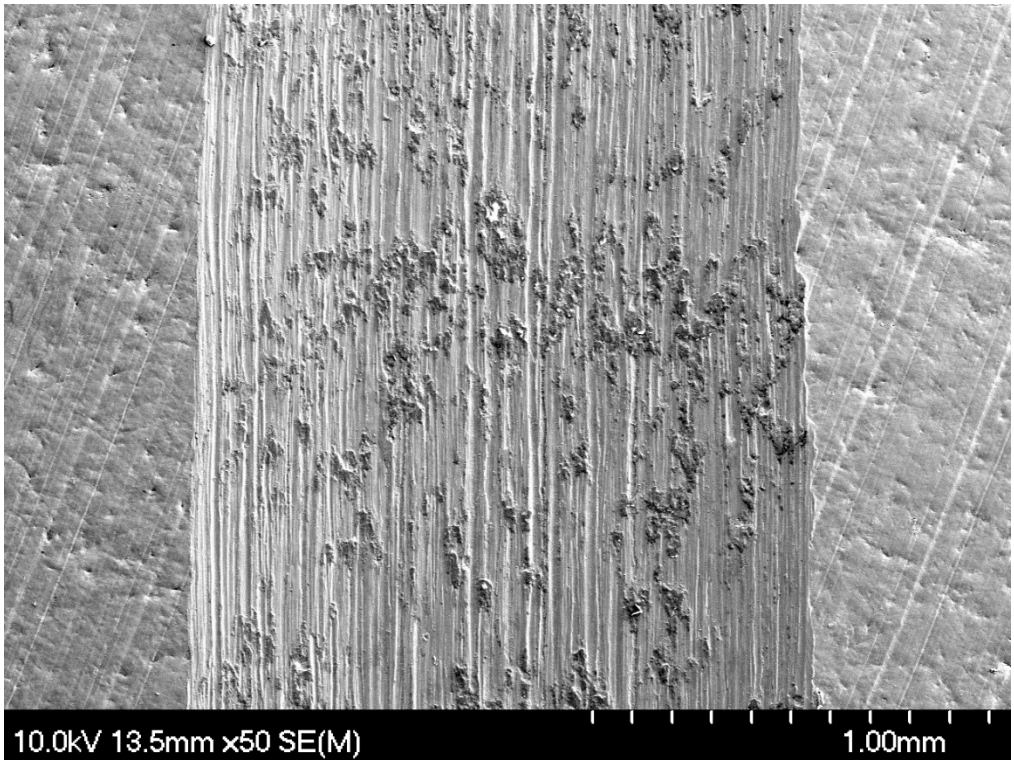

Figure 4—42: SEM image of a wear track on Ti-6Al-4V peened at 1000 mm/s.

The wear tracks of all the peened samples demonstrated features of adhesive wear and wear debris scattered along the wear track. The sample wear tracks all showed the characteristic ‘stick-slip’ wear behaviour of titanium, as described in other works [3]. Regions of sheared asperities are interspersed along the length of the wear tracks, surrounded by regions of deep grooves caused by ploughing. Examples of the stick-slip features found in the samples are presented in Figure 4–43 and Figure 4–44.

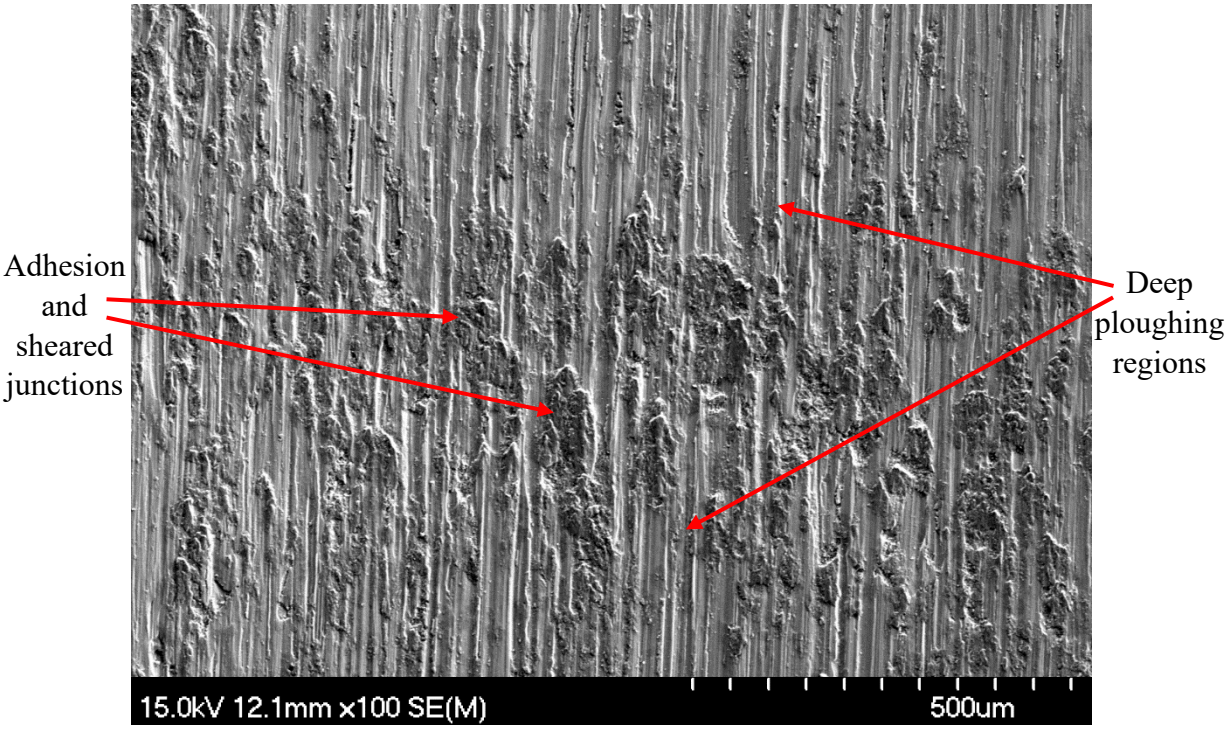

Figure 4—43: SEM image of adhesive wear features on Ti-6Al-4V peened at 800 mm/s.

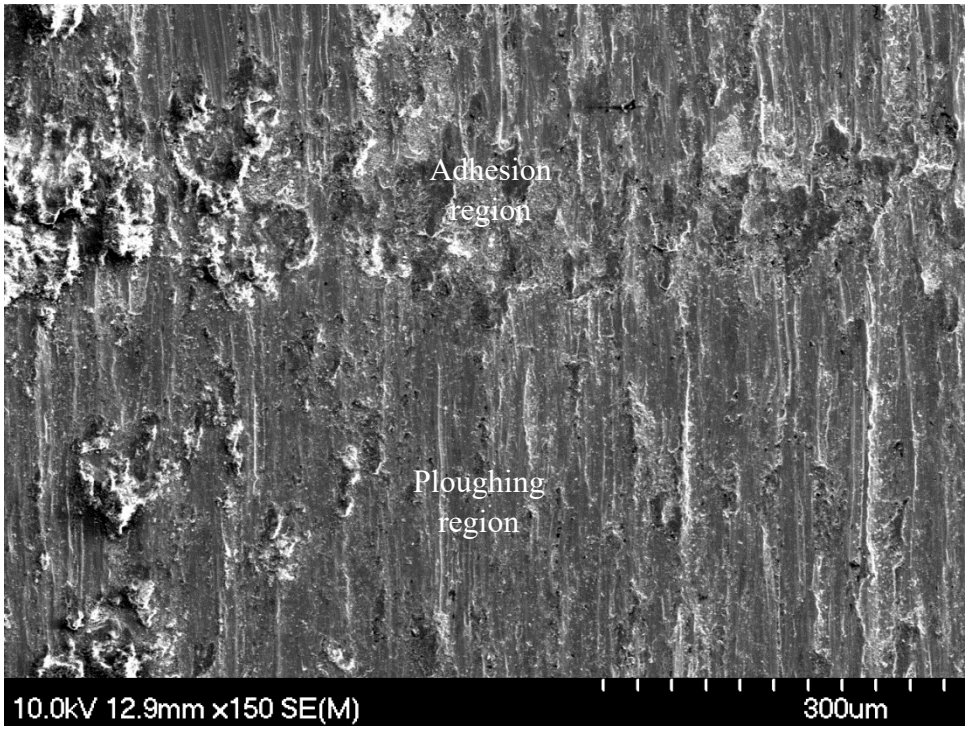

Figure 4—44: SEM image of adhesion and ploughing regions in a wear track on Ti-6Al-4V peened at 800 mm/s.

The number and size of the adhesion regions decreases with increasing traverse rate. This is likely a result of decreasing surface roughness, as fewer and smaller surface asperities are present with increasing traverse rate. Hence, larger junctions are formed on the surfaces of materials peened with low traverse rates.

A significant number of fine particles were found to be dispersed in the wear tracks of samples peened at 900 and 1000 mm/s. This may be indicative of severe oxidation wear or substantial two-body abrasive wear. Oxidation debris is generated by cyclic formation and removal of an oxide layer, which is formed when the material becomes exposed to the atmosphere [3]. Three-body abrasive wear is the result of material transfer and detachment from the counter surface, which then collect in the wear track and abrade the metal [33, 34]. Figure 4–45 displays the extremely fine particles, which can be seen covering the wear track.

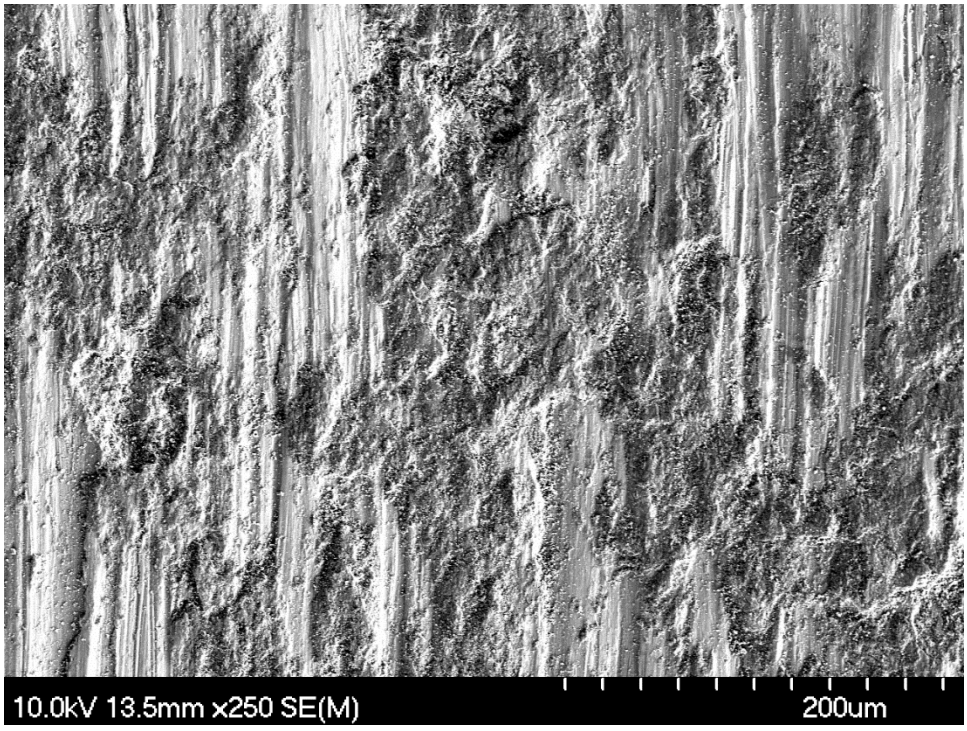

Figure 4—45: SEM image of fine particles covering a wear track on Ti-6Al-4V peened at 1000 mm/s.

The samples were further analysed with EDS element concentration mapping, to attempt to observe the extent of oxidation. The EDS maps are presented in Figures 4–46 to 4–52.

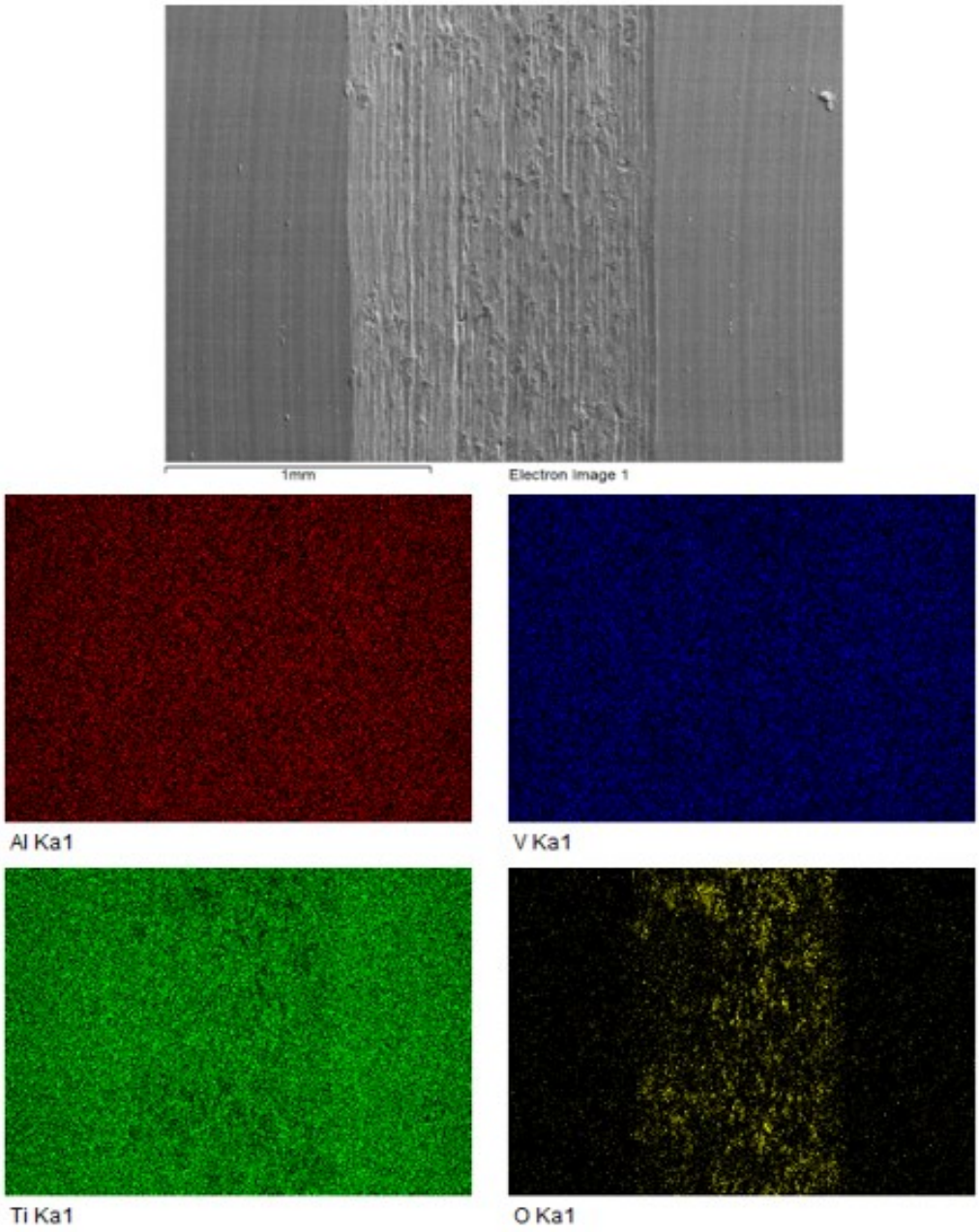

Figure 4—46: EDS mapping of a wear track on unpeened Ti-6Al-4V.

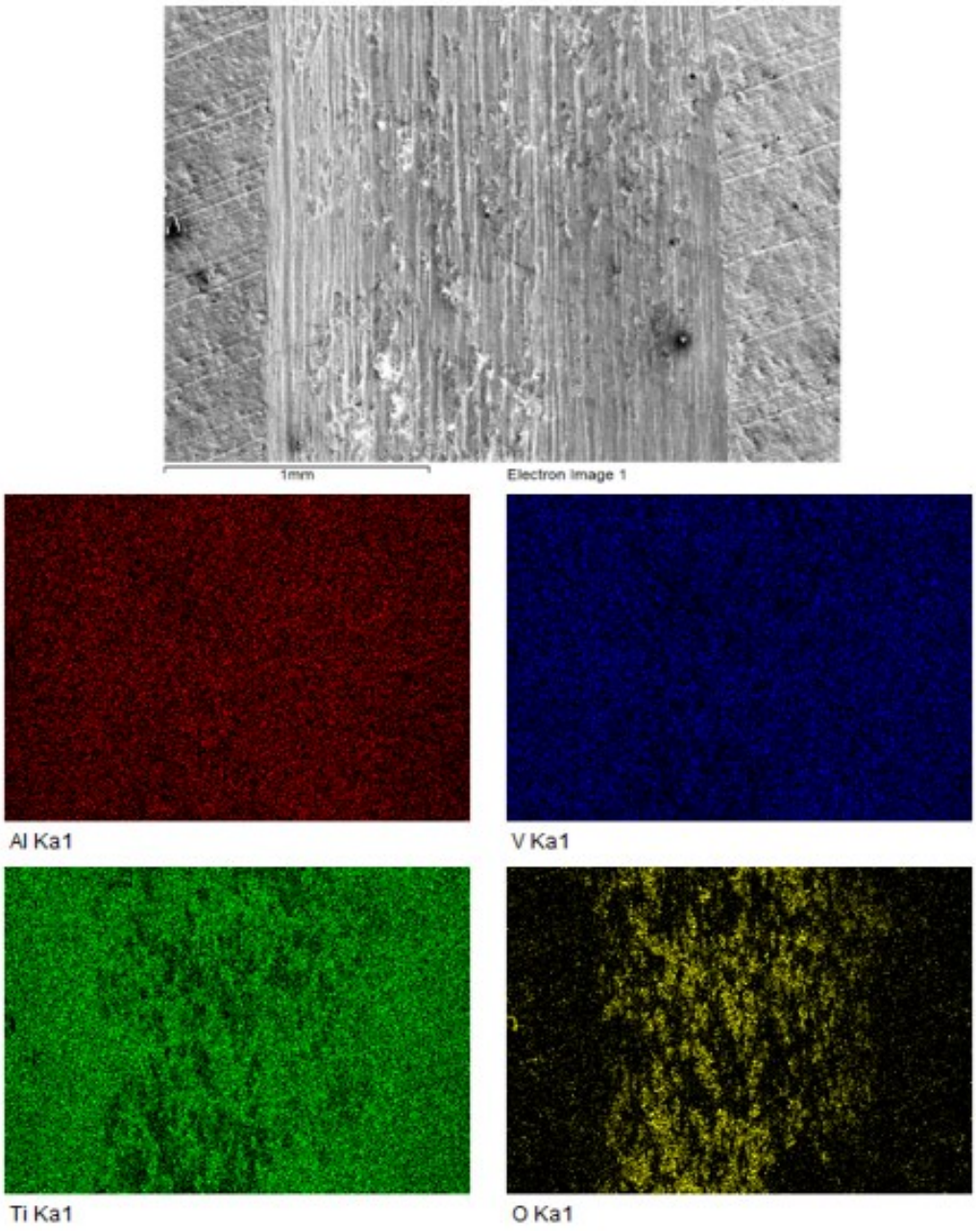

Figure 4—47: EDS mapping of a wear track on Ti-6Al-4V peened at 500 mm/s.

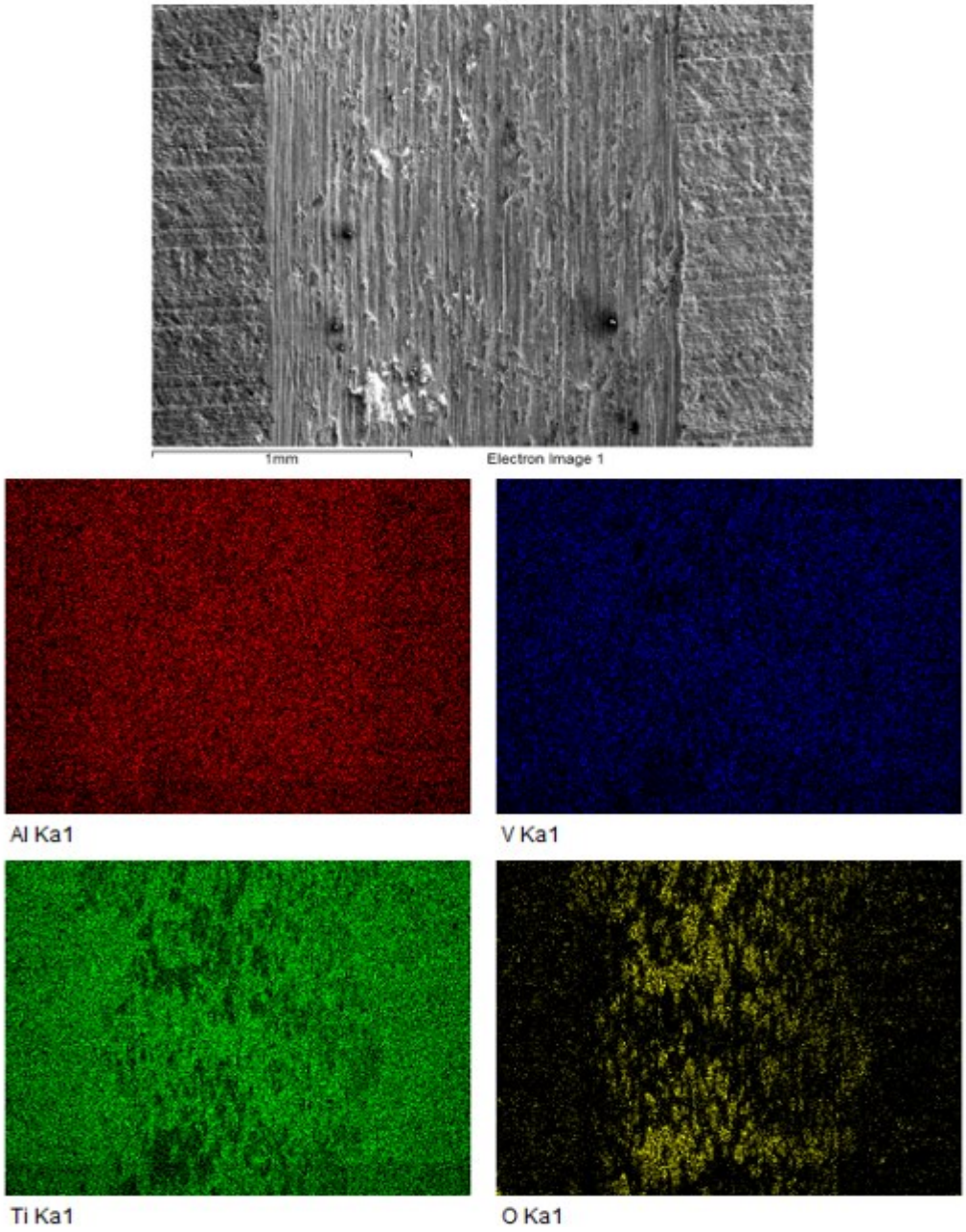

Figure 4—48: EDS mapping of a wear track on Ti-6Al-4V peened at 600 mm/s.

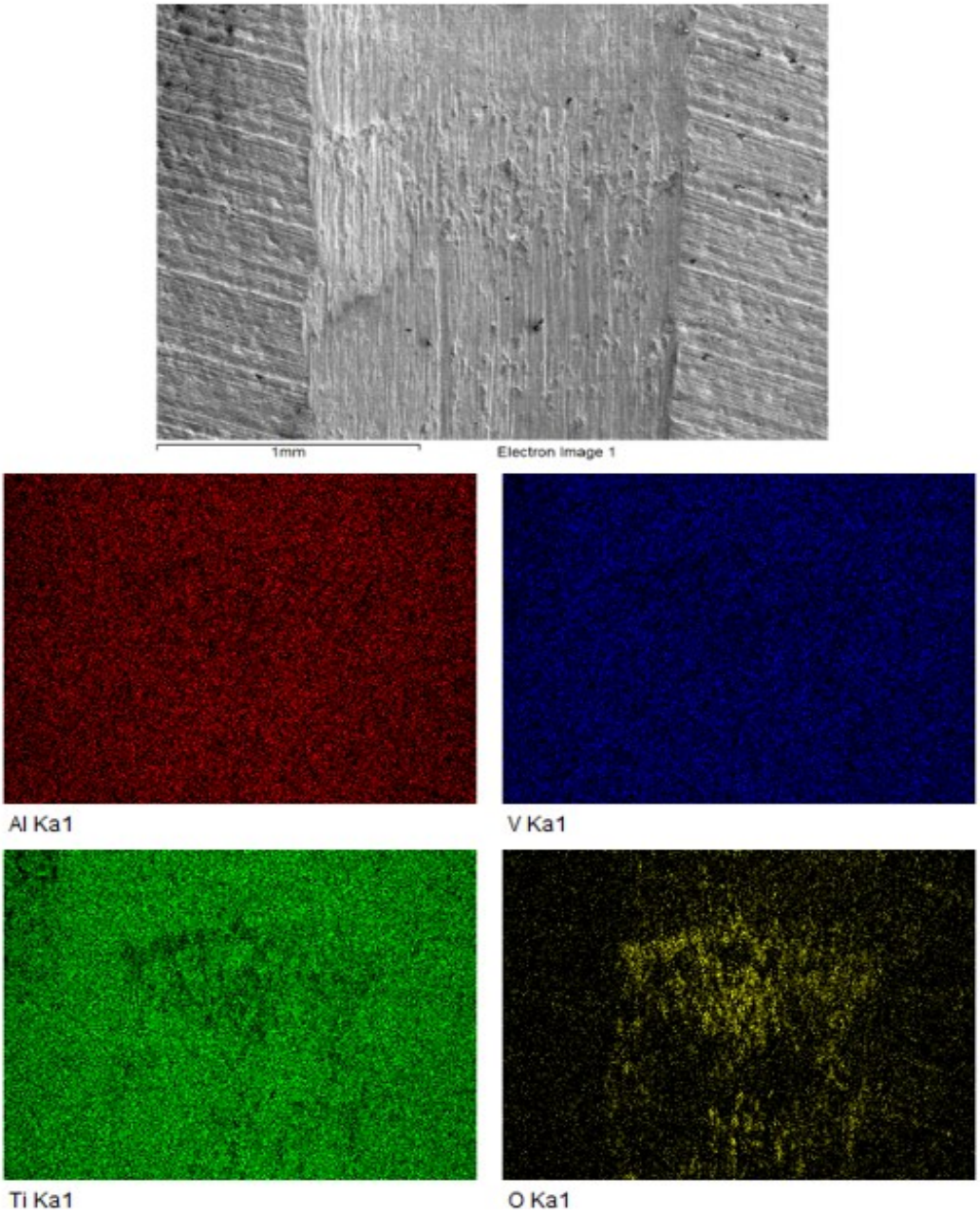

Figure 4—49: EDS mapping of a wear track on Ti-6Al-4V peened at 700 mm/s.

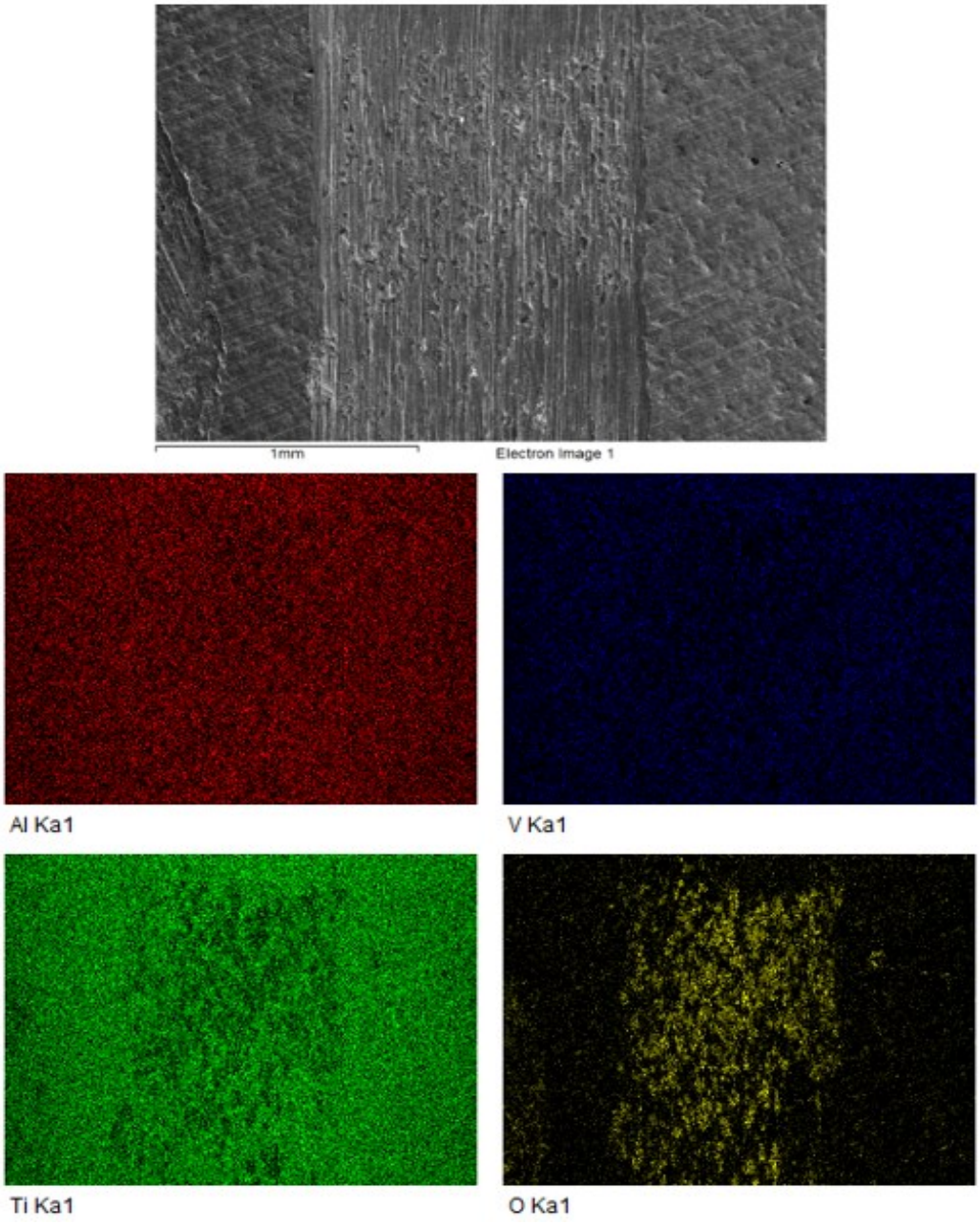

Figure 4—50: EDS mapping of a wear track on Ti-6Al-4V peened at 800 mm/s.

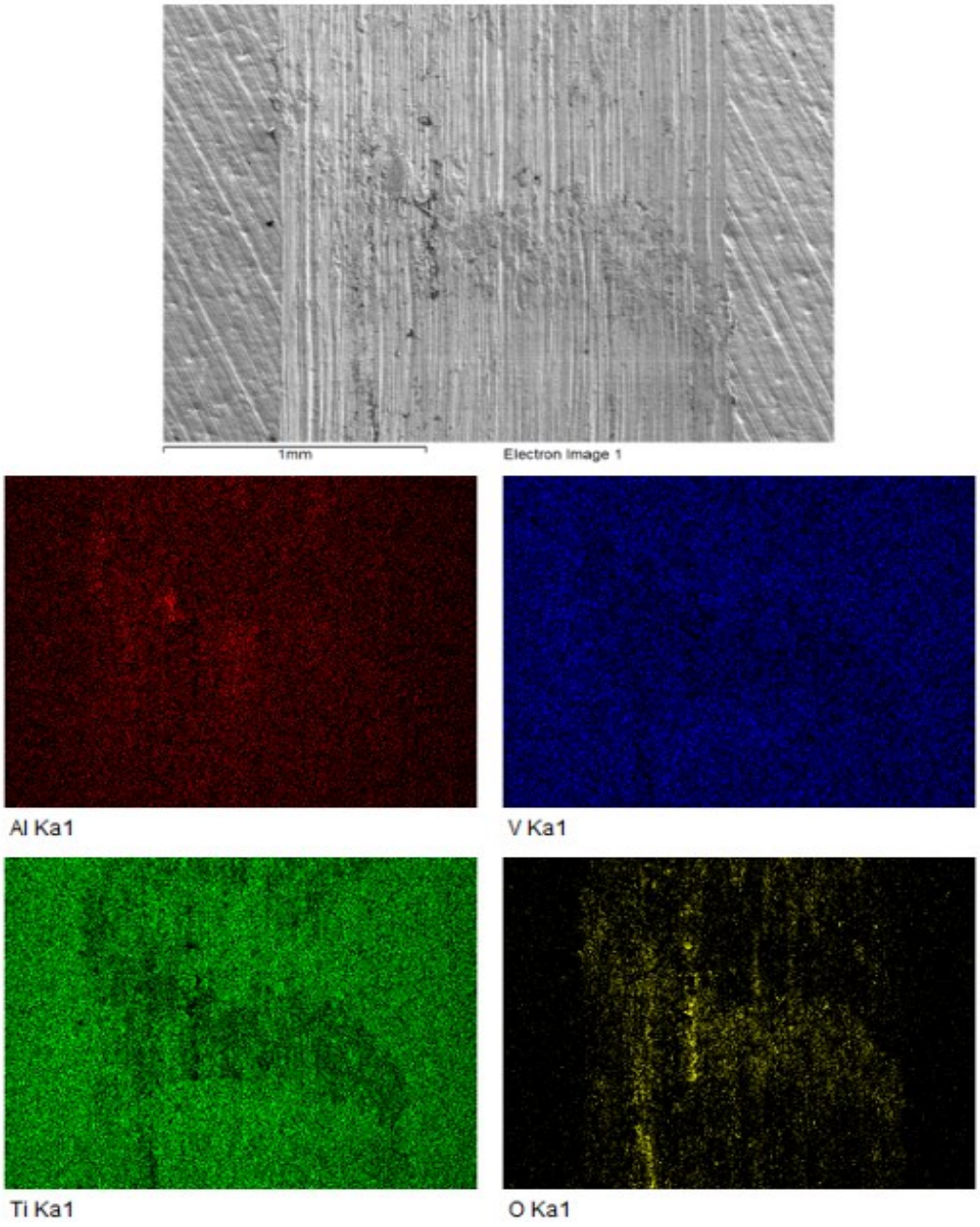

Figure 4—51: EDS mapping of a wear track on Ti-6Al-4V peened at 900 mm/s.

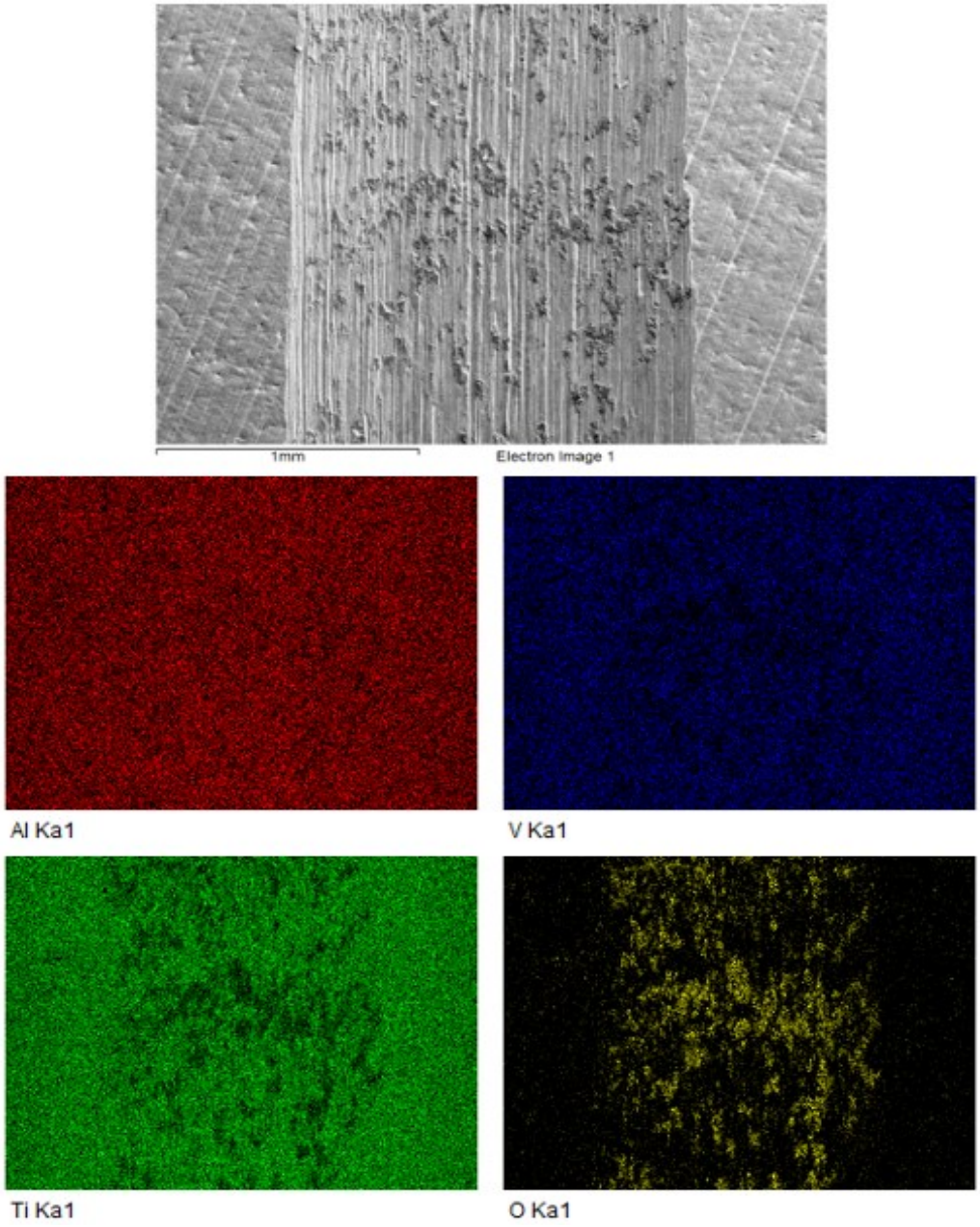

Figure 4—52: EDS mapping of a wear track on Ti-6Al-4V peened at 1000 mm/s.

EDS mapping of the wear tracks show localised oxygen concentrations indicative of oxidation wear in all samples. The oxygen concentrations appear to be localised in regions of adherence within the wear tracks. As the junctions are ruptured, the metal becomes exposed to the atmosphere and oxidation occurs. Hence, the oxidation layer is formed primarily at regions of adhesion and junction ruptures. Oxidation was present in

all samples, suggesting that oxidative wear was not the primary wear mechanism for any samples. However, samples treated at lower traverse speeds appear to have more concentrated oxidation than samples treated at traverse speeds above 800 mm/s. This supports the idea that these samples suffered more adhesive wear than samples peened at traverse speeds above 800 mm/s since a greater number of junctions are ruptured.

The gathered data and images suggest that the primary wear mechanism for traverse rates below 800 mm/s is adhesive wear. This is likely due to their high surface roughness that allows for larger junctions to form and rupture. In samples peened at traverse rates above 800 mm/s, the primary wear mechanism appears to be two-body abrasion. The harder surface material is converted into fine particulates that harshly abrade softer titanium subsurface material, resulting in a high specific wear rate. In comparison to the unpeened material, UPWJ did not improve the wear resistance of Ti-6Al-4V wrought alloy.

Chapter 5: Conclusions and Recommendations

In this study, samples of wrought Ti-6Al-4V were subjected to UPWJ with applied traverse speeds, ranging from 200 to 1000 mm/s in 100 mm/s increments. The UPWJ peening process increased the surface roughness of all samples in comparison to the baseline, unpeened material. However, it was also noted that the surface roughness decreased with increasing traverse speed. The surface roughness appeared to plateau starting at 700 mm/s, to a roughness of 1.06 ± 0.03 μm. Multiple single-pass scratch tests under constant load were completed on the unpeened and peened materials, the resulting scratches were analysed with SEM and CLSM. The scratch hardness of the materials was calculated following measurements of the scratch widths. Below a traverse speed of 800 mm/s, the scratch hardness of wrought Ti-6Al-4V was not improved by UPWJ. Traverse speeds of 800 mm/s and above enhanced the scratch hardness of the material. From CLSM measurements, the scratch hardness was increased from 3.61 ± 0.24 μm to 5.61 ± 0.30 μm using a traverse speed of 1000 mm/s. By SEM measurements, the scratch hardness of Ti-6Al-4V treated at 1000 mm/s was 6.29 ± 0.41 μm, in comparison to 3.65 ± 0.20 μm for the unpeened material. The dynamic coefficient of friction recorded during scratch testing demonstrated minor instabilities at all traverse speeds, although the data showed increased variation at the lower examined traverse speeds. Reciprocating wear testing was also performed on all samples and the worn surfaces were subsequently assessed with CLSM, SEM, and EDS. Analysis of the volume loss allows calculation of specific wear rate for each of the samples. The specific wear rates determined for the peened samples demonstrated a significant increase after peening, when compared to the unpeened material due to increased adhesive and abrasive wear. A traverse speed of 800 mm/s was found to produce the highest wear resistance (i.e., the lowest specific wear rate) of the peened materials. The wear tracks of samples peened with lower traverse speeds (below 800 mm/s) exhibited many features of adhesive wear. The wear tracks of samples peened at traverse speeds above 800 mm/s were found to contain features of minor adhesive wear and major abrasive wear. EDS demonstrated consistent oxidative wear across all traverse speeds. From these findings, the following conclusions of this project were developed:

1. UPWJ increases surface roughness of wrought Ti-6Al-4V, which decreases and eventually plateaus with increased traverse speed, as there is less exposure time to the water hammer effect and subsequent plastic deformation.

2. The scratch hardness of wrought Ti-6Al-4V is likely to be significantly enhanced with UPWJ with a traverse speed above 800 mm/s. At lower traverse rates and higher surface roughness, the peened material is more susceptible to ploughing. At higher traverse speeds, the benefits from induced compressive stress may overcome the detrimental effects of increased surface roughness.

3. UPWJ resulted in greater stability of coefficient of friction with decreasing traverse speed. This is largely due to decreasing surface roughness at higher traverse speeds.

4. UPWJ has a detrimental influence upon the wear resistance of Ti-6Al-4V. At low traverse speeds, the primary wear mechanism is adhesive wear. At higher traverse speeds, abrasive wear becomes the primary wear mechanism.

5. A traverse speed of 800 mm/s is the most beneficial of the tested traverse speeds. It resulted in the lowest wear rate while maintaining an improved scratch resistance and relatively low surface roughness.

To further gain insight of the influence of traverse speed in UPWJ peening on the surface properties of wrought Ti-6Al-4V, the following work is recommended:

1. Scratch and wear testing of the samples' cross-sections up to the peened surface, to determine the depth of scratch hardening that may be achieved with UPWJ peening. Nano-indentation may also be utilised to further aid this process, by performing indentation arrays on the sample cross-section. This allows for measurement of the material's elastic properties with depth.

2. Perform corrosion testing on the peened and unpeened Ti-6Al-4V material, to determine the effects of UPWJ peening on surface corrosion resistance.
3. Testing slightly polished samples, to determine the effects of UPWJ peening without the intrusive effects of increased surface roughness.
4. Perform wear testing with lubrication to assess how lubrication may require adjustment after UPWJ peening as well as the material's tribological response with lubrication. In biomedical applications, implants are heavily lbricated with bodily fluids, this is commonly simulated in research environments using a bovine serum as a lubricant.
5. Assess a broader range of UPWJ peening parameters, to determine how variation of other peening parameters, such as the frequency and stand-off distance, may influence the tribological behaviour of wrough Ti-6Al-4V.

The recommended work may provide insight into the possible applications of UPWJ peening for titanium alloys. In particular, in biomedical fields an increased surface roughness has been found to be advantageous for artificial hip implants. An increased surface roughness has been observed to promote osteointegration, as proteins and bacteria are able to attach more easily to a rough surface than a smooth surface [21-23, 36]. Despite the decreased wear resistance of the wrought Ti-6Al-4V after UPWJ peening, the increased surface roughness may prove beneficial for artificial joint implants and promoting healing. However, much more research is required to understand the relationship between osteointegration and surface roughness, as well as the mechanical properties of materials treated with UPWJ peening.

Bibliography

[1] A. Bloyce, “Surface engineering of titanium alloys for wear protection,” *Journal of Engineering Tribology*, vol. 212, pp. 467-476, 1998.

[2] G. Chen et al., “Effect of wet shot peening on Ti-6Al-4V alloy treated by ceramic beads,” *Transactions of Nonferrous Metals Society of China*, vol. 24, pp. 690-696, 2014.

[3] H. Dong, “Tribological properties of titanium-based alloys,” in *Surface Engineering of Light Alloys: Aluminium, Magnesium, and Titanium Alloys*, United Kingdom: Elsevier, 2010, pp. 58-80.

[4] F. H. Froes, M. Qian, “Titanium background, alloying behavior and advanced fabrication techniques – an overview,” in *titanium in Medical and Dental Applications*, United Kingdom: Elsevier, 2018, pp. 23-37.

[5] B. K. C. Ganesh, N. Ramanaih, P.V. Chandrasekhar Rao, “Dry sliding wear behavior of Ti-6Al-4V implant alloy subjected to various surface treatments,” *Transactions of the Indian Institute of Metals*, vol. 65, no. 5, pp. 425-434.

[6] V. Sáenz de Viteri, E. Fuentes, “Titanium and titanium alloys as biomaterials,” in *Tribology – Fundamentals and Advancements*, J. Gegner, Croatia: InTech, 2013, pp. 155-181.

[7] C. Veiga, J. P. Davim, A.J.R. Loureiro, “properties and applications of titanium alloys: a brief review,” *Reviews on Advanced Materials Science*, vol. 32, pp. 14-34, 2012.

[8] C. Leinenbach, D. Eifler, “Fatigue and cyclic deformation behaviour of surface-modified titanium alloys in simulated physiological media,” *Biomaterials*, vol. 27, pp. 1200-1208, 2006.

[9] J. C. Williams, R. R. Boyer, “Opportunities and issues in the application of titanium alloys for aerospace components,” *Metals*, vol. 10, no. 6, 2020.

[10] N. Huang, Y. X. Leng, P. D. Ding, “Surface engineering titanium alloys for biomedical devices,” in *Surface Engineering of Light Alloys: Aluminium, Magnesium, and Titanium Alloys*, United Kingdom: Elsevier, 2010, pp. 568-602.

[11] M. Thomas, M. Jackson, “The role of temperature and alloy chemistry on subsurface deformation mechanisms during shot peening of titanium alloys,” *Scripta Materialia*, vol. 66, pp. 1065-1068, 2012.

[12] P. D. Miller, J. W. Holladay, “Friction and wear properties of titanium,” *Wear*, vol. 2, pp. 133-140, 1958.

[13] D. Kümmel et a., “Surface engineering of a titanium alloy for tribological applications by nanosecond-pulsed laser,” *Tribology International*, vol. 150, pp. 2020.

[14] X. Luo, N. Dang, X. Wang, “The effect of laser shock peening, shot peening and their combination on the microstructure and fatigue properties of Ti-6Al-4V titanium alloy,” *International Journal of Fatigue*, vol. 153, 2021.

[15] A. Gomez-Gallegos et al., “Studies on titanium alloys for aerospace application,” *Defect and Diffusion Forum*, vol. 386, pp. 419-423, 2018.

[16] V. A. R. Henriques, “Titanium production for aerospace applications,” *Journal of Aerospace Technology and Management*, vol. 1, no. 1, pp. 7-17, 2009.

[17] I. Inagaki et al., “Application and features of titanium for the aerospace industry,” *Defect and Diffusion Forum*, vol. 385, pp. 22-27, 2018

[18] A. P. Mouritz, “Aerospace materials: past, present and future,” in *Introduction to Aerospace Materials*, United Kingdom: Woodhead Publishing, 2012, pp. 15-38.

[19] R. R. Boyer, “An overview on the use of titanium in the aerospace industry,” *Materials Science and Engineering*, vol. 213, pp.103-114, 1996.

[20] R. R. Boyer, “Titanium for aerospace: rationale and applications,” *Advanced Performance Materials,* vol. 2, pp. 349-368, 1995

[21] X. Liu, P. K. Chu, C. Ding, “Surface modification of titanium, titanium alloys, and related materials for biomedical applications,” *Materials Science and Engineering: R: Reports,* vol. 47, pp. 49-121, 2004.

[22] C. Richard, “Innovative surface treatments of titanium alloys for biomedical applications,” *Materials Science Forum*, vol. 879, pp. 1570-1575, 2016.

[23] N. Lin et al., “Surface texture-based surface treatments on Ti6Al4V titanium alloys for tribological and biological applications: a review,” *Materials*, vol. 11, no. 4, 2018.

[24] F. Bai et al., “A novel ultrasonic cavitation peening approach assisted by water jet,” *Applied Sciences*, vol. 8, no. 11, 2018.

[25] M. Ijiri et al., “Effect of water jet peening using ultrasonic waves on pure Al and Al-Cu alloy surfaces,” *International Journal of Lightweight Materials and Manufacture*, vol. 1, pp. 246-251, 2018.

[26] M. Ijiri, T. Yoshimura, “Sustainability of compressive residual stress on the processing time of water jet peening using ultrasonic power,” *Heliyon*, vol. 4, 2018.

[27] G. Stolárik et al., “Ultrasonic pulsating water jet peening: influence of pressure and pattern strategy,” *Materials*, vol. 14, no. 20, 2021.

[28] J. Foldyna et al., “Utilization of ultrasound to enhance high-speed water jet effects,” *Ultrasonics Sonochemistry*, vol. 11, pp. 131-137, 2004.

[29] M. Srivastava et al., “Surface integrity and residual stress analysis of pulsed water jet peened stainless steel surfaces,” *Measurement*, vol. 143, pp. 81-92, 2019.

[30] P. Siahpour et al., “Surface characteristics and residual stress generation in Ti-6Al-4V following ultrasonic pulsed water jet peening,” *Surface and Coatings Technology*, vol. 445, 2022.

[31] M. Peters et al., “Titanium alloys for aerospace applications,” *Advanced Engineering Materials*, vol. 5, no. 6, pp. 419-427, 2003.

[32] J. T. Terwey et al., “Energy-based modelling of adhesive wear in the mixed lubrication regime,” *Lubricants*, vol. 8, no. 16, 2020.

[33] A. Tsujimoto et al., “Wear of resin composites: current insights into underlying mechanisms, evaluation methods and influential factors,” *Japanese Dental Science Review*, vol. 54, pp. 76-87, 2018.

[34] M. Kandeva-Ivanova, A. Vencl, D. Karastoyanov, *Adavnced Tribological Coatings for Heavy-Duty Applications: Case Studies*, Bulgaria: Prof. Marin Drinov Publishing House of Bulgarian Academy of Sciences, 2016

[35] A. Świetlicki, M. Szala, M. Walczak, "Effects of shot peening and cavitation peening on properties of surface layer of metallic materials – a short review," *Materials*, vol. 15, no. 7, 2022.

[36] M. Lieblich et al., "On the fatigue behavior of medical Ti6Al4V roughened by grit blasting and abrasiveless waterjet peening," *Journal of the Mechanical Behavior of Biomedical Materials*, vol. 63, pp. 390-398, 2016.

[37] M. K. Kulekci, U. Esme, "Critical analysis of processes and apparatus for industrial surface peening technologies," *The International Journal of Advanced Manufacturing Technology*, vol. 74, pp. 1551-1565, 2014.

[38] M. John et al., "Peening techniques for surface modification: processes, properties, and applications," *Materials*, vol. 14, no. 14, 2021.

[39] M. Srivastava et al., "Residual stress and surface properties of stainless-steel welded joints induced by ultrasonic pulsed water jet peening," *Measurement*, vol. 127, pp. 453-462, 2018.

[40] A. Azhari, C. Schindler, B. Li, "Effect of waterjet peening on aluminum alloy 5005," *The International Journal of Advanced Manufacturing Technology*, vol. 67, pp. 785-795, 2013.

[41] H. Soyama, F. Takeo, "Effect of various peening methods on the fatigue properties of titanium alloy Ti6Al4V manufactured by direct metal laser sintering and electron beam melting," *Materials*, vol. 13, no. 10, 2020.

[42] J. Poloprudský et al., "Surface and subsurface analysis of stainless steel and titanium alloys exposed to ultrasonic pulsating water jet," *Materials*, vol.14, no.18, 2021.

[43] A. H. Mahmoudi et al., "Effects of water jet peening on residual stresses, roughness, and fatigue," *Surface Engineering*, vol. 37, pp. 972-981, 2021.

[44] M. Srivastava et al., “Ultrasonically generated pulsed water jet peening of austenitic stainless-steel surfaces,” *Journal of Manufacturing Processes*, vol. 32, pp. 455-468, 2018.

[45] M. Srivastava et al., “Potential of using water jet peening as a surface treatment process for welded joints,” *Procedia Engineering*, vol. 149, pp. 472-480, 2016.

[46] S. R. Daniewicz, S. D. Cummings, “Characterization of a water peening process,” *Journal of Engineering Materials and Technology*, vol. 121, no. 3, pp. 336-340, 1999.

[47] M. A. Islam, Z. Farhat, J. Bonnell, “High pressure water-jet technology for the surface treatment of Al-Si Alloys and repercussion on tribological properties,” *Journal of Surface Engineered Materials and Advanced Technology*, vol. 1, no. 3, pp. 112-120, 2011.

[48] S. Hloch et al., “Effect of pressure of pulsating water jet moving along stair trajectory on erosion depth, surface morphology and microhardness,” *Wear*, vol. 452, 2020.

[49] D. D. Arola, M. L. McCain, “Abrasive waterjet peening: a new method of surface preparation for metal orthopedic implants.” *Journal of Biomedical Materials Research*, vol. 53, no. 5, pp. 536-546, 2000.

[50] D. Arola et al., “Waterjet and abrasive waterjet surface treatment of titanium: a comparison of surface texture and residual stress,” *Wear*, vol. 249, pp. 943-950, 2002.

[51] S. Barriuso et al., “Roughening of metallic biomaterials by abrasiveless waterjet peening: characterization and viability,” *Wear*, vol. 270, pp. 634-639, 2011.

[52] G. Sundararajan, M. Roy, “Hardness testing” in *Encyclopedia of Materials: Science and Technology*, K. H. J. Buschow et al.: Elsevier, 2001, pp. 3728-3736.